Master Thesis

GROWTH OF THIN FILMS AND THIN FILM TRANSFER FOR METAMATERIAL SYNTHESIS

Syntesis of Semiconductor Thin Film on Metal Thin Film

30th May 2025

Physics and Technology / Nanomaterials and Nanophysics, Julia Petersen
Department of Materials and Production, Aalborg University

AALBORG UNIVERSITET
STUDENTERRAPPORT

w/
Department of Materials and Production
Physics and Technology / Nanomaterials and Nanophysics
Fibigerstræde 16
9220 Aalborg Øst

Title:
Growth of Thin Films and Thin Film Transfer for Metamaterial Synthesis

Project:
Master Thesis

Project period:
3rd September 2024 to 30th May 2025

Project group:
Julia Petersen

Supervisor:
Kjeld Pedersen

Number of pages:
84

Number of appendices:
5

Finish date:
30th May 2025

Abstract:

Growth of different thin films was performed by physical vapour deposition (PVD) and molecular beam epitaxy (MBE). The thin films produced were Au with PVD and GaN with MBE. The Au thin films were grown on a quartz glass substrate with no intermediate layer. For the GaN thin films, different substrates were tested to grow the thin film. Substrates such as Si(100) and muscovite mica were used and heated during deposition. For Si(100) substrate, the Ga source temperature was optimised to be 970 °C and afterwards the sample temperature was optimised. The sample temperatures for this substrate where 650 °C, 710 °C, 725 °C and 760 °C.
The muscovite mica samples had two different sizes to ensure the best possible heat diffusion through the sample. The two sizes were $25 \times 25 \times 0.15$ mm and $9 \times 32 \times 0.15$ mm. For both of the sizes heat distribution simulations were made in COMSOL[1]. The big muscovite mica samples had sample temperatures of 550 °C to 850 °C with a temperature step of 50 °C. The lowest temperature was to see if it was possible to deposit and the highest temperature was to ensure where the threshold for heating muscovite mica would be. For the smaller muscovite mica samples, sample temperatures of 650 °C to 800 °C with a temperature step of 50 °C, were made. The final temperature of this sample size where 770 °C and 780 °C.
Optical microscopy, atomic force microscopy (AFM) and photoluminescence measurements were produced for all samples. Only for the GaN with the Si(100) substrate, XRD measurements were produced. For the assembly three different methods were used, 3-mercaptopropyl(trimethoxysilane) (MPTS), silver epoxy and adhesive tape lift-off.

Preface

This master's thesis was written by Julia Petersen, who is a 4^{th} semester master's student at Nanomaterial and Nanophysics, at Aalborg University. This thesis was written in the period from 3^{rd} September to May 30^{th}. This thesis was supervised by Professor Kjeld Pedersen, from the Department of Materials and Production. This thesis focuses on the growth of metal thin films and semiconductor thin films and afterwards the transfer of the semiconducting thin films onto the metal thin films. The topic of this thesis was different assembly methods and achieving the semiconducting material to be grown on different substrates. For the growth, the sample temperature was simulated by COMSOL[1]. They were then characterised by optical microscopy, atomic force microscopy and photoluminescence. All the laboratory work and simulation work is described in the method section, and some of the results are presented in the results section, and the rest are presented in the appendix. The results were then discussed and lastly summed up in a conclusion.

All the references were in the IEEE citation style and they are summarised in the bibliography. An generative AI was used for corrections and assistance in different aspects. Figures were named "X.X" [example figure 2.3], tables were named "X.X" [example table 3.4], and equations were named "(X.X)" [example equation (2.6)]. Figures with no citation were made by Julia Petersen.

Julia Petersen
jpete20@student.aau.dk

Aalborg University, 30^{th} May 2025

Resume

Dette speciale fokuserer på udviklingen af metoder til vækst og overførsel af tyndfilm med henblik på syntese af metamaterialer, gennem kombinationen af tyndfilms metal så som Au og halvleder så som GaN. Tyndfilmene blev fremstillet ved hjælp af henholdsvis physical vapour deposition (PVD) for Au og molecular beam epitaxy (MBE) for GaN. Formålet var at undersøge, hvordan disse materialer kan kombineres uden at danne uønskede fejl i groningen eller kombination af materiale mellemlag, som kan forringe de optiske eller elektriske egenskaber.

Au blev groet direkte på kvartsglas uden et bindende mellemlag, mens GaN blev dyrket på både Si(100) og muscovite mica. For at optimere vækstbetingelserne blev temperaturen af både Ga kilden og substraterne varieret. Til Si(100) blev Ga temperaturen optimeret til 970 °C, og de resterende temperaturer blev afprøvet i området 650 °C til 760 °C. For muscovite mica blev der anvendt to forskellige størrelser af substratet, og der blev udført detaljerede varmesimuleringer i COMSOL Multiphysics[1] for at undersøge varmefordelingen på de to forskellige substrater. Dette blev gjort for at undersøge hvor stor en forskel på temperatur der vil være når GaN bliver deponeret. De temperatuerer der blev undersøgt for muscovite mica var fra 550 °C til 850 °C.

Karakteriseringen af de fremstillede tyndfilm blev gjort ved hjælp af optisk mikroskopi, atomar kraft mikroskopi (AFM), fotoluminescens spektroskopi og x-ray diffraction (XRD). XRD blev kun udført på substratet af Si(100). Disse metoder blev anvendt til at vurdere ruhed, krystalstruktur og optiske egenskaber. Fotoluminescens blev brugt til at analysere båndgab og defekter i GaN filmene. Det blev observeret, at substratvalget og substrat temperaturen havde stor betydning for GaN filmens kvalitet og defektstruktur. For GaN på Si(100) blev der bl.a. fundet krystalfaser og relevante fotoluminescence toppe, mens muscovite mica gav anledning til højere variation i ruhed og optiske egenskaber, men også for Van der Waals samling.

Der blev eksperimenteret med tre forskellige metoder til at samle de to typer af tyndfilm: kemisk overfladefunktionalisering med 3-mercaptopropyl(trimethoxysilan) (MPTS), anvendelse af sølv-epoxy og mekanisk lift-off med tape. Hver metode blev evalueret i forhold til vedhæftning og potentiale for anvendelse i videre integration af funktionelle materialer. Den mest lovende metode viste sig at være MPTS-behandling.

Contents

1 Intro

Today's electronic industry uses semiconductors, a material between a conducting material and an insulator. Before the semiconductor, around the 1900s to 1950s, vacuum tubes were the primary electronic component. These tubes were fragile, and bulky, produced a lot of heat and required a lot of power. In 1948 the transistor was invented at Bell Laboratories. The transistors were smaller, lightweight, had long lifetimes and used less power than the vacuum tube.[2]

From this advance, Jack Kilby of Texas Instruments created in 1958 a semiconductor chip with resistors and capacitors. This was the catalyst for further advances in the electronics industry. The physical chemist Gordon E. Moore predicted in 1965 that the number of components on a chip would be doubled every year, which he then 10 years later corrected to be every two years instead. This became Moore's law.[2, 3, 4]

For the past years, the material often used for semiconductors was silicon[2]. With the increasing research made in the past years, semiconductors are made of elements from group III-V or II-VI. These semiconductors are currently used in a variety of different electronics, such as optoelectronic devices or photovoltaic cells.[5]

A variety of different semiconductors have been researched and things like oxide semiconductors, thin film transistors, transparent electrodes and doped semiconductors with magnetic impurities, have been produced.[5]

Not only are semiconductors used in microchips, but also for light-emitting diodes (LED). These forms of LEDs have a short wavelength and are thereby in the blue-violet range. This can thereby be used for things such as laser light to focus the laser light and get a smaller spot. The most efficient semiconducting alloy material for this is the group III nitrides, such as AlN or GaN. They have the characteristic wide bandgap.[6]

In this project, the GaN semiconducting material is studied. To form GaN the two elements need to be in a vacuum environment with Ga rich and N_2 rich conditions. Ga is in general a soft and silvery blue metal which has similar chemical properties as Al. The Ga has a melting point of 302.98 K and a boiling point of 2676 K and has a low vapour pressure even at higher temperatures.[7]

For the growth of the GaN both high pressure and temperature are needed to ensure the best crystallinity. The GaN crystal structure is a wurtzite structure and is usually grown with heteroepitaxy growth on sapphire. The semiconductor suffers from different defects when grown, such as lattice defects, point defects and dislocations. To understand these defects an understanding of the surface and interfaces are essential.[5, 8]

Sapphire is one of the most used substrates for GaN growth due to its relatively good lattice match. The two materials have different thermal coefficients which creates expansions in substrate and thin film, and is a remarkable problem when the diameter of the sapphire increases. The possibility of growing GaN on different substrates, such as Si is starting to become

interesting in research. The Si despite the low cost, electrical and thermal properties, has lattice mismatch with GaN, and thermal mismatch.[9, 10]

Muscovite mica with the chemical structure $KAl_2(Al, Si_3)O_{10}(OH)_2$, is available in large quantities and has low cost. It is also lightweight, transparent, and structurally flexible. It is possible to deposit GaN on top of muscovite mica by molecular beam epitaxy (MPE). Muscovite mica is an insulator and is an atomically flat material that consists of weakly bound sheets. These sheets are bound by electrostatic interactions with the K atoms. This substrate is part of research with Van der Waals epitaxy, which aims to grow mismatched layers with a reduced amount of lattice strain. This has been successfully done by pulsed laser deposition reported by Matsuki, N. et al[11].[11, 12, 13, 14]

Choosing a "pseudo substrate" is to choose what substrate to deposit the thin film and then transfer it to a different substrate, material or thin film. This technique is good for two reasons. Firstly ensure high quality in the thin film and reduce dislocations in the film. Secondly, it ensures that the two-dimensional growth does not need an intermediate layer or buffer layer, that in the end can react with the thin film.[15]

There are different ways of lift-off for thin films such as optically, chemically or mechanically. One of them is optical, which is a method using a laser, where GaN is grown on a substrate and then lifted off the substrate by letting the laser penetrate the substrate to heat the interface. Another one is chemical where a sacrificial layer between substrate and thin film is grown and etched away in a chemical. Lastly, the mechanical method can for example be done with adhesive tape.[16, 17]

After the lift-off of the thin film, the freestanding film can be assembled onto other thin films, such as a Au film. A Au thin film has become important to technology and research since it has chemical inertness, high work function, favourable optical properties, large atomic mass and high conductivity.[18]

To combine these thin films to create another material is the interest of this project. To create this without creating alloys or an insulating layer between the two thin films. Especially with a homogenous thin film on top of another thin film.

Theory 2

2.1 Index System for Crystal Structures

This section is based on chapter 1 from the book by Kittel, C. et al. *Kittel's Introduction to Solid State Physics* (2005)[19].

For crystals, the orientation of the crystal plane can be determined by three points in the plane, and they are not collinear. The lattice constants (a_1, a_2, a_3) can specify the points in the plane if each point is on a different crystal axis. From figure 2.1, the plane in the crystal is described by the lattice constants and can be in a primitive or nonprimitive cell. The reciprocal is used from these numbers and then reduced to three integers, with the same ratio. From this, the index of the plane is described by (hkl).

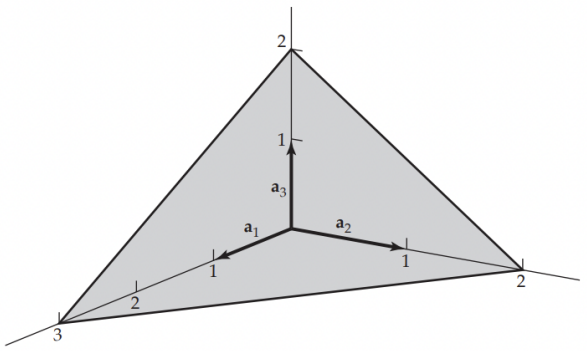

Figure 2.1. *A plane that is at the points of $3\boldsymbol{a}_1$, $2\boldsymbol{a}_2$, $2\boldsymbol{a}_3$, giving the miller indices of (233) for this plane. Taken from [19].*

Examples of the different planes in a cubic crystal can be seen in figure 2.2, where the (100) plane will mainly be used in this project.

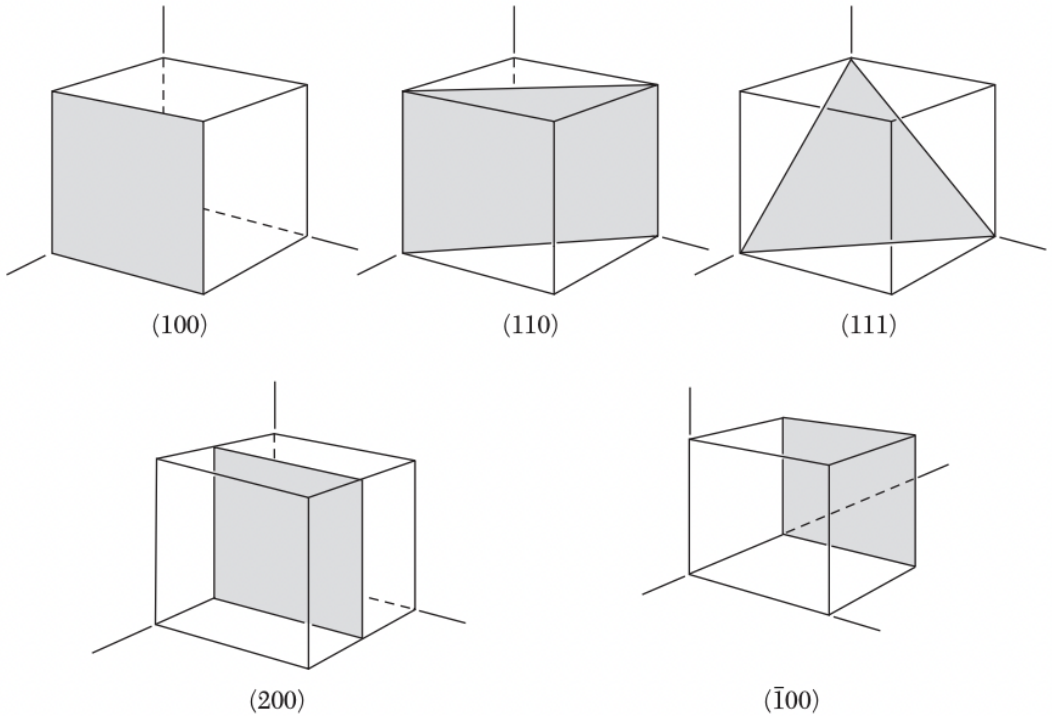

Figure 2.2. *Representation of the different miller indices in a cubic crystal. Taken from [19].*

2.1.1 GaN Crystal Structure

The crystal structure for GaN is ordered in a wurtzite lattice. From figure 2.3, the crystal structure is shown with the lattice parameters a and c and the internal parameter u. Where the lattice values are $a = 3.190$ Å, $c = 5.189$ Å and the internal parameter $u = 0.377$.[20, 21]

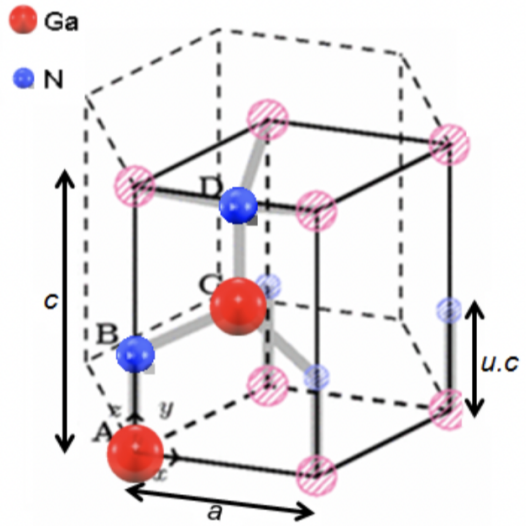

Figure 2.3. *Crystal structure of GaN with the crystal parameters a and c and the internal parameter u. Ga as red atoms and N as blue atoms. Taken from [20]*

The wurtzite structure of GaN gives a wide direct band gap of around 3.4 eV. Thereby the photons traveling in the crystal have a similar energy as the wide direct band gap. Having a

direct band gap means that the optical transition in this gap is ”allowed”, thus making them much stronger than indirect band gaps.[20, 21]

The photoluminescence of a perfect GaN crystal is shown in figure 2.4. Here the black graph is the perfect GaN crystal and has a distinct maximum at 3.48 eV, which is the bound exciton and at 3.40 eV is the first longitudinal optical (LO) phonon mode. At around 3.27 eV, the donor-acceptor pair is shown plus the LO phonons. The broad maximum in this figure is the yellow luminescence of the crystal.[22]

Not only is the photoluminescence of a perfect crystal shown but also a GaN crystal that was doped with Fe, which is the red graph. This shows that when the crystal is doped the donor-acceptor pair is gone, but then a Fe induced vacancy is introduced instead at around 1.30 eV.[22]

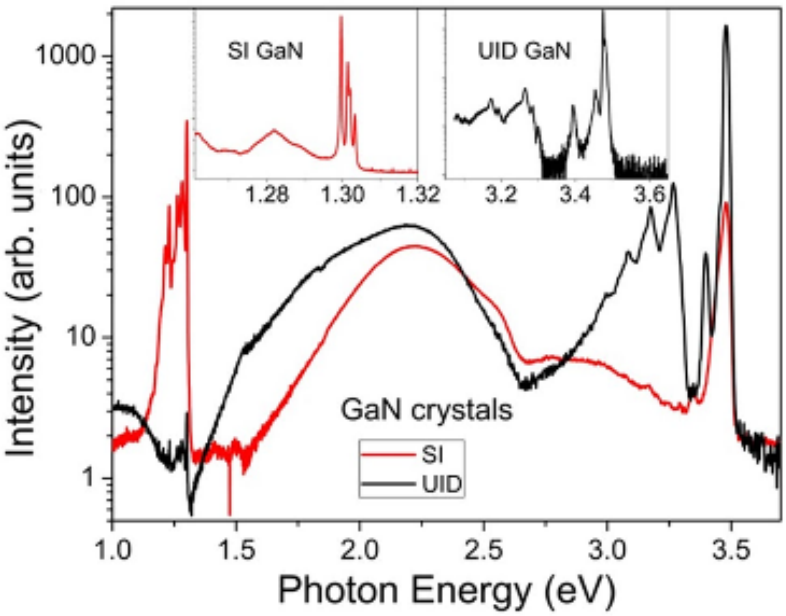

Figure 2.4. *Photoluminescence of a perfect crystal is shown where the black graph is the perfect crystal and the red graph is the doped crystal. Taken from [22].*

2.2 Thin Film Growth

This section is based on chapter 14 of the book by Oura, K. et al. *Surface Science: An Introduction* (2013)[23]. The growth of thin films is when the adsorbate is covered by more than a monolayer. There are different ways these thin films can grow, which are

- Layer-by-layer
- Island
- Layer-plus-island

For layer-by-layer, the atoms are binding stronger to the substrate than to each other, thereby creating a two-dimensional growth. The island growth is when the atoms bind stronger to each other than to the substrate. For layer-plus-island growth, the first layer consists of atoms binding strongly to the substrate, and afterwards, the atoms bind strongly to each other to create the islands on top.

These different forms of growth can be described by the surface or interface tension (γ). Tension is defined as the minimum work that needs to be overcome to make the surface or interface per unit area. The tension γ is thereby also the force per unit length of a boundary, where it is the contact point of the substrate. The force equilibrium can thereby be described as:

$$\gamma_S = \gamma_{S/F} + \gamma_F \cos\varphi \tag{2.1}$$

Where γ_S is the tension of the substrate, $\gamma_{S/F}$ is the tension at the interface of the substrate and the film, and γ_F is the film tension. Here φ is the wetting angle of the island. This is illustrated in figure 2.5.

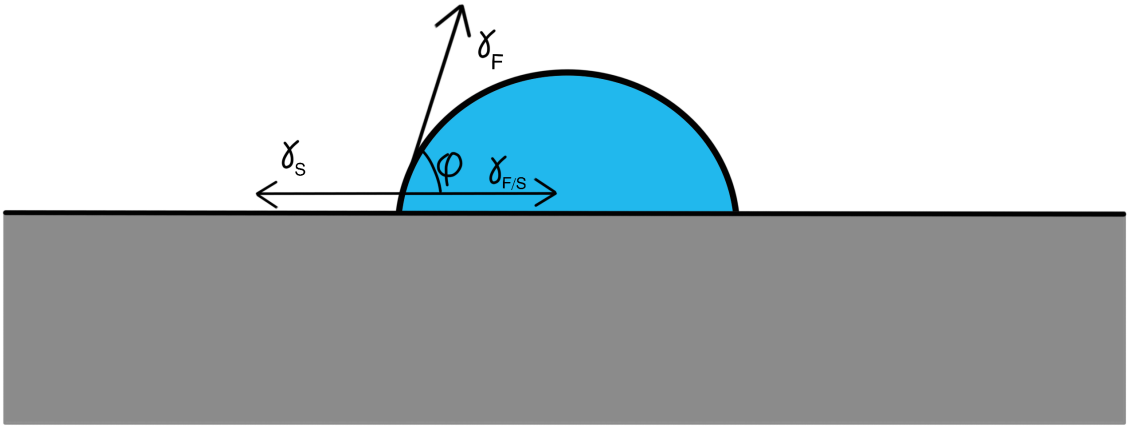

Figure 2.5. *Schematic of island on a substrate were γ_S is the surface tension substrate, γ_F surface tension of film and $\gamma_{S/F}$ is surface tension at the interface.*

The different growth modes can be described by changing the wetting angle as seen in figure 2.5 and equation (2.2).

$$\begin{aligned} \text{Layer-by-layer:} \quad & \gamma_S \geq \gamma_{S/F} + \gamma_F \quad (\varphi = 0) \\ \text{Island:} \quad & \gamma_S \leq \gamma_{S/F} + \gamma_F \quad (\varphi > 0) \end{aligned} \tag{2.2}$$

For the layer-plus-island growth, first, the layer-by-layer condition is fulfilled, and then the island condition.

2.2.1 Epitaxy Growth

There are two ways of epitaxy growth when growing thin films: homoepitaxial growth and heteroepitaxial growth. In homoepitaxy growth, the substrate and the film growing on the substrate are of the same material. In heteroepitaxy, the substrate and film are of different materials. In this project, heteroepitaxy was used.

2.2.2 Heteroepitaxy

In heteroepitaxy growth, there is the problem of strain effects when growing the thin film. Different materials have different lattice constants, which means that the thin films do not always have an ideal lattice match. This non-ideal lattice match is described by the misfit (ε), which is the relative difference of the lattice constants:

$$\varepsilon = \frac{b - a}{a}. \tag{2.3}$$

Elastic strain can give low misfits by deformation of the lattice in a way that the strained film gets the same periodicity as the substrate at the interface. At the interface, the thin film gets the periodicity of the substrate, and at the perpendicular plane, it can become distorted to remain the volume of the unit cell. This is because of the elastic strain in the crystalline structure. Figure 2.6 shows what happens when the misfit gets higher since the strain is relieved by the dislocations at the interface. For the dislocations, the distance is defined as:

$$d = \frac{ab}{|b - a|}. \tag{2.4}$$

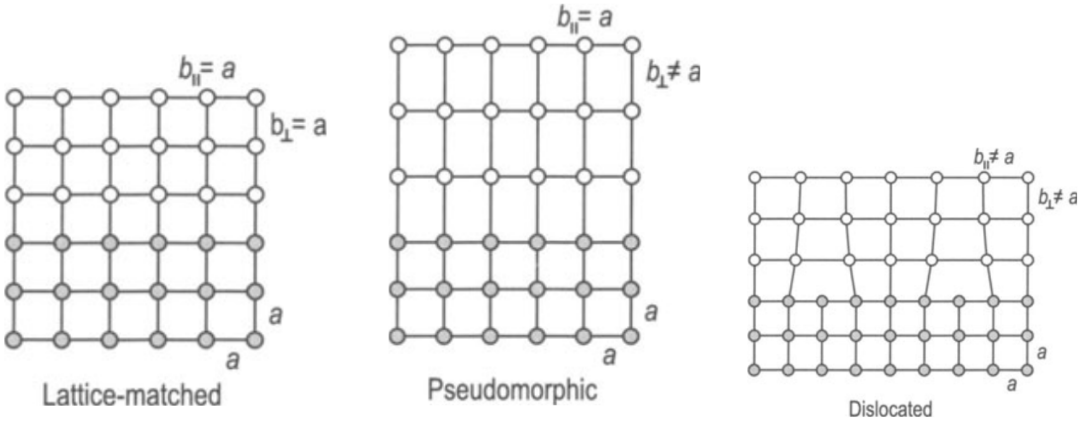

(a) **(b)** **(c)**

Figure 2.6. *Shows the different lattice mismatches where* ***(a)*** *is lattice matched,* ***(b)*** *is pseudomorphic mismatch and* ***(c)*** *is dislocated mismatch. Taken from[23]*

The free density energy determines which growth mode is happening. In figure 2.7a, the lattice misfit per energy is plotted, where in the beginning, the strained energy (E_ε) is more favourable. After a critical misfit point (ε_c), the dislocations (E_D) become more energy favourable. In figure 2.7b, the film thickness dependent on energy is plotted, where the strain growth is favourable in the beginning and after the critical film thickness (h_c), the dislocated growth is more favourable.

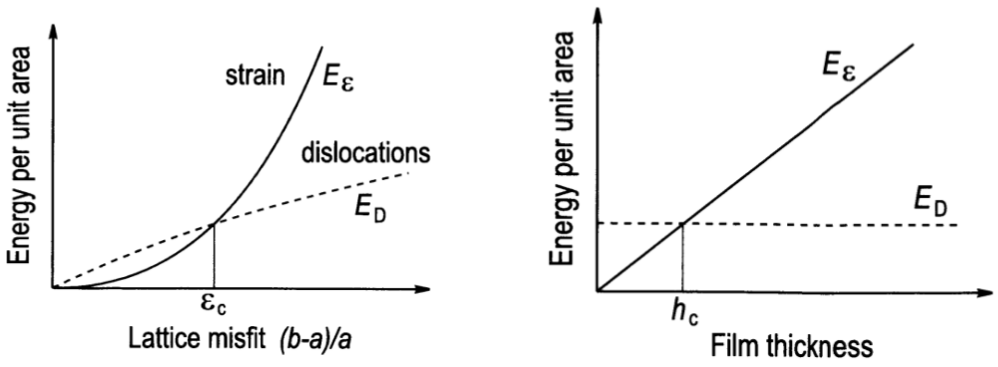

(a) **(b)**

Figure 2.7. *Schematic of lattice energy per unit area, were* ***(a)*** *is per lattice misfit and* ***(b)*** *is per film thickness. Here ε_c is the critical misfit and h_c is the critical film thickness. Taken from[23]*

2.2.3 Molecular Beam Epitaxy

For molecular beam epitaxy (MBE), the atoms or molecules are delivered to the surface of the sample for thin film deposition. For the growth of the thin film onto the substrate, the substrate is heated at a constant temperature. This ensures that the atoms arriving at the surface migrate over the surface to the lattice sites. It also ensures that the induced diffusion intermixing between the already grown layer and the bulk material is not too high. All of this occurs under ultra-high vacuum for deposition.

2.2.4 Physical Vapor Deposition

Physical vapour deposition (PVD) uses the physical process of either thermal evaporation or impact process. By using this process the particles that will be deposited will be transformed into the gaseous state. For this process, the pressure needed is below about 10^{-1} mbar. In this project, heating is used.[24]

This method uses the heating of atoms or molecules of a solid or liquid to increase the kinetic energy in the material, and thereby overcome the separation energy to evaporate. These evaporated particles consist of atoms, molecules and clusters. There are different ways to achieve heating of the material. The one used in this project is evaporation by heating from a boat or wire, consisting of a refractory metal, such as tungsten, tantalum or carbon. This metal is then heated by an electrical current. This works if the material to evaporate has a lower melting point than the wire material.[24]

2.3 Assembly Methods

2.3.1 Surface Modification

Various methods can be used to modify the surfaces of two different samples with two different substrates. By modification of the surfaces, the samples can be assembled depending on the modification. By using self-assembled monolayers (SAM), the surface can make a chemical bond to the SAM. This implies surfaces like noble metal, metal oxides and semiconductors.[25]

Silanes

There are different forms of silanes, such as (3-Aminopropyl) triethoxysilane (APTES), (3-Glycidyloxypropyl) trimethoxysilane (GPTMS), and 3-mercaptopropyl(trimethoxysilane) (MPTS). All of them have the characteristic silane group, which will react to the surface by either hydrogen bonds or covalent bonding. The silane used in this project is the MPTS, which has a sulfur group at the other end. This is shown in Figure 2.8.[25]

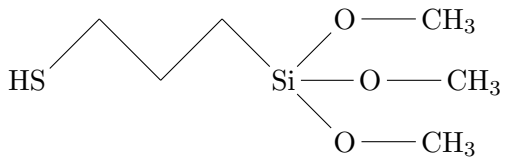

Figure 2.8. *Chemical structure of MPTS (3-mercaptopropyl(trimethoxysilane)).*

The alkoxysilane group of the molecule can then bind to a variety of minerals and metal surfaces by covalent bonds. This is done through complex hydrolysis/condensation reaction to form the Si−O−R bonds. Where R is any form of atom or metal surface.[26]

2.3.2 Silver Epoxy

For silver epoxy, Ag particles are mixed with epoxy resin. Ag has one of the highest thermal conductivities of 427 W/mK.[27]

Epoxy resin is a low-molecular-weight pre-polymer, which contains more than one epoxide group. An epoxide group is shown in figure 2.9. Here the R could be any form of polymer. Epoxy resins are thermosetting resins, which means that it is an irreversible process. Depending on the epoxy resin and curing agent it can be used for different applications.[28]

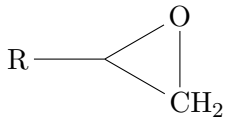

Figure 2.9. *An epoxide group where R is a placeholder for any form of polymer.*

In this project, it is used as an assembly method. The silver epoxy that was used had an epoxy resin made of diglycidyl ether of bisphenol-A (DGEBA), shown in figure 2.10. The way it is produced is by letting epichlorohydrin react with bisphenol-A in the presence of a basic catalyst. The properties of this chemical depend on the length of the repeating polymer unit. For this specific epoxide, it can be either low-molecular-weight or high-molecular-weight, which either is liquid or more viscous liquid/solid, respectively.[28]

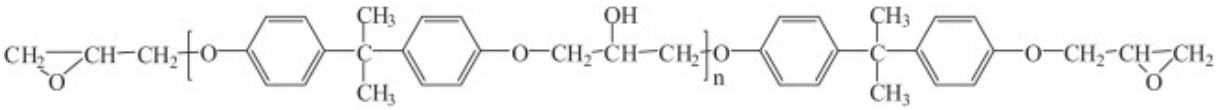

Figure 2.10. *Chemical structure of DGEBA, where n denotes that this part of the polymer can be repeated n times. Taken from [28].*

Curing Agent

For the epoxy to be cured, it needs a curing agent. There exists a wide range of curing agents, such as alkali curing agents, anhydrides, catalytic and amine-type. In this project, the amine-type curing agent is used. This type of curing agent is one of the basic curing agents for epoxy

resins. The amine type reacts with the epoxy ring by nucleophilic addition. Figure 2.11 shows how the amine is used to cure an epoxide by the nucleophilic addition.[28]

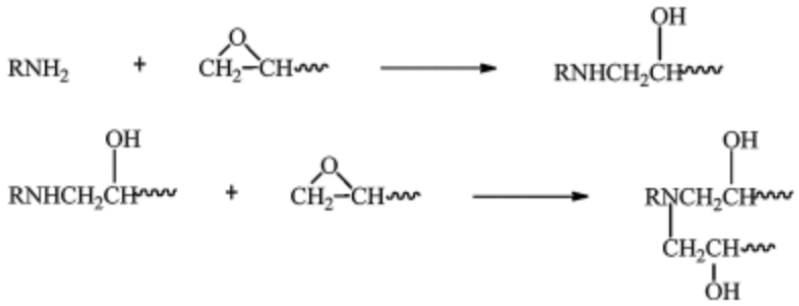

Figure 2.11. *Chemical reaction of amine with epoxide. Taken from [28].*

2.3.3 Lennard-Jones Potential

Atoms can bind in different ways such as ionic bonding and covalent bonding. The Lennard-Jones potential (LJ) describes a sum of a simple pair potential between two atoms, as seen in figure 2.12. It describes a weak Van der Waals bond with reliable bond energies and bond lengths.[29]

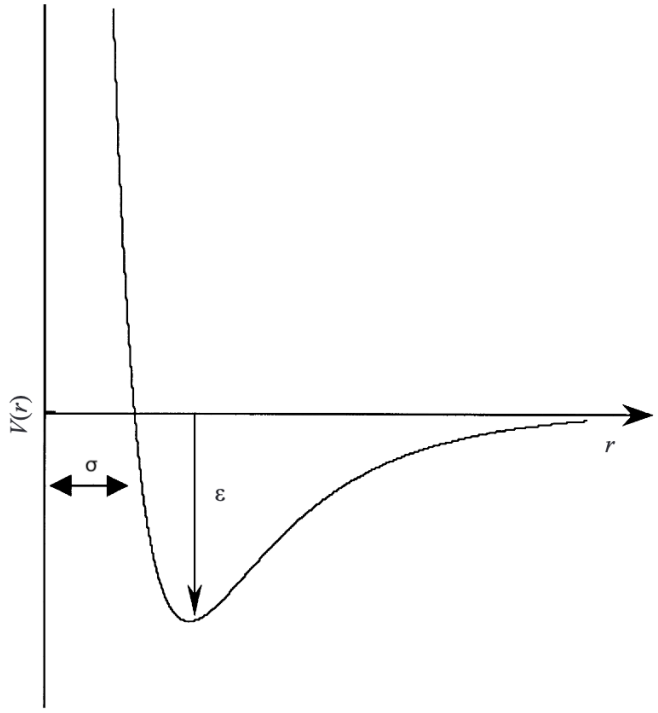

Figure 2.12. *Lennard Jones potential for interaction of atoms. Energy on the y-axis and distance on the x-axis. Taken from [29].*

The LJ is described by,

$$V^{LJ}(r) = 4\varepsilon \left[\left(\frac{\sigma}{r}\right)^{12} - \left(\frac{\sigma}{r}\right)^{6} \right]. \tag{2.5}$$

Here r is the distance between the atoms, ε is the bond energy and σ is the bond length. Thereby the attractive interactions are due to dipoles of the atoms and the repulsive part is due

to electron clouds overlapping. The repulsive part is also called the Pauli exclusion principle, which also forces the electrons into higher states.[29]

Equation (2.5) shows that the attractive part of the potential is $\left(\frac{\sigma}{r}\right)^6$, where it decays with the distance because of the dipole-dipole interaction. The repulsive part of the equation is $\left(\frac{\sigma}{r}\right)^{12}$ and decays more rapidly than the attractive part. From this, the repulsive term is dominant at short distances and the attractive term is dominant at long distances. The bottom of the well is the equilibrium of the atom pair at 0 K. The bond energy of the two atoms is defined as the bottom of the well to infinity of the bond energy. The curvature of the bottom of the well defines the frequency of the two atoms swinging.[29]

2.4 Heat Conduction in Solids

This section is based on chapter 1 of the book of Hahn D. W. and Özisik N. M. *Heat Conduction* (2012)[30].

Heat conduction can be derived from the differential or integral form of heat conduction, which is often called the heat equation. Here the differential control volume equation is derived. The assumption made for this is that it is a continuum so that all the properties do not vary on the microscopic scale. The heat equation is for a solid which is homogeneous, stationary and isotropic, where there is heat generation in the body. The internal heat generation in a solid is mainly due to nuclear or chemical reactivity, electrical current, and absorption of light i.e. laser. These are in general a function of time and/or position.

Figure 2.13 shows the differential control volume in cartesian coordinates. From this, the volume and mass of it is defined as,

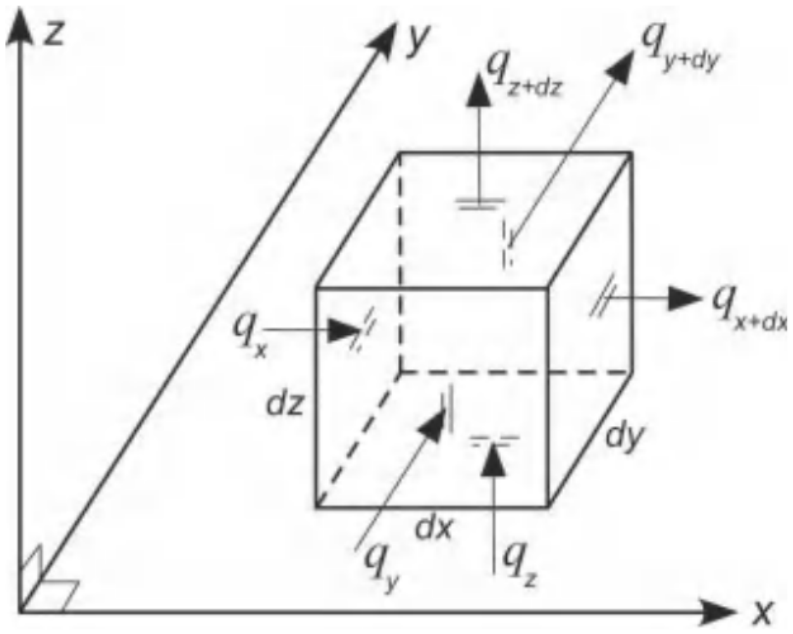

Figure 2.13. *Image for the differential control volume, for derivations of the heat equation. Taken from [30].*

$$\begin{aligned} dv &= dx\ dy\ dz \\ dm &= \rho dx\ dy\ dz \end{aligned} \tag{2.6}$$

Here ρ is the mass density of the control volume with the units of $\frac{\mathrm{kg}}{\mathrm{m}^3}$. For the assumption of a continuum the equation (2.7) is considered.

$$\varepsilon \ll L_c^3 \tag{2.7}$$

Where ε is a volume much larger than the individual atoms and L_c is the smallest length scale of interest for the heat transfer. When this equation is valid then the continuum assumption is fulfilled.

After this assumption, we can look at the general statement of conservation of energy, which is based on the first law of thermodynamics.

$$\left(h + \frac{1}{2}\overline{V}^2 + gz\right)_{\text{in}} \delta\dot{m} - \left(h + \frac{1}{2}\overline{V}^2 + gz\right)_{\text{out}} + \delta\dot{Q} + \delta\dot{E}_{\text{gen}} - \delta\dot{W} = \frac{dE_{\text{cv}}}{dt} \tag{2.8}$$

where h is the specific enthalpy, $\overline{V}$ is the velocity of the fluid, gz is the potential energy per unit mass, $\delta\dot{m}_{\text{in}}$ and $\delta\dot{m}_{\text{out}}$ is the mass flow rates in and out of the controlled volume, $\delta\dot{Q}$ is the net heat transfer into the controlled volume, $\delta\dot{E}_{\text{gen}}$ is the generated energy within the controlled volume, $\delta\dot{W}$ is the work transfer rate out of the controlled volume and $\frac{dE_{\text{cv}}}{dt}$ is the rate of change in energy inside the controlled volume. When the mass flow rates and the rate of work done by the control volume are zero, then the heat equation for the quiescent medium can be derived. Thereby the rate of change in energy can be expanded as,

$$\frac{dE_{\text{cv}}}{dt} = \frac{d}{dt}\left[\left(u + \frac{1}{2}\overline{V}^2 + gz\right)_{\text{cv}} dm\right]. \tag{2.9}$$

Here u is the internal energy with units of $\frac{\mathrm{J}}{\mathrm{kg}}$. This is an intensive scalar property, which is related to the thermodynamic state of the system. If any changes in the kinetic energy and potential energy are neglected the change in energy can be described as,

$$\delta\dot{Q} + \delta\dot{E}_{\text{gen}} = \frac{d(u\,dm)}{dt} \tag{2.10}$$

The net heat is described by the heat rate in and out of the controlled volume, which is,

$$\delta\dot{Q} = (q_x - q_{x+dx}) + (q_y - q_{y+dy}) + (q_z - q_{z+dz}) \tag{2.11}$$

The individual terms of the heat rate can be described by Fourie's law and the respective cross-sectional area. Thereby the one in the x direction can be described as,

$$q_x = -kA_x\frac{\partial T}{\partial x} \qquad \text{where} \qquad A_x = dy\,dz. \tag{2.12}$$

For the y and z direction it is essentially the same, thus $A_y = dx\,dz$ and $A_z = dx\,dy$, respectively. To describe the individually exiting heat rates a Taylor series expansion is used neglecting the higher-order terms. For the x direction it becomes,

$$q_{x+dx} = q_x + \frac{\partial q_x}{\partial x}dx = -kA_x\frac{\partial T}{\partial x} + \frac{\partial}{\partial x}\left(-kA_x\frac{\partial T}{\partial x}\right)dx. \tag{2.13}$$

By combining equation (2.12) and (2.13) the net heat rate entering the controlled volume becomes,

$$q_x - q_{x+dx} = \frac{\partial}{\partial x}\left(k\frac{\partial T}{\partial x}\right) dx\, dy\, dz \tag{2.14}$$

The same applies to the net heat rate in the y and z direction. These definitions can then be inserted in equation (2.11) giving,

$$\delta\dot{Q} = \frac{\partial}{\partial x}\left(k\frac{\partial T}{\partial x}\right) + \frac{\partial}{\partial y}\left(k\frac{\partial T}{\partial y}\right) + \frac{\partial}{\partial z}\left(k\frac{\partial T}{\partial z}\right) \tag{2.15}$$

The definition of the internal energy generation can be calculated from the volumetric rate of the internal energy generation g. The volumetric rate of internal energy generation is in general described as $g = g(\hat{r}, t)$ and therefore the internal energy generation can be described as,

$$\delta\dot{E}_{\text{gen}} = g\, dx\, dy\, dz. \tag{2.16}$$

For the rate of change of energy in the controlled volume, the definition can be described by introducing the constant volume specific heat c_v with units of $\frac{\text{J}}{\text{kg}\cdot\text{K}}$. This is defined as $c_v \equiv \frac{\partial u}{\partial T}\big|_v$ and becomes

$$u = c_v T + u_{\text{ref}}. \tag{2.17}$$

It is known that for an incompressible solid or fluid, it is defined as $c_v = c_p = c$, where c_p is the specific heat of constant pressure. By inserting the above expression into the right-hand side of the equation (2.10) the net rate of change of energy within the controlled volume becomes,

$$\frac{d(u\, dm)}{dt} = \rho c\frac{\partial T}{\partial t} dx\, dy\, dz. \tag{2.18}$$

For the equation to hold the assumption that the properties ρ and c are constant.

Now equation (2.15), (2.16) and (2.18) can be introduced to equation (2.10) to become the general heat equation in the cartesian coordinate system,

$$\frac{\partial}{\partial x}\left(k\frac{\partial T}{\partial x}\right) + \frac{\partial}{\partial y}\left(k\frac{\partial T}{\partial y}\right) + \frac{\partial}{\partial z}\left(k\frac{\partial T}{\partial z}\right) + g = \rho c\frac{\partial T}{\partial t}. \tag{2.19}$$

Each of the different terms has the units of $\frac{W}{m^3}$. The above equation is thereby the net rate of heat conducted per differential volume plus the rate of energy generated internally per volume, which gives the net rate stored per differential volume.

If the thermal conductivity for the general heat equation is a constant the equation can be rewritten as,

$$\frac{\partial^2 T}{\partial x^2} + \frac{\partial^2 T}{\partial y^2} + \frac{\partial^2 T}{\partial z^2} + \frac{g}{k} = \frac{1}{\alpha}\frac{\partial T}{\partial t}. \tag{2.20}$$

Thereby each term in the equation has the units $\frac{\text{K}}{\text{m}^2}$, since the thermal diffusivity is defined as

$$\alpha = \frac{k}{\rho c} \tag{2.21}$$

where the units are $\frac{\text{m}^2}{\text{s}}$. Thermal diffusivity is a thermal physical property of the medium. This physical property represents the flow of heat. This means that the higher the thermal diffusivity the faster the response of the medium to thermal perturbations, and the faster the change in propagation is through the medium.

Method 3

3.1 Deposition of Au

A machine that Professor Kjeld Pedersen built was used to deposit Au on quartz glass outside of the clean room. The start parameters for the machine and the parameters for deposition of Au on the different samples are shown in table 3.1.

Table 3.1. *Parameters for growing Au on quartz glass.*

Sample	Temperature [°C]	Current [A]	Voltage [V]	Effect [W]	Pressure [mbar]
Start	10	5	–	–	$1{\cdot}10^{-6}$
1	10	55	9.3	511.5	$3{\cdot}10^{-6}$
2	10	55	9.3	511.5	$6{\cdot}10^{-6}$
3	10	55	9.4	517	$2{\cdot}10^{-6}$
4	10	55	9.4	517	$2{\cdot}10^{-6}$

3.2 Deposition of GaN

The machine used was built by Professor Kjeld Pedersen and technician Peter Kjær Kristensen. A sample was placed inside the load lock for deposition. The deposition was done with Ga and N rich conditions in an ultra-high vacuum. The N was cracked with microwaves to create a plasma. The following parameters for the different samples can be seen in the table 3.2. Here T_S is the temperature of the substrate and T_{Ga} is the temperature of the Ga source for deposition. The parameter T_{FS} is the temperature of the samples getting flashed to remove the O layer on the surface of the sample. t_{FS} is the time used to flash the sample $<$ 1000 °C. Here the samples marked with * are the samples where they got flashed in the deposition chamber, else they were flashed in the loading chamber except for samples 1 and 2. The deposition time for all samples was around 3 hours.

Table 3.2. *Deposition parameters of GaN.*

Sample	Substrate	T_S [°C]	Power [A]	T_{Ga} [°C]	t_{FS} [s]	thickness [nm]
1	Si(100)	25	–	950	–	≈ 100
2	Si(100)	650	2	950	–	≈ 100
3	Si(100)	650	2	950	10	≈ 100
4*	Si(100)	650	2	970	10	≈ 100
5*	Si(100)	710	3	970	10	≈ 100
6*	Si(100)	725	3.1	970	10	≈ 100
7*	Si(100)	760	3.7	970	10	≈ 100
8	Mica	550	1	970	–	–
9	Mica	600	1.5	970	–	–
10	Mica	650	1.9	970	–	–
11	Mica	700	2.8	970	–	–
12	Mica	750	3.7	970	–	–
13	Mica	800	4.6	970	–	–
14	Mica	850	5.7	970	–	–
15	Mica (small)	650	1.9	970	–	–
16	Mica (small)	700	2.8	970	–	–
17	Mica (small)	750	3.7	970	–	–
18	Mica (small)	800	4.6	970	–	–
19	Mica (small)	770	3.5	970	–	–
20	Mica (small)	770	3.5	970	–	–
21	Mica (small)	780	4.0	970	–	–
22	Mica (small)	780	4.0	970	–	–

3.3 Optical Microscope

The Optical microscope from Zeiss was used with the AxioCam MRc camera and the SMC 2009 controller. Bright field with reflective light and transmitted light was used to examine the surface samples. A magnification of ×2.5, ×10, ×20 and ×50 was used for all the samples.

3.4 Atomic Force Microscopy

The MDT-Ntegra atomic force microscope (AFM) was used to take images of the surface. The surface roughness of the different samples was investigated using the semi-contact mode. The tip parameters that were used are shown in table 3.3.

Table 3.3. *Cantilever parameters.*

Spring constant $\left[\frac{N}{m}\right]$	Resonant frequency [kHz]	Model
1.45 - 15.1	87 - 230	NSG01
17 - 34	230 - 380	ScanSense
3.5 - 6	77 - 114	ScanSens

For roughness of the samples images of 3×3 μm were made to get the most accurate measurements.

3.5 Photoluminescence Spectroscopy

Photoluminescence spectroscopy was done using a machine built by Professor Kjeld Pedersen. The setup uses a UV diode with a wavelength of 280 nm, which leads to a filter that lets it hit the sample. The light is detected in a spectrometer through an optical fibre. The input filter is a short pass filter, and the filter for detection is a long pass filter, which both have a wavelength of 300 nm. All the measurements were done at room temperature. The parameters that are used for photoluminescence are shown in table 3.4.

Table 3.4. *Parameters for measurements.*

Parameter	Value
Detector chip	-40 °C
Output slit size	1000 μm
Input slit size	500 μm
Exposure time	0.2 s
Accumulations	60
Accumulation cycle time	1 Hz
DAC	100

3.6 X-Ray Diffraction

The Empyrean X-ray diffractometer machine from PANalytical was used to make X-ray diffraction (XRD) spectra for the samples on Si(100). All samples were rotated while taking the measurements, and all the samples were taken from 0 to 80 degrees.

3.7 Assembly

3.7.1 MPTS Assembly

The method for assembly of the samples was inspired by Boden, C. A. et al.[25] and Tingting, Y. et al.[31]. Before the samples were used, they were rinsed with acetone and isopropanol, then dried with N_2. Different parameters were then changed to get the best possible result. The different parameters that were changed were the time the sample spent in the ozone and time in the desiccator. The various times are shown in table 3.5. The try where there is a * was the one that got MPTS deposited directly on the surface.

Table 3.5. *The different parameters changed to assemble the two thin films.*

Try	Assembly sample	Ozone time [hour]	Vacuum time [hour]	MPTS/Toluene mix	Weight
1	GaN 20 and Au 1	$\approx 1/2$	≈ 1	1/3	–
2	GaN 20 and Au 1	≈ 1	≈ 2	1/3	–
3	GaN 21 and Au 2	≈ 3	≈ 3	1/3	–
4	GaN 21 and Au 2	≈ 2	≈ 3	1/3	Yes
5	GaN 21 and Au 2	≈ 24	≈ 24	1/3	Yes
6*	GaN 21 and Au 2	≈ 24	–	–	Yes
7	GaN 21 and Au 2	≈ 24	≈ 24	1/1	Yes

For the desiccator treatment of try number 1, the sample was left there for around 5 minutes after the vacuum pump was turned off. For the second try and afterwards, the vacuum pump

was on for the whole vacuum time. After the ozone treatment and the desiccator treatment, the assembled sample was baked in an oven at 100°C for 1 hour, with a weight on top of the samples.

3.7.2 Silver Epoxy Assembly

Samples GaN 21 and Au 2 were first cleaned with acetone and isopropanol and then dried with N_2. They were then assembled with silver epoxy from Chemtronics[32]. The sample sandwich was baked in an oven for 70°C for 1 hour, with weight on top. 24 hours after the sample was baked, it was placed in a beaker with Tetrahydrofuran (THF) and left there overnight.

3.7.3 Tape Lift-off Assembly

GaN sample 22 and Au sample 3 were cleaned with acetone and isopropanol, and then dried with N_2. Adhesive tape was used for GaN lift-off. This was done 2 more times on the GaN of the first adhesive tape lift-off from the sample. The GaN on the first adhesive tape was placed in a beaker with isopropanol in an ultrasonic bath until everything came off. The GaN flake was then deposited on the Au sample, and left to dry.

3.8 COMSOL Simulation

To heat the muscovite mica samples, a Si(100) wafer was placed underneath to create a heating element. This is done since mica is an insulating material. Therefore the temperature difference is important to look at for the whole sample. For simulations, the program COMSOL Multiphysics[1] (version 6.2) was used. The heat distribution from Si(100) to muscovite mica was simulated with two different geometries for the two samples of different sizes. The geometries are shown in Figure 3.1. where both samples have a Si(100) sample with the size of $10 \times 35 \times 0.5$ mm.

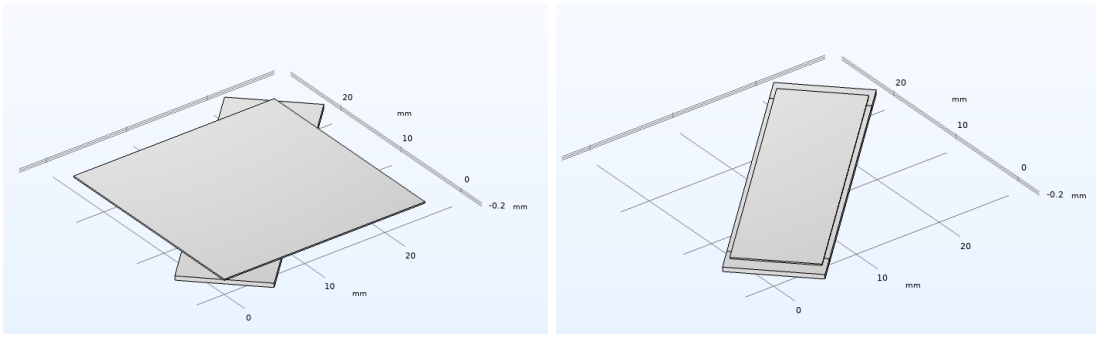

(a) *25 × 25 × 0.15 mm* **(b)** *9 × 32 × 0.15 mm*

Figure 3.1. *The two different muscovite mica samples.*

For the simulation, there was made a time-dependent study, where thermal conductivity (k), density (ρ) and heat capacity at constant pressure (C_p) are from the two materials. The simulations' surroundings were held at a constant temperature of 293.15 K. The surface-to-ambient radiation was defined to be the muscovite mica sample where the surface emissivity (ε) was from the material and the ambient temperature at 293.15 K. Then one end of the sample was heated in a time from 0 min to 1 min with a time step of 0.01 min. This was done for temperatures from 823.15 K to 1123.15 K with a temperature step of 50 K.

Results 4

4.1 Grown Au Surface

Several Au surfaces were grown on a quartz glass substrate, where optical images and AFM images were taken to examine the surface. These thin films were grown to be around 50 nm in thickness.

4.1.1 Optical and AFM Imaging

Sample number 1 of the grown Au on quartz glass is shown in figure 4.1. For figure 4.1a the magnification was ×10 and shows a few visible imperfections on the surface. For figure 4.1b the magnification was ×20, where it shows the surface with transmitted light, to better see the imperfections.

Different AFM images were taken of the Au surfaces to examine the roughness of the surface. For sample 1, the roughness depends on the place of the sample. Some areas on the sample have more Au islands and other places are more smooth, as observed in figure 4.1c. In table 4.1a the roughness of sample 1 can be observed and the average roughness is around 2.3 nm.

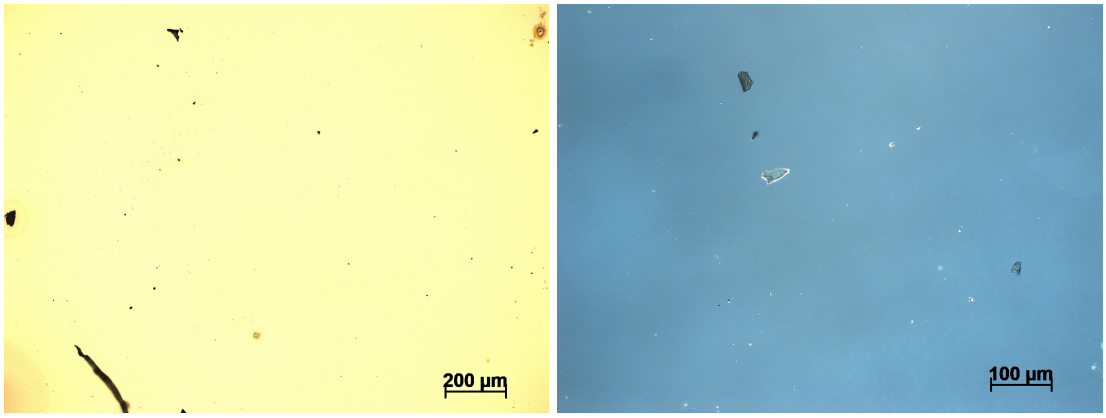

(a) **(b)**

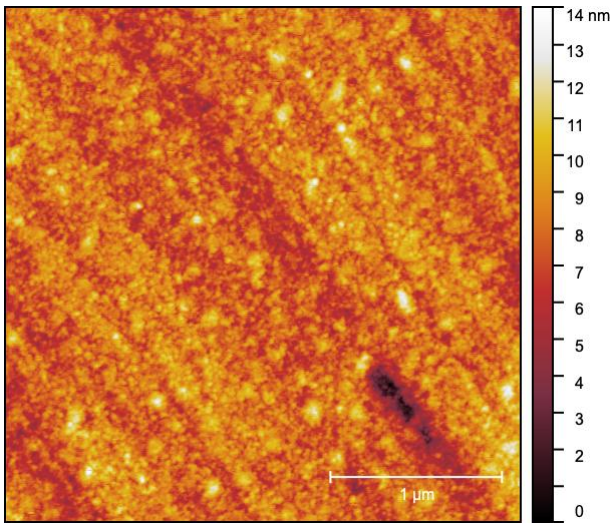

(c)

Figure 4.1. *Sample 1, Au surface on quartz glass without binding material between Au and quartz glass taken in an optical microscope and AFM. Here* ***(a)*** *is taken with a magnification of ×10 and* ***(b)*** *is with a ×20 magnification and with transmitted light.* ***(c)*** *is the AFM image of the surface.*

Sample 2 of the Au samples is shown in figure 4.2. Here the Au has a homogeneous surface with a few imperfections. This is also observed in the image taken with transmitter light, which shows the surface to be blue. The AFM image shows many grains spread over the surface, with an average roughness of 1.7 nm, shown in table 4.1b.

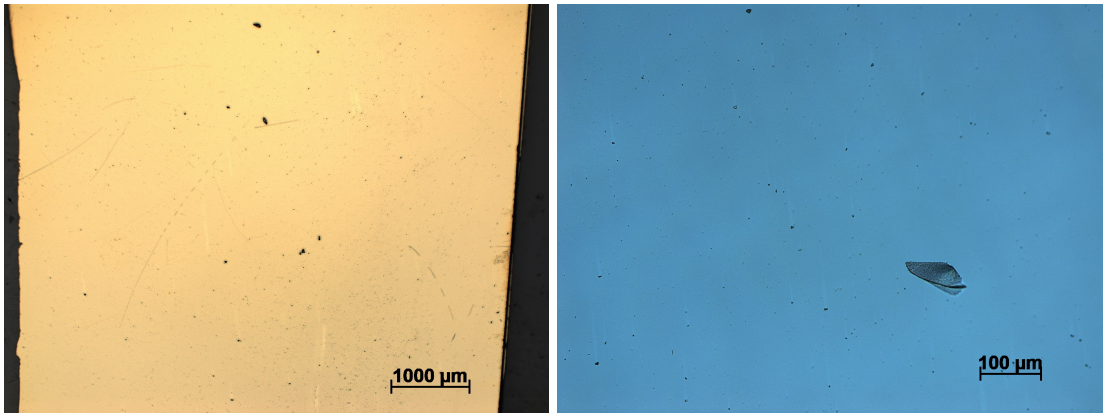

(a) **(b)**

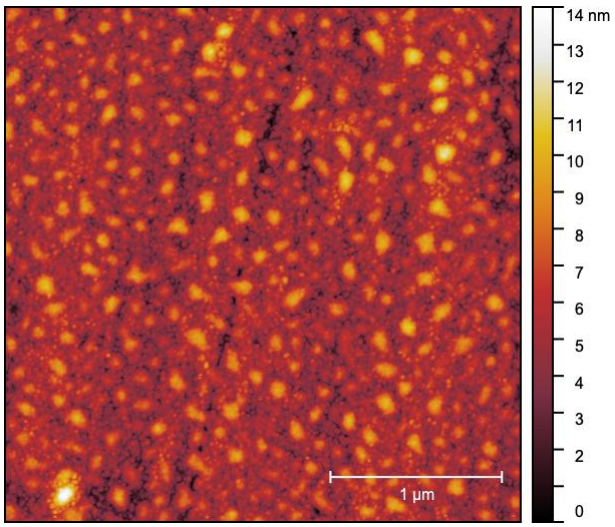

(c)

Figure 4.2. *Sample 2, Au surface on quartz glass without binding material between Au and quartz glass taken in an optical microscope and AFM. Here* ***(a)*** *is taken with a magnification of ×10 and* ***(b)*** *is with a ×20 magnification and with transmitted light.* ***(c)*** *is the AFM image of the surface.*

Samples 3 and 4 were grown in the deposition chamber at the same time. Sample 4 is shown in Appendix 7. Figure 4.3 shows sample 3 with a homogenous surface and one big scratch. The image of the transmitted light shows a few grains of imperfections throughout the surface. From the AFM image, the surface shows some big grains on top of the surface. This makes the average roughness 4.0 nm, shown in table 4.1c.

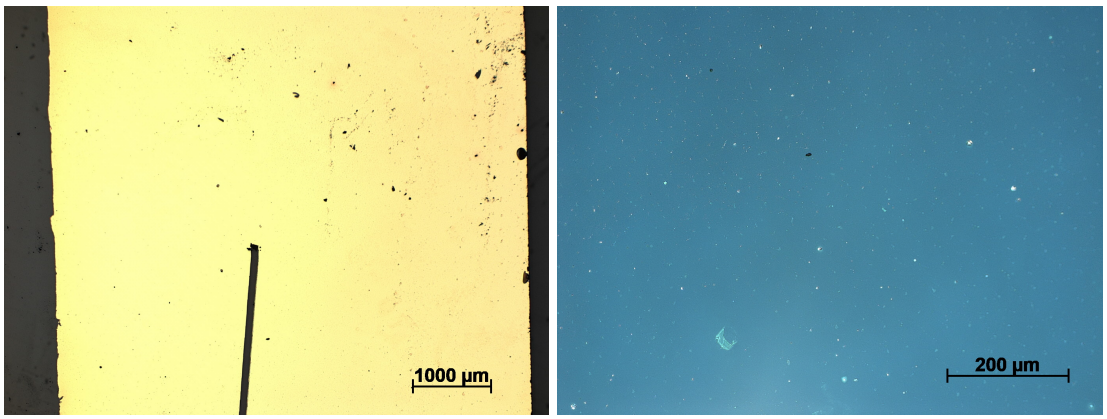

(a) **(b)**

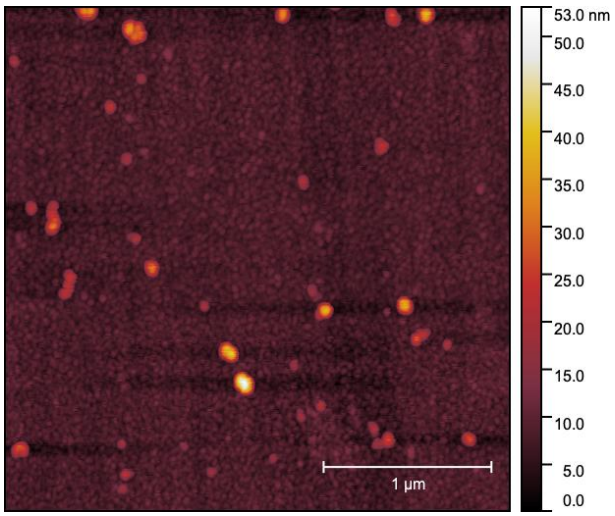

(c)

Figure 4.3. *Sample 3, Au surface on quartz glass without binding material between Au and quartz glass taken in an optical microscope and AFM. Here* ***(a)*** *is taken with a magnification of ×10 and* ***(b)*** *is with a ×20 magnification and with transmitted light.* ***(c)*** *is the AFM image of the surface.*

Table 4.1. *Roughness of the Au surface on different wafer places taken from the 3×3 images.*

(a) *Sample 1*

Image number	RMS [nm]
1	1.4
2	1.3
3	10.3
4	1.2
5	1.3
6	1.1
7	1.4
8	1.2
9	2.5
10	1.4
Average	2.3

(b) *Sample 2*

Image number	RMS [nm]
1	1.4
2	1.5
3	1.8
4	4.0
5	1.5
6	1.3
7	1.5
8	1.1
9	1.3
10	1.1
Average	1.7

(c) *Sample 3*

Image number	RMS [nm]
1	2.0
2	2.4
3	3.7
4	1.9
5	2.8
6	2.9
7	4.0
8	5.5
9	8.2
10	6.1
Average	4.0

(d) *Sample 4*

Image number	RMS [nm]
1	0.9
2	0.6
3	0.5
4	0.9
5	1.0
6	0.6
7	0.8
8	0.6
9	0.6
10	0.7
Average	0.7

4.2 Grown GaN

The growing process for GaN was done with substrates of Si(100) and muscovite mica. For all samples, the optical images were taken with reflected light. Optical images, AFM images and photoluminescence measurements were made to look at the surface and to check if the grown GaN had the ideal structure for its band gap energy. The band gap energy was calculated by equation (4.1)

$$E_g = \frac{hc}{\lambda}, \tag{4.1}$$

where E_g is the band gap energy, h is the Planck constant, c is the speed of light and λ is the wavelength.

Only for the GaN on Si(100) samples, XRD measurements were made, to check the thin film structures.

4.2.1 Optical, AFM and Photoluminescence For GaN on Si(100)

The first test sample that was made can be seen in Appendix 10. The other results of different temperatures on Si(100) are shown in Appendix 8. Sample 1 is seen in figure 4.4 where the surface of GaN on a Si(100) substrate can be observed. Here, figure 4.4a is the surface with a magnification of ×50, and figure 4.4b is at the edge of the GaN surface with the same magnification. The GaN is grown to be around 100 nm in thickness. The surface shows a homogeneous layer with a few imperfections.

AFM images were made to check the roughness of the different samples. In figure 4.4c the image of a 3×3 μm is shown for sample 1. A lot of small grains can be observed on the surface. Table 4.2a shows the roughness of the surface from different places of sample 1 with the grown GaN. The average roughness of this sample is around 2.2 nm.

From figure 4.4d, the photoluminescence measurement is shown for sample 1. Three maxima can be observed in the graph. The first maximum is around 280 nm, which is the pump light leaking through the pass filter. This maximum can be observed again around 560 nm which is the second-order diffraction of the monochromator grating. The very small maximum from the black box is around 367 nm, which gives a band gap energy of 3.38 eV.

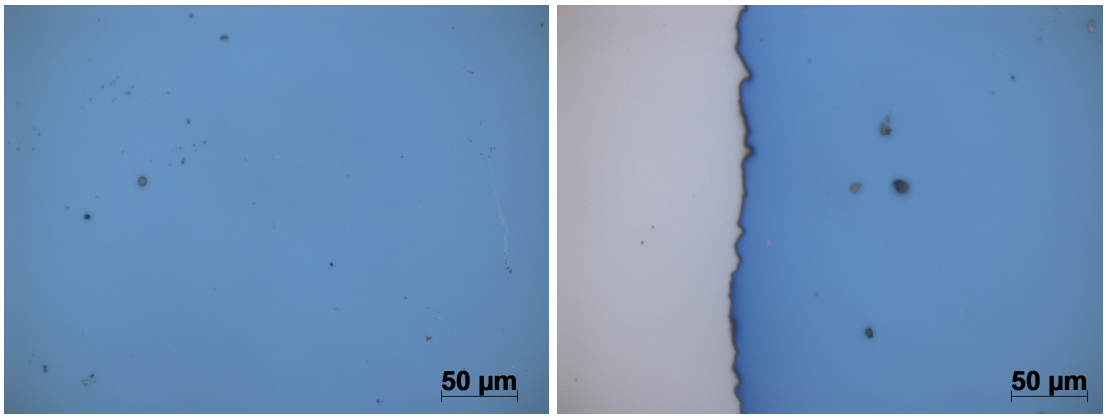

(a) **(b)**

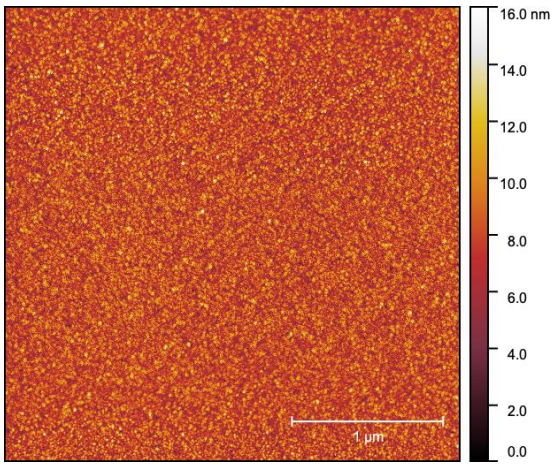

(c)

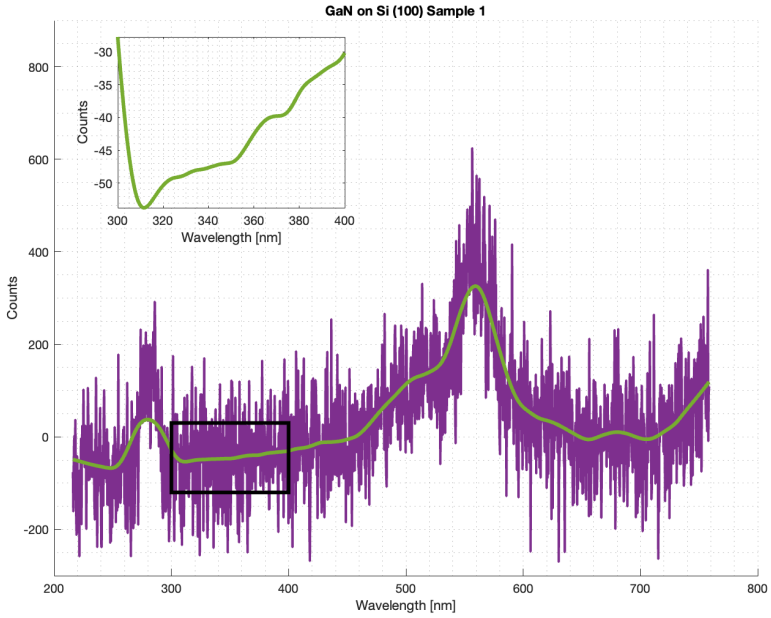

(d)

Figure 4.4. *Grown GaN on a Si(100) substrate where* ***(a)*** *is the optical image of the middle of the surface and* ***(b)*** *is the edge of the sample, both with a magnification of ×50.* ***(c)*** *is the AFM image.* ***(d)*** *is the photoluminescence measurement where the green line is the smoothened data of the purple raw data. The zoomed part on the graph is from the black box.*

The optical image for sample 5 shows a homogeneous surface with a circular formation of grains and a yellow circle around the grains. The rest of the sample also shows a homogeneous surface. The AFM image of this sample shows many closely packed grains, which gives an RMS value of 15.3 nm. Photoluminescence of this sample shows a more defined maximum at around 351 nm, giving a band gap energy of 3.53 eV. It also shows a broad maximum starting from around 500 nm to around 800 nm which indicates a defect in the crystal.

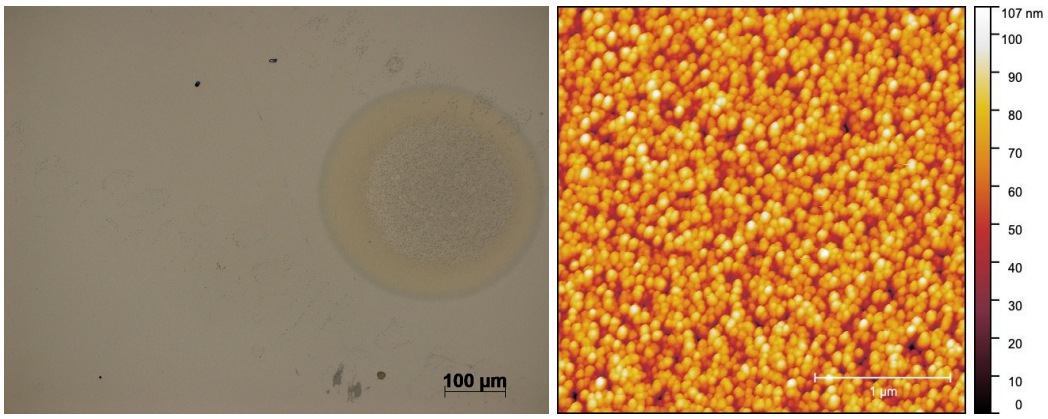

(a) **(b)**

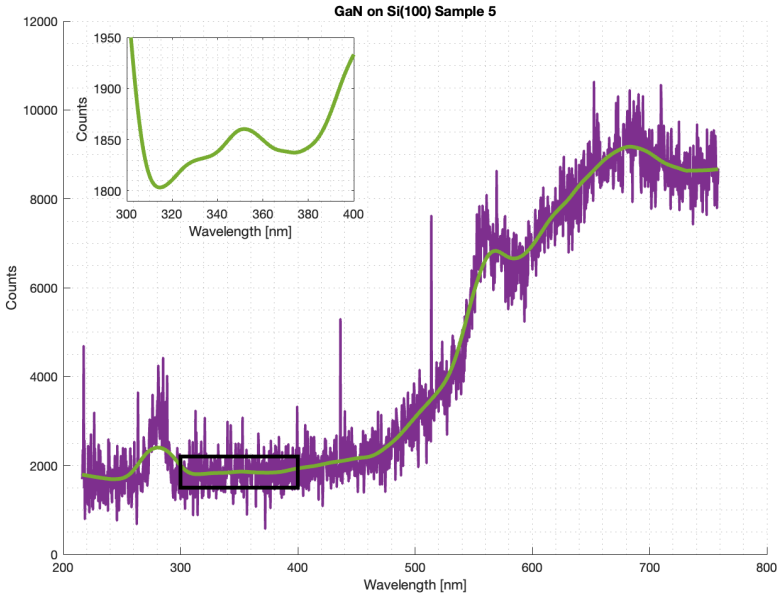

(c)

Figure 4.5. *Grown GaN on a Si(100) substrate where* ***(a)*** *is the optical image of the surface with a magnification of* $\times 50$ *and* ***(b)*** *is the AFM image.* ***(c)*** *is the photoluminescence measurement where purple is the raw data, green is the smoothed data and the zoomed graph is from the black box on the original graph.*

For sample 7, the surface was different depending on the wafer position. The two different positions are shown in figure 4.6a and 4.6b, where it is the sample in the middle and one of the edges, respectively. The middle of the surface is homogeneous without visible grains. The surface on the edge is of different colours and shows many grains. The grains in the AFM image are closely packed, giving an RMS of 18.5 nm. The photoluminescence of this sample shows only one very broad maximum at around 610 nm, which is a strong defect of luminescence. The maximum which is examined is the one from the black box. Here the maximum is small and at around 370 nm. This gives a band gap energy of 3.35 eV.

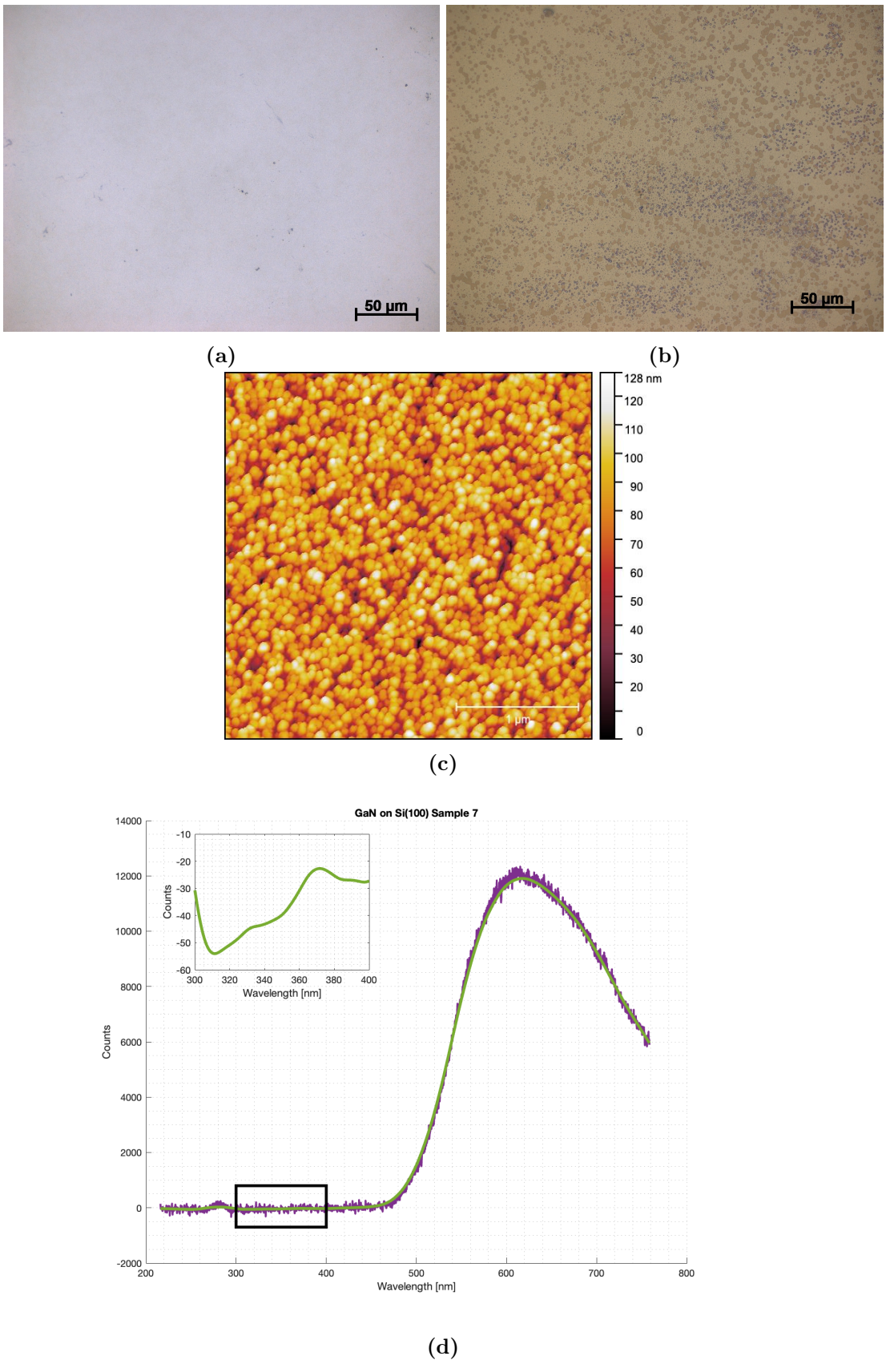

Figure 4.6. *Grown GaN on a Si(100) substrate where* ***(a)*** *is the optical image of the surface with a magnification of ×50 on the middle of the sample and* ***(b)*** *is the optical image on the edge of the sample with the same magnification.* ***(c)*** *is the AFM image.* ***(d)*** *is the photoluminescence measurement from the middle of the sample, where purple is the raw data, green is the smoothed data and the zoomed graph is from the black box on the original graph.*

Table 4.2. *Roughness of the grown GaN on Si(100) substrate taken from the 3×3 μm AFM images*

(a) *Sample 1*

Image number	RMS [nm]
1	1.6
2	2.9
3	3.0
4	1.6
5	2.0
6	2.0
7	2.1
8	2.1
9	2.3
10	2.8
Average	2.2

(b) *Sample 2*

Image number	RMS [nm]
1	24.2
2	25.1
3	24.7
4	25.0
5	23.7
6	24.1
7	22.3
8	22.5
9	23.4
10	23.7
Average	23.9

(c) *Sample 3*

Image number	RMS [nm]
1	27.2
2	26.0
3	27.3
4	24.3
5	22.6
6	22.6
7	26.4
8	26.7
9	26.8
10	25.4
Average	25.5

(d) *Sample 4*

Image number	RMS [nm]
1	22.1
2	12.9
3	12.0
4	12.1
5	13.6
6	14.5
7	15.5
8	18.2
9	15.2
10	18.8
Average	15.5

(e) *Sample 5*

Image number	RMS [nm]
1	14.2
2	14.2
3	13.3
4	13.9
5	16.6
6	15.4
7	17.6
8	18.2
9	16.4
10	13.3
Average	15.3

(f) *Sample 6*

Image number	RMS [nm]
1	11.9
2	11.3
3	15.3
4	12.3
5	13.3
6	12.4
7	14.0
8	13.8
9	13.4
10	14.9
Average	13.3

(g) *Sample 7*

Image number	RMS [nm]
1	16.6
2	17.6
3	18.2
4	17.7
5	17.1
6	18.0
7	18.1
8	17.5
9	20.5
10	23.3
Average	18.5

XRD

The following articles were used to analyse all the data shown in this section. The article of Nasr, F. B. et al. (2016)[33] was used for some of the GaN peaks. Then Saron K. M. A. et al. (2021)[34] was used for both the GaN and Si(100) peaks. To ensure that the peak for Si(100) is at around 69.4, the article from Kumar G. et al. (2022)[35] was used. Articles from Masilamani, G. et al. (2012)[36], Kang, B. et al. (2011)[37] and Martínez-Ara, L. A. et al. (2019)[38] were

used to ensure that the peaks in the XRD data were indeed the different GaN and Si structures. XRD data for samples 2 to 4 and 6 are displayed in Appendix 8.1.1. The XRD data shows that for samples 3 to 7 GaN has an orientation of GaN(002), GaN(200) and GaN(112). Orientations of GaN(100) and GaN(101) are observed for samples from 4 to 7. Sample number 5 from figure 4.7b shows a peak for GaN(002) with nearly the same intensity as the Si(100) peak.

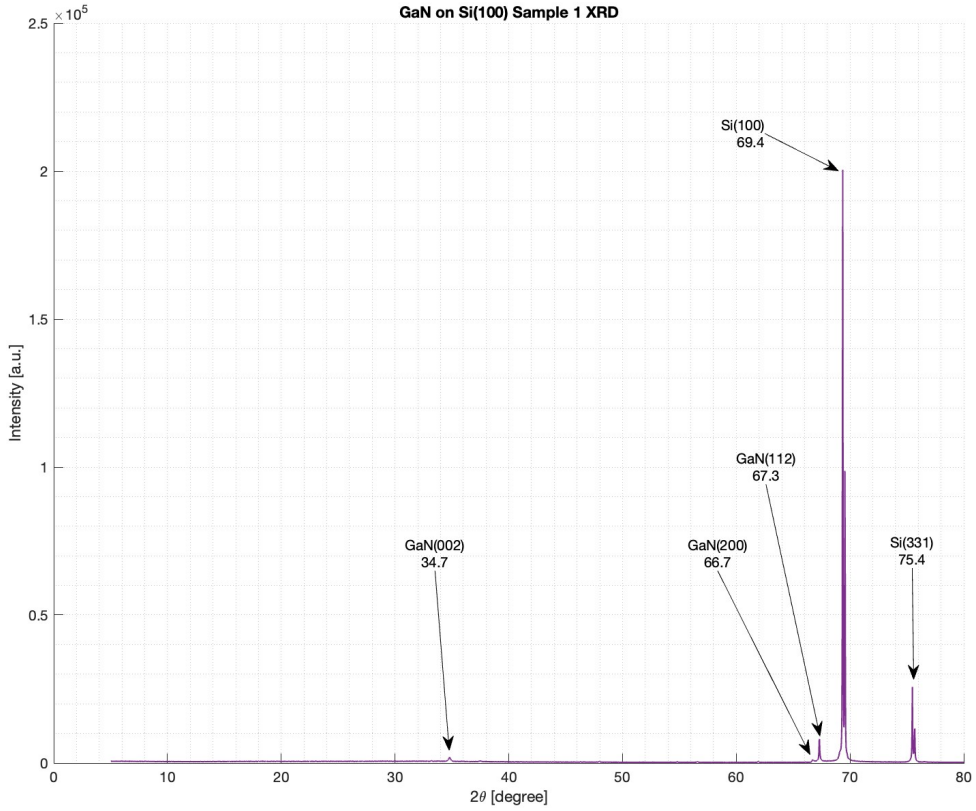

(a)

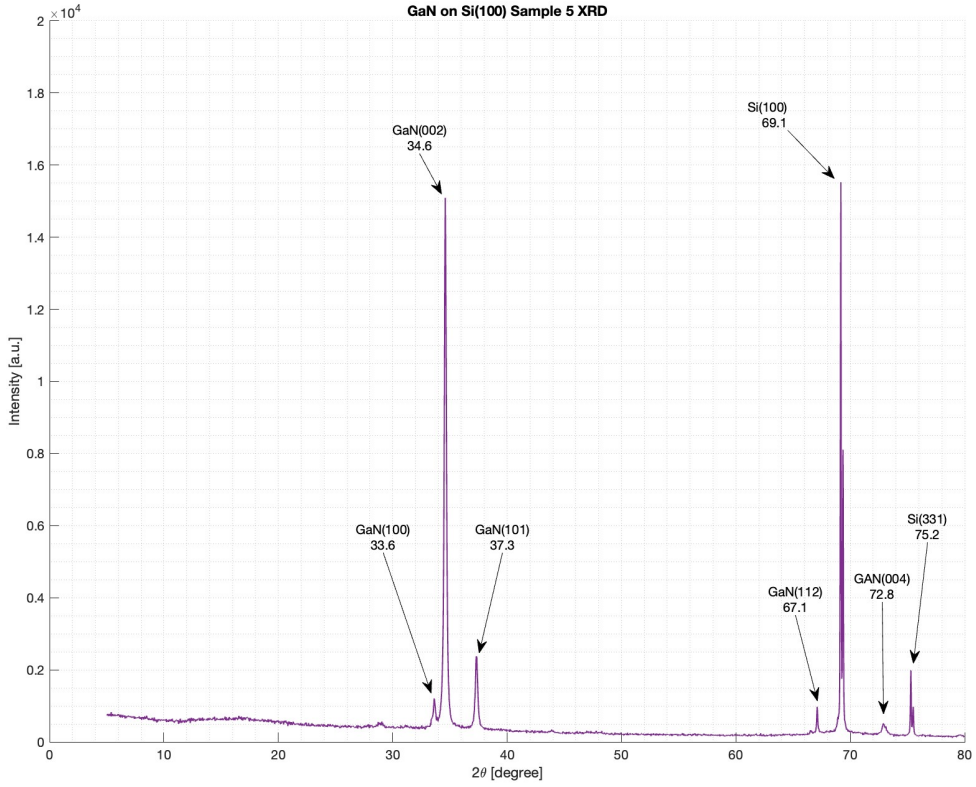

(b)

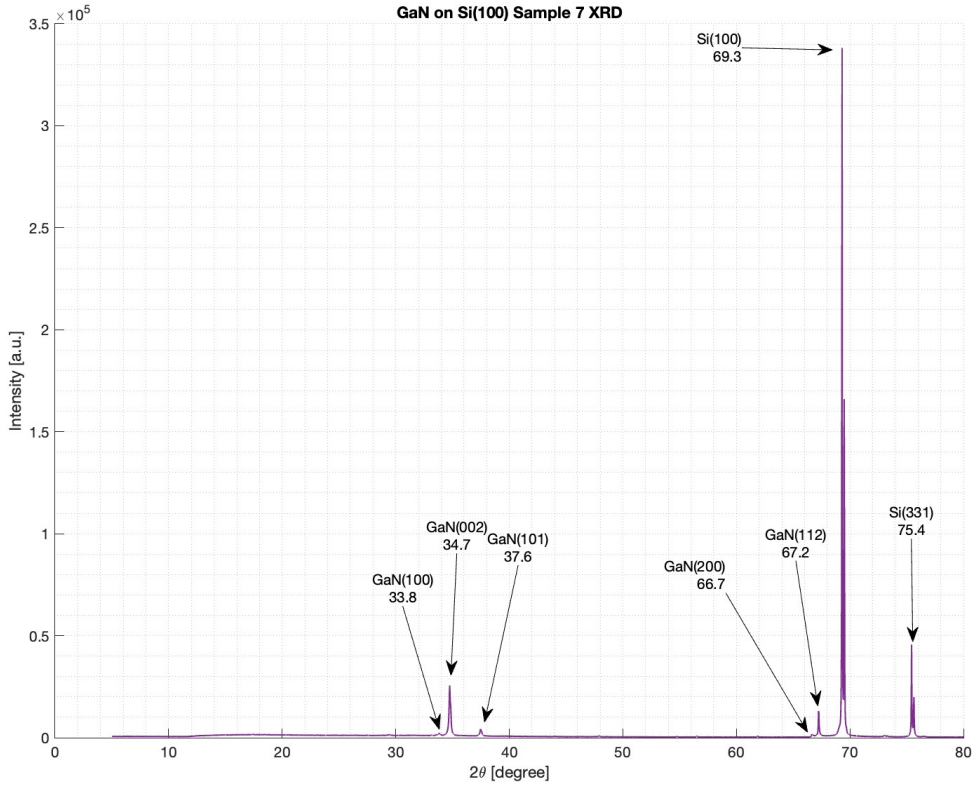

(c)

Figure 4.7. *The XRD data is shown with its defined peaks of the different crystal orientations for both the GaN and Si(100). Here* ***(a)*** *is sample 1,* ***(b)*** *is sample 5 and* ***(c)*** *is sample 7.*

4.2.2 Optical, AFM and Photoluminescence for GaN on Muscovite Mica

The results for samples 8, 12 and 14, where GaN was deposited on mica are displayed in this section. The rest of the results for this type of substrate are shown in Appendix 8.2.

Sample 8 is shown in figure 4.8, where the optical image shows a homogeneous surface with few imperfections at the mica plate boundaries. The AFM image of this sample shows a lot of small grains and gives an RMS value of 2.0 nm, which is displayed in table 4.3a. For the photoluminescence, there can be observed 2 distinct maxima. This can be observed in every photoluminescence measurement, since this is the pump light leaking through the pass filter, at 280 nm and again at 560 nm. The maximum at around 560 nm is also broad which is defects in the crystal. For this sample, there is no distinct maximum from the black box.

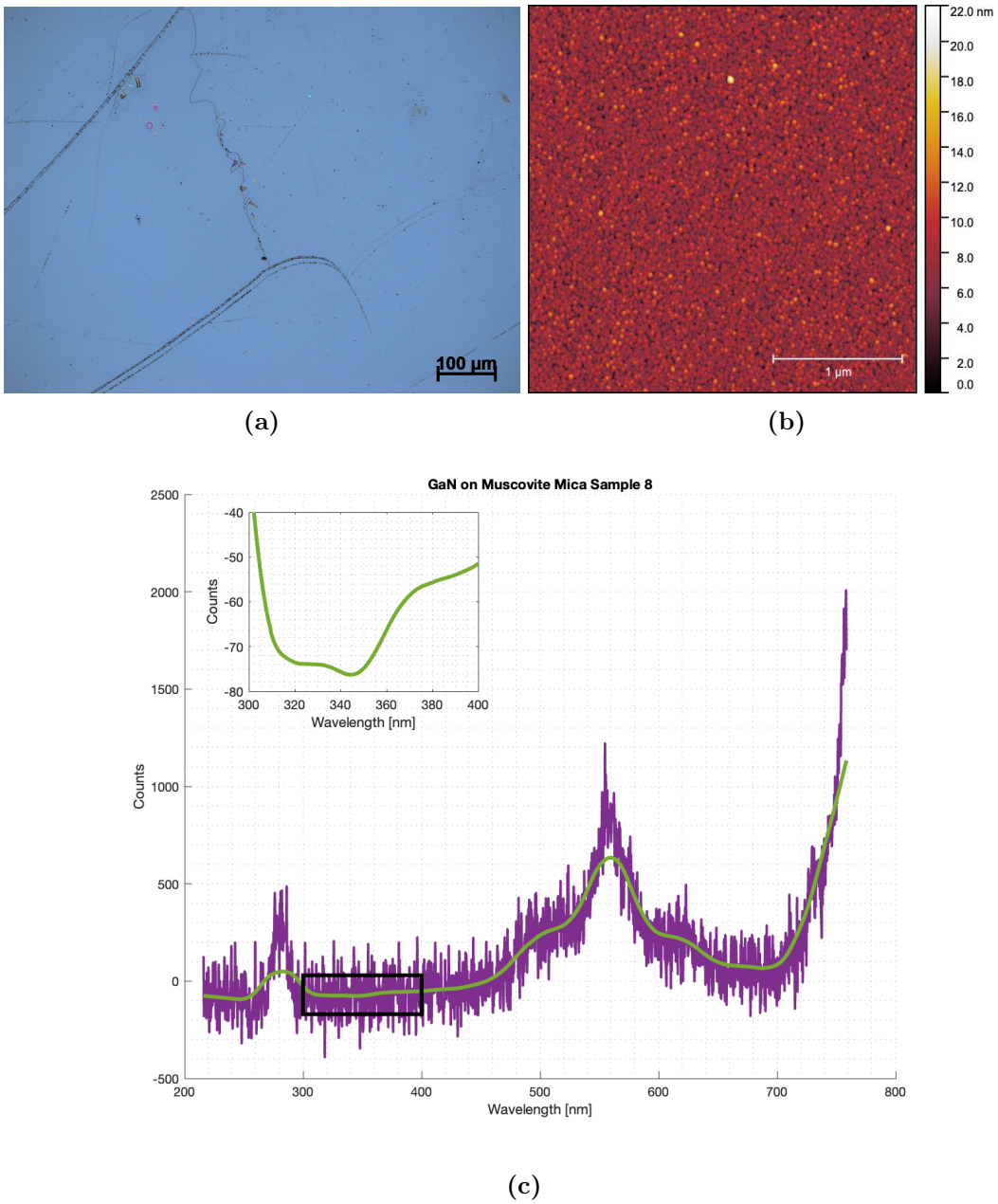

Figure 4.8. *Grown GaN on a muscovite mica substrate where* ***(a)*** *is the optical image of the surface with a magnification of* $\times 20$ *and* ***(b)*** *is the AFM image.* ***(c)*** *is the photoluminescence measurement where purple is the raw data, green is the smoothed data, and the zoomed graph is from the black box on the original graph.*

The optical image for sample 12 shows a homogeneous thin film with few imperfections, which are some circles in the image. For the AFM image, bigger grains can be observed, making the surface rougher. The RMS value for this surface is, therefore, around 6.0 nm. The photoluminescence for this sample shows a distinct maximum in the graph in the black box. The maximum here is around 372 nm and 391 nm, giving a band gap energy of 3.33 eV and 3.17 eV, respectively.

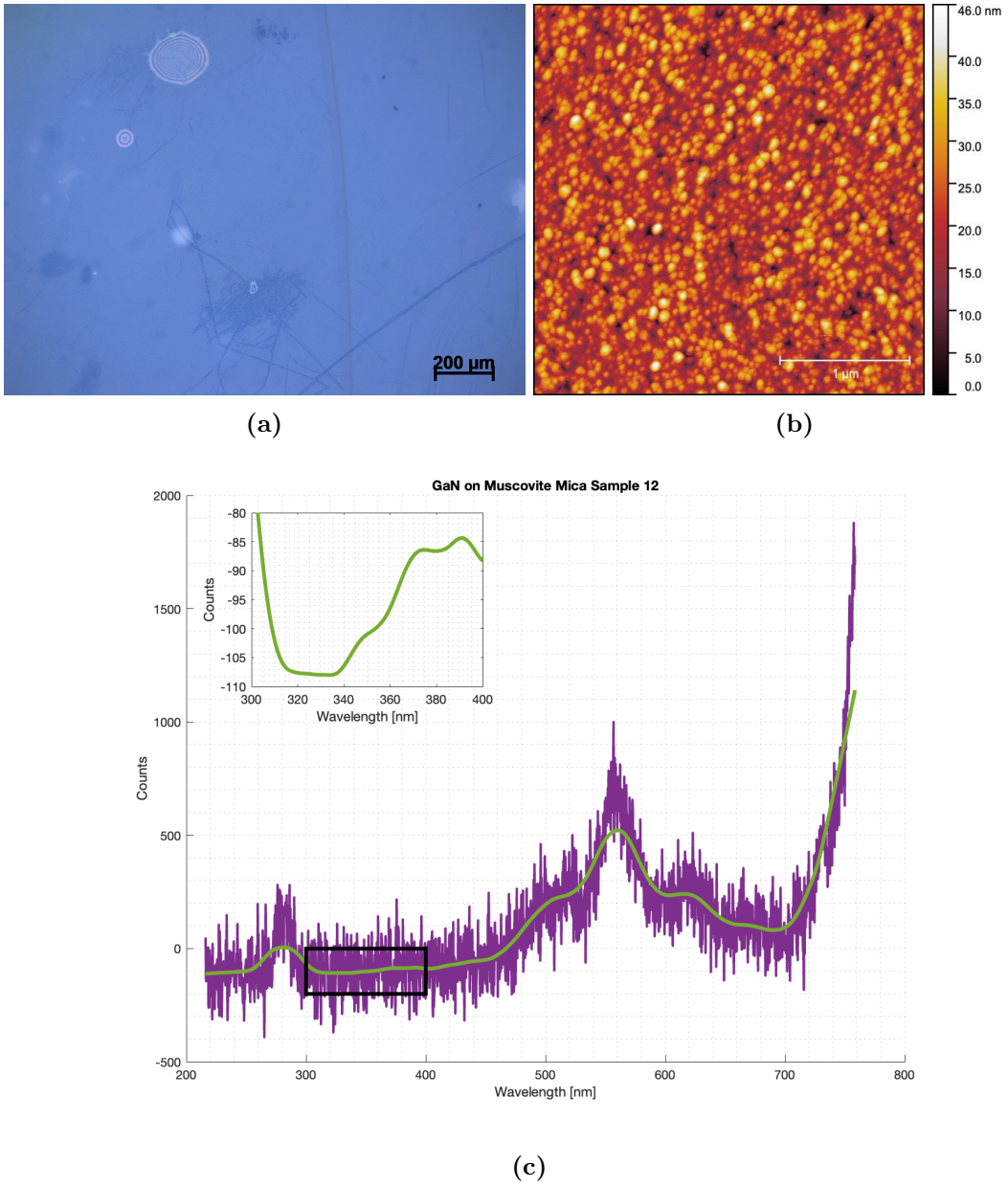

Figure 4.9. *Grown GaN on a muscovite mica substrate where* ***(a)*** *is the optical image of the surface with a magnification of* $\times 10$ *and* ***(b)*** *is the AFM image.* ***(c)*** *is the photoluminescence measurement where purple is the raw data, green is the smoothed data, and the zoomed graph is from the black box on the original graph.*

Sample 14 only shows two optical images of the surface and a photoluminescence measurement. The optical images show two different places on the surface. Here, the heat from the heat source destroyed one end of the substrate. The substrate and thin film layer are intact in the optical image of the middle of the sample. It shows a uniform surface in the middle

of the wafer. For the photoluminescence measurements, the maximum observed at 300 - 400 nm shows two small maxima. One of the two maxima is at 332 nm, corresponding to a band gap energy of 3.73 eV. The second small maximum is around 371 nm, giving a band gap energy of 3.34 eV.

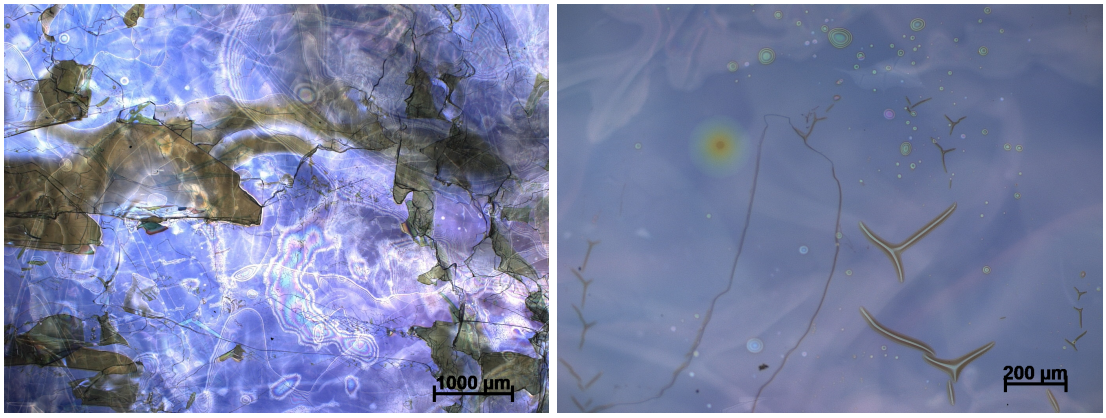

(a) **(b)**

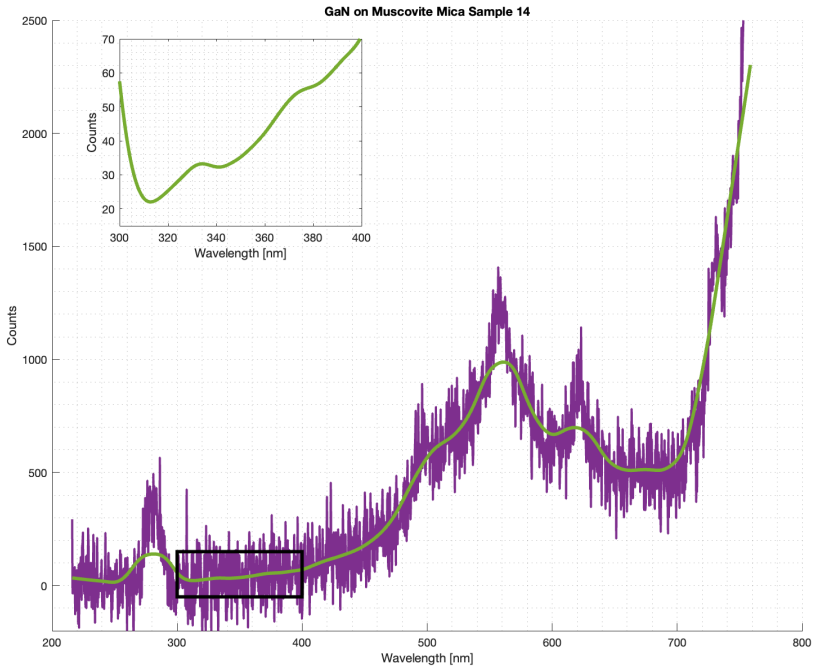

(c)

Figure 4.10. *Grown GaN on a muscovite mica substrate where* ***(a)*** *is the optical image of the surface with a magnification of* $\times 2.5$ *and* ***(b)*** *is another optical image of the surface with a magnification of* $\times 10$. ***(c)*** *is the photoluminescence measurement where purple is the raw data, green is the smoothed data, and the zoomed graph is from the black box on the original graph.*

Table 4.3. *Roughness of the grown GaN on muscovite mica substrate taken from the 3×3 μm AFM images*

(a) *Sample 8*

Image number	RMS [nm]
1	2.4
2	2.2
3	2.1
4	1.9
5	1.9
6	1.9
7	1.9
8	1.8
9	1.9
10	2.0
Average	2.0

(b) *Sample 9*

Image number	RMS [nm]
1	3.0
2	3.3
3	3.2
4	3.2
5	3.0
6	3.2
7	3.3
8	3.1
9	3.4
10	3.4
Average	3.2

(c) *Sample 10*

Image number	RMS [nm]
1	3.4
2	3.6
3	3.5
4	3.6
5	3.5
6	1.8
7	3.4
8	3.7
9	3.9
10	2.1
Average	3.3

(d) *Sample 11*

Image number	RMS [nm]
1	2.3
2	2.3
3	3.2
4	3.3
5	2.9
6	1.5
7	1.7
8	1.9
9	1.8
10	3.1
Average	2.4

(e) *Sample 12*

Image number	RMS [nm]
1	6.0
2	6.2
3	6.2
4	6.2
5	3.9
6	6.1
7	6.3
8	6.4
9	6.3
10	6.3
Average	6.0

(f) *Sample 13*

Image number	RMS [nm]
1	1.0
2	2.5
3	1.1
4	0.9
5	0.9
6	3.0
7	2.9
8	2.7
9	2.9
10	2.9
Average	1.9

(g) *Sample 14*

Image number	RMS [nm]
1	–
2	–
3	–
4	–
5	–
6	–
7	–
8	–
9	–
10	–
Average	–

Small Muscovite Mica Samples

The muscovite mica samples were cut into smaller pieces to ensure that the sample had the same size as the Si(100) wafer underneath the sample. Here samples 15, 20, 21 and 22 are displayed and the rest of the results with this size of substrate are displayed in Appendix 8.2.1.

Sample 15 is shown in figure 4.11, where the optical image shows few imperfections and a homogeneous surface. The AFM image shows many small grains around the surface with

small islands spread over the surface. The measured average RMS value is around 0.4 nm. The photoluminescence measurement shows one broad maximum in the black box of the graph. This maximum is around 363 nm, giving a band gap energy of 3.42 eV.

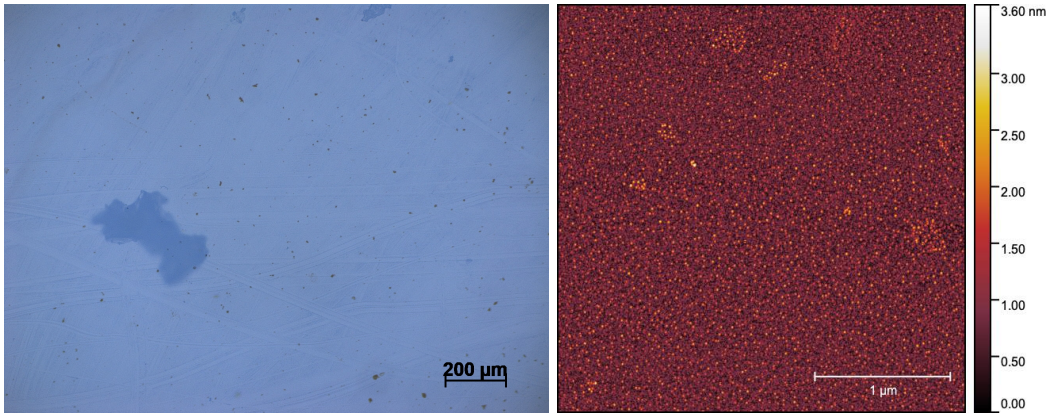

(a) **(b)**

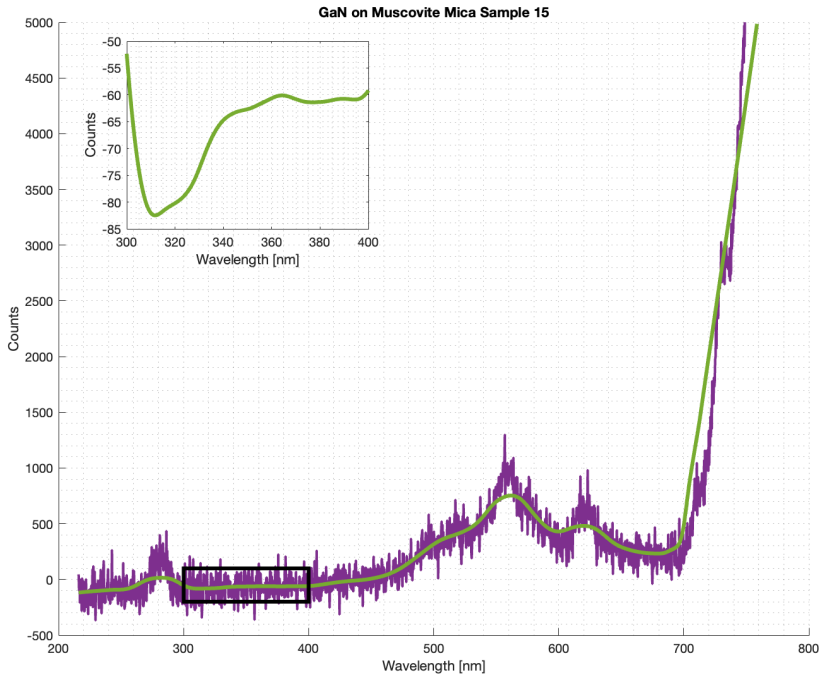

(c)

Figure 4.11. *Grown GaN on a muscovite mica substrate where* ***(a)*** *is the optical image of the surface with a magnification of* $\times 10$ *and* ***(b)*** *is the AFM image.* ***(c)*** *is the photoluminescence measurement where purple is the raw data, green is the smoothed data, and the zoomed graph is from the black box on the original graph.*

Figure 4.12 shows sample 20 where the optical image shows a homogeneous surface with few imperfections. From the AFM image, the grains are small and leave nearly no space between them. This gives an average roughness of about 4.4 nm, as seen in table 4.4f. From the photoluminescence graph, the maximum of interest is small and broad. This maximum is around 356 nm and gives a band gap energy of around 3.48 eV.

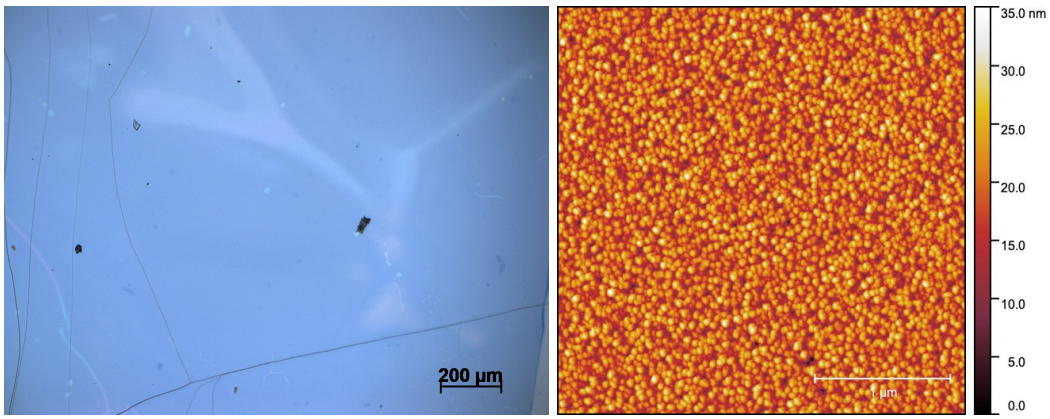

(a) (b)

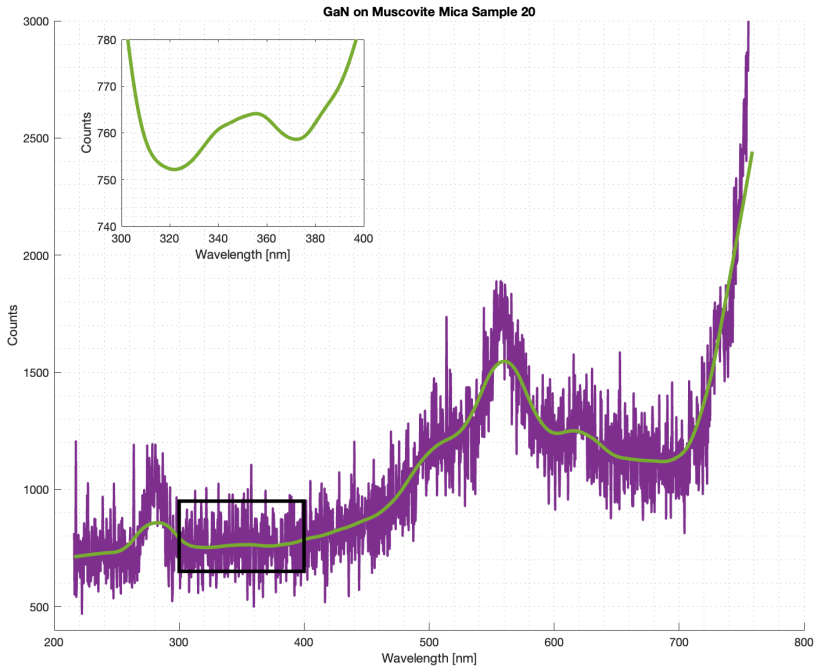

(c)

Figure 4.12. *Grown GaN on a muscovite mica substrate where* ***(a)*** *is the optical image of the surface with a magnification of* $\times 10$ *and* ***(b)*** *is the AFM image.* ***(c)*** *is the photoluminescence measurement where purple is the raw data, green is the smoothed data, and the zoomed graph is from the black box on the original graph.*

The optical image of sample 21 shows a homogeneous surface with some imperfections. There are some bubbles on the surface within a substrate domain. The AFM image shows many grains with some space between specific grains, giving an average roughness of around 4.4 nm. The photoluminescence graph shows the maximum of interest to be around 363 nm and is a broad maximum. This gives a band gap energy of around 3.41 eV.

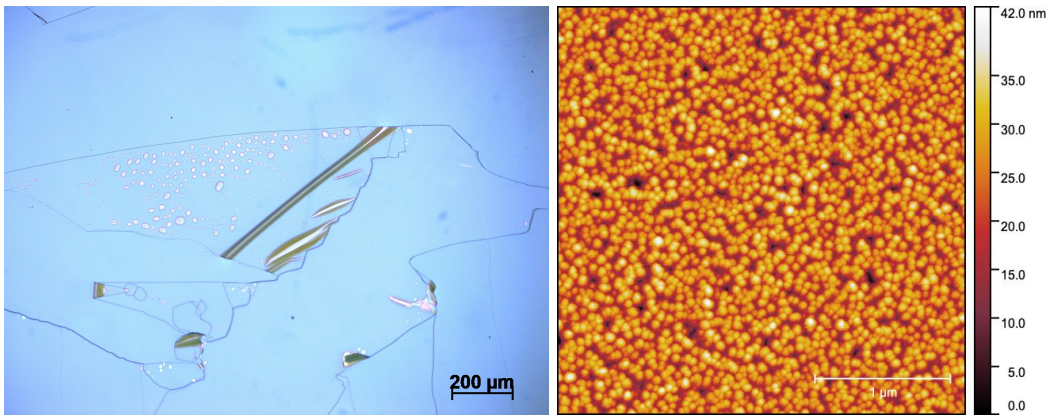

(a) (b)

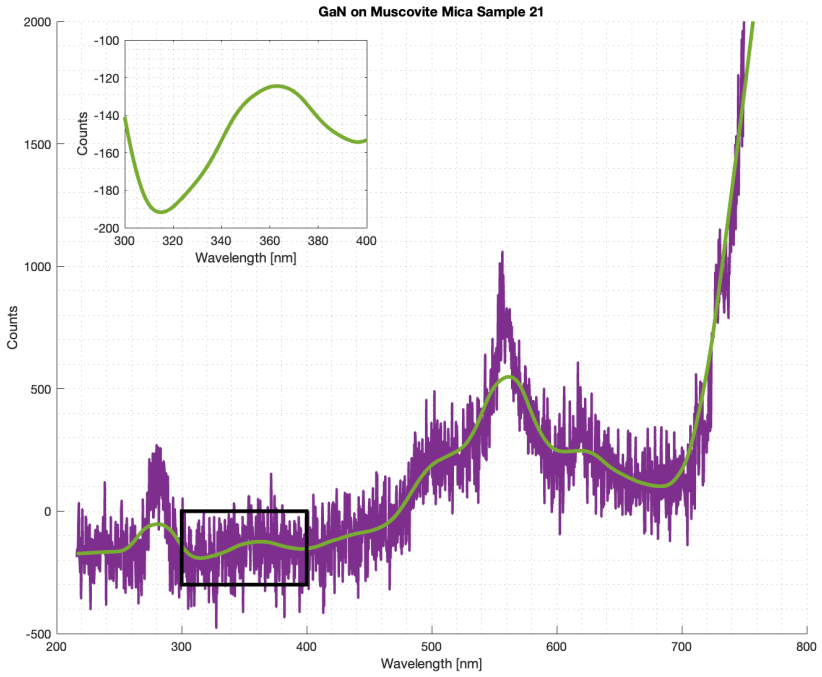

(c)

Figure 4.13. *Grown GaN on a muscovite mica substrate where* ***(a)*** *is the optical image of the surface with a magnification of* $\times 10$ *and* ***(b)*** *is the AFM image.* ***(c)*** *is the photoluminescence measurement where purple is the raw data, green is the smoothed data, and the zoomed graph is from the black box on the original graph.*

For sample 22 the optical image shows many small grains on the surface. Besides the small grains, the surface shows a continuous film on the mica substrate. The AFM image shows many grains with nearly no space in between. There are grains on top of grains which gives an RMS of around 7.7 nm. The photoluminescence graph shows a maximum at the desired place, which is around 350 nm. Thus giving a band gap energy of around 3.54 eV for this thin film.

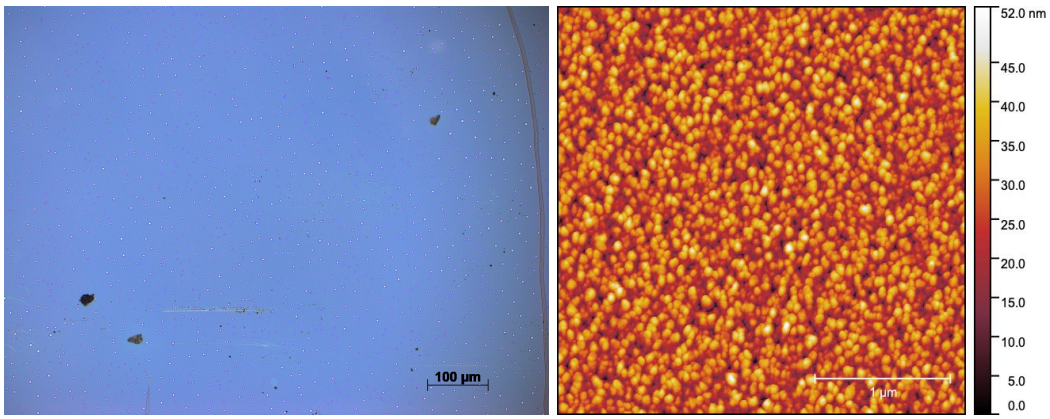

(a) **(b)**

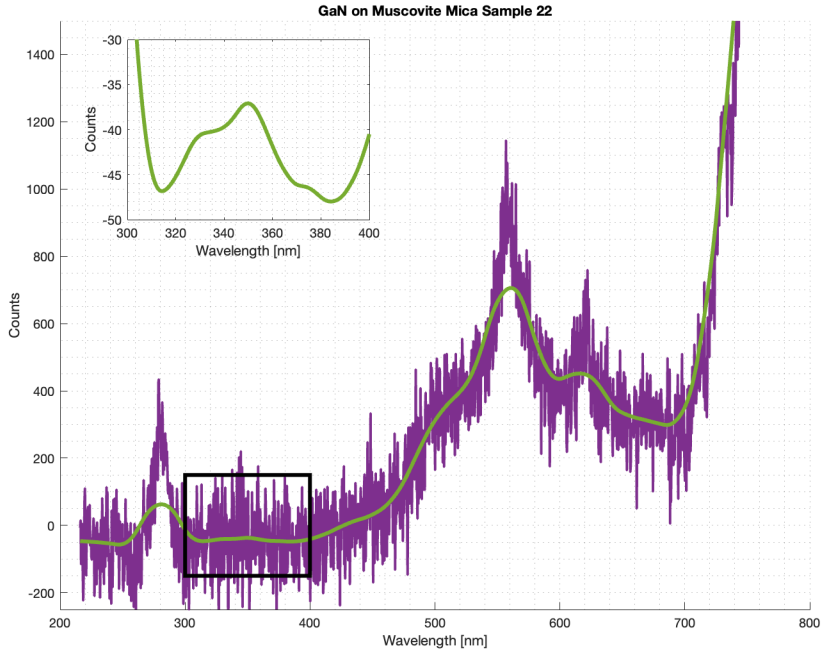

(c)

Figure 4.14. *Grown GaN on a muscovite mica substrate where* ***(a)*** *is the optical image of the surface with a magnification of* $\times 20$ *and* ***(b)*** *is the AFM image.* ***(c)*** *is the photoluminescence measurement where purple is the raw data, green is the smoothed data, and the zoomed graph is from the black box on the original graph.*

Table 4.4. *Roughness of the grown GaN on muscovite mica substrate taken from the 3×3 μm AFM images*

(a) *Sample 15*

Image number	RMS [nm]
1	0.4
2	0.7
3	0.4
4	0.4
5	0.3
6	0.5
7	0.5
8	0.4
9	0.3
10	0.3
Average	0.4

(b) *Sample 16*

Image number	RMS [nm]
1	2.8
2	3.0
3	3.0
4	3.0
5	2.7
6	2.8
7	3.0
8	2.9
9	2.8
10	2.9
Average	2.9

(c) *Sample 17*

Image number	RMS [nm]
1	4.3
2	4.8
3	4.4
4	4.8
5	4.5
6	4.5
7	4.5
8	4.6
9	4.3
10	4.3
Average	4.5

(d) *Sample 18*

Image number	RMS [nm]
1	4.7
2	4.4
3	3.9
4	4.9
5	4.6
6	5.2
7	5.3
8	5.2
9	5.4
10	5.4
Average	4.9

(e) *Sample 19*

Image number	RMS [nm]
1	7.2
2	4.3
3	7.0
4	7.6
5	5.9
6	8.9
7	8.7
8	7.1
9	7.4
10	9.0
Average	7.3

(f) *Sample 20*

Image number	RMS [nm]
1	4.5
2	4.6
3	4.4
4	4.6
5	4.5
6	4.5
7	4.3
8	4.3
9	4.3
10	4.3
Average	4.4

(g) *Sample 21*

Image number	RMS [nm]
1	7.1
2	5.7
3	4.2
4	3.0
5	4.8
6	5.2
7	2.3
8	1.9
9	5.3
10	4.5
Average	4.4

(h) *Sample 22*

Image number	RMS [nm]
1	7.8
2	7.4
3	7.4
4	7.5
5	7.3
6	7.2
7	8.2
8	7.9
9	8.3
10	8.1
Average	7.7

4.3 Heat Distribution In Mica

The heat distribution in muscovite mica was simulated in COMSOL[1] to investigate the heat from Si(100) to muscovite mica. Samples 8 to 18 were simulated to check the temperature difference from one end of the sample to the other end. Here samples 8, 14, 15 and 18 are displayed. The rest of the simulated results are shown in Appendix 9.1.

Figure 4.15 shows sample 8, with the 25 × 25 × 0.15 mm muscovite mica sample. At the

beginning of the simulation, there is one end that is heated. After 1 min, the muscovite mica is heated by the Si(100). It shows that the heat is distributed to the muscovite mica all over the sample where it is connected to the heating element. Figures 4.15c and 4.15d show the same sample, only with a cut through the horizontal. Here it shows that after the 1 minute simulation time, the end where the sample temperature is 550 °C, is evenly distributed from the Si(100) heating element to the mica sample. The middle of the sample shows that the mica sample has little heat distribution outwards through the broader part of the sample. At the end of the sample, the temperature difference is around 180 °C from the heat source place. This trend is shown in all the simulations for mica $25 \times 25 \times 0.15$ mm.

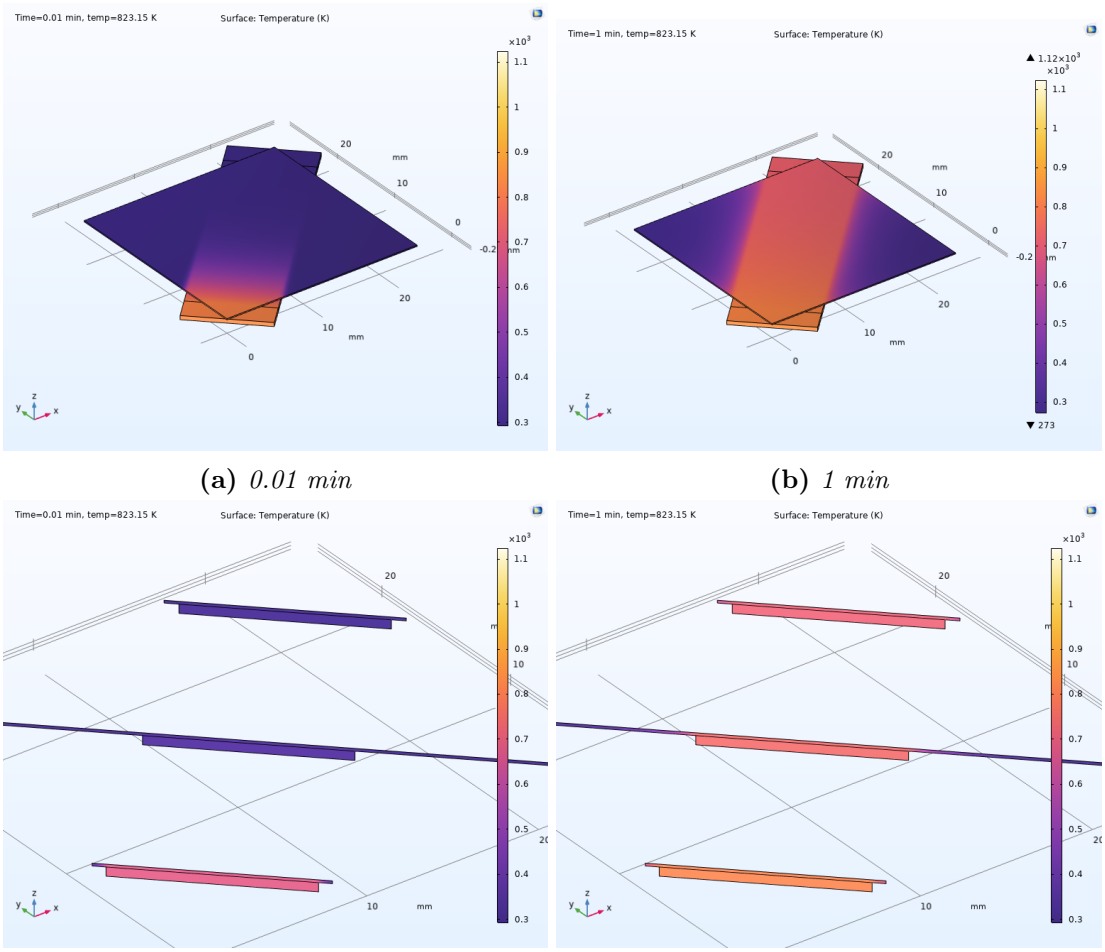

(a) *0.01 min* **(b)** *1 min*

(c) *0.01 min* **(d)** *1 min*

Figure 4.15. *Sample 8 simulated from 0.01 min to 1 min with a temperature of 550 °C and steps of 0.01 min. Both the whole surface and with cutouts from the sample are shown.*

Sample 14 is shown in figure 4.16, where from the simulation beginning, the 850 °C is already reached at the heated place. After 1 minute the heat has distributed through the muscovite mica sample. The sample has a temperature difference of around 200 °C. From the cutout, the heat is observed to go further out on the rest of the muscovite mica sample than the heating heating element.

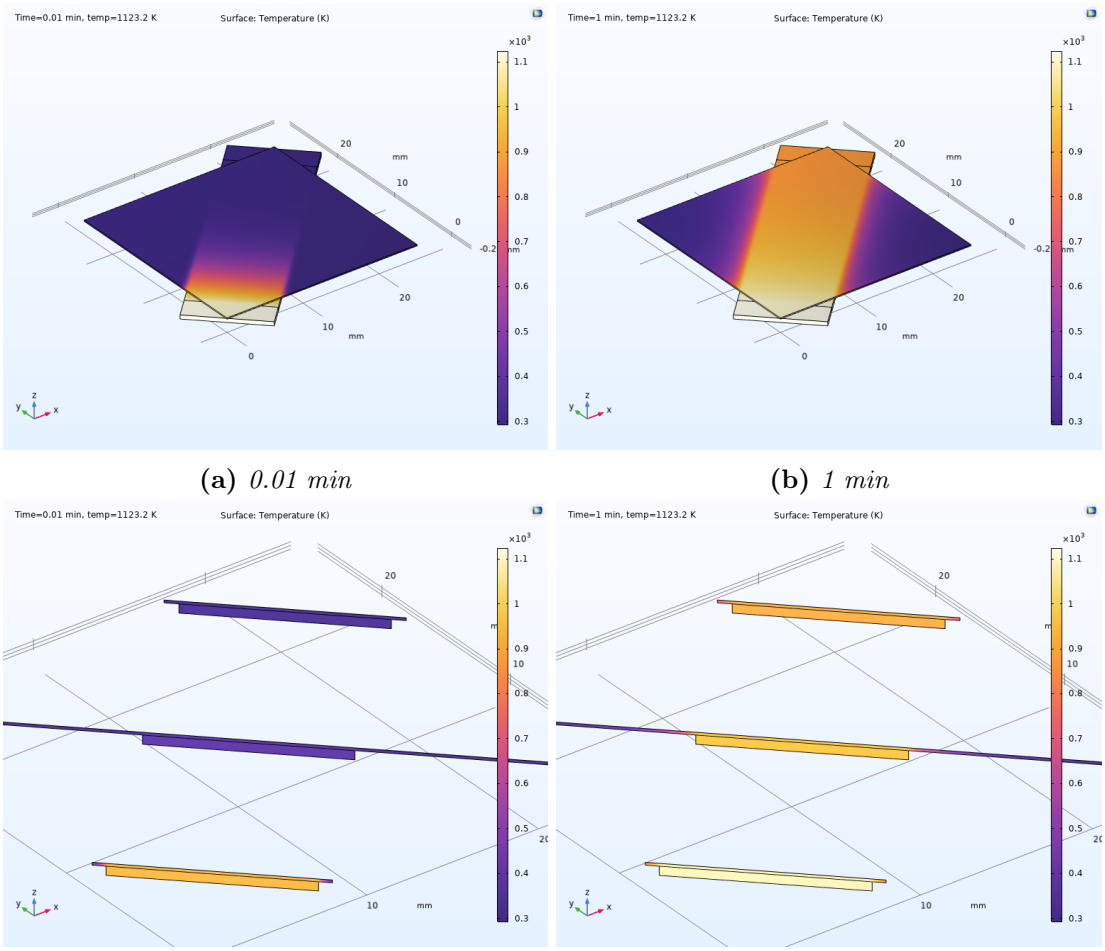

(a) *0.01 min* **(b)** *1 min*

(c) *0.01 min* **(d)** *1 min*

Figure 4.16. *Sample 14 simulated from 0.01 min to 1 min with a temperature of 850 °C with steps of 0.01 min. Both the whole surface and the cutout of the sample are shown.*

Sample 15 shows the smaller mica sample which shows a uniformly heated sample, where the applied temperature is 650 °C. The temperature difference of the sample is around 150 °C. The cutout of the sample also shows an evenly distributed heat transport through the sample from bottom to top.

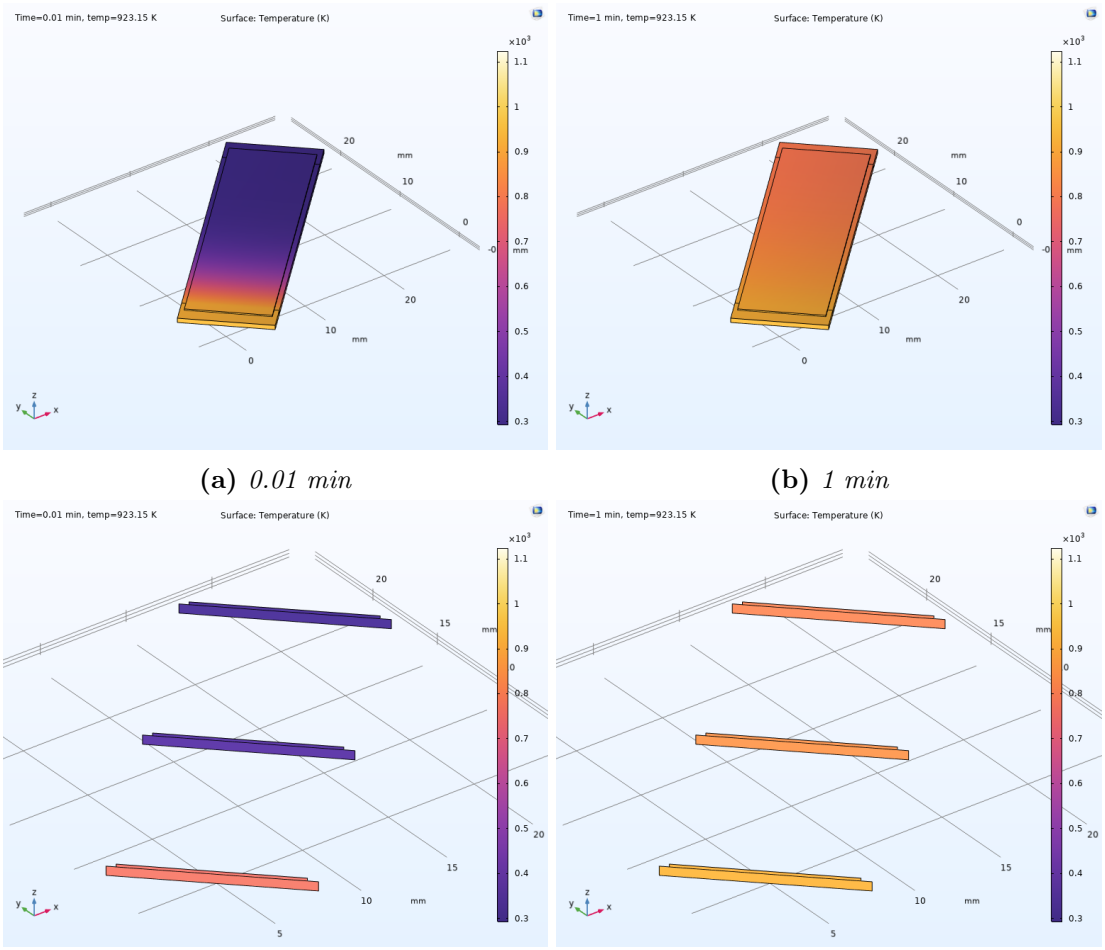

(a) *0.01 min* **(b)** *1 min*

(c) *0.01 min* **(d)** *1 min*

Figure 4.17. *The simulated sample 15 with a simulation time of 0.01 min to 1 min with a time step of 0.01 min. The applied temperature is 650 °C where both the whole sample and the cutout are shown.*

Sample 18 shows an applied temperature of 800 °C at the beginning of the simulation. After 1 min, the heat has distributed through the whole sample, where a temperature difference through the sample is observed to be around 200 °C. From the cutout of the sample, the heat from the bottom to the top is evenly distributed.

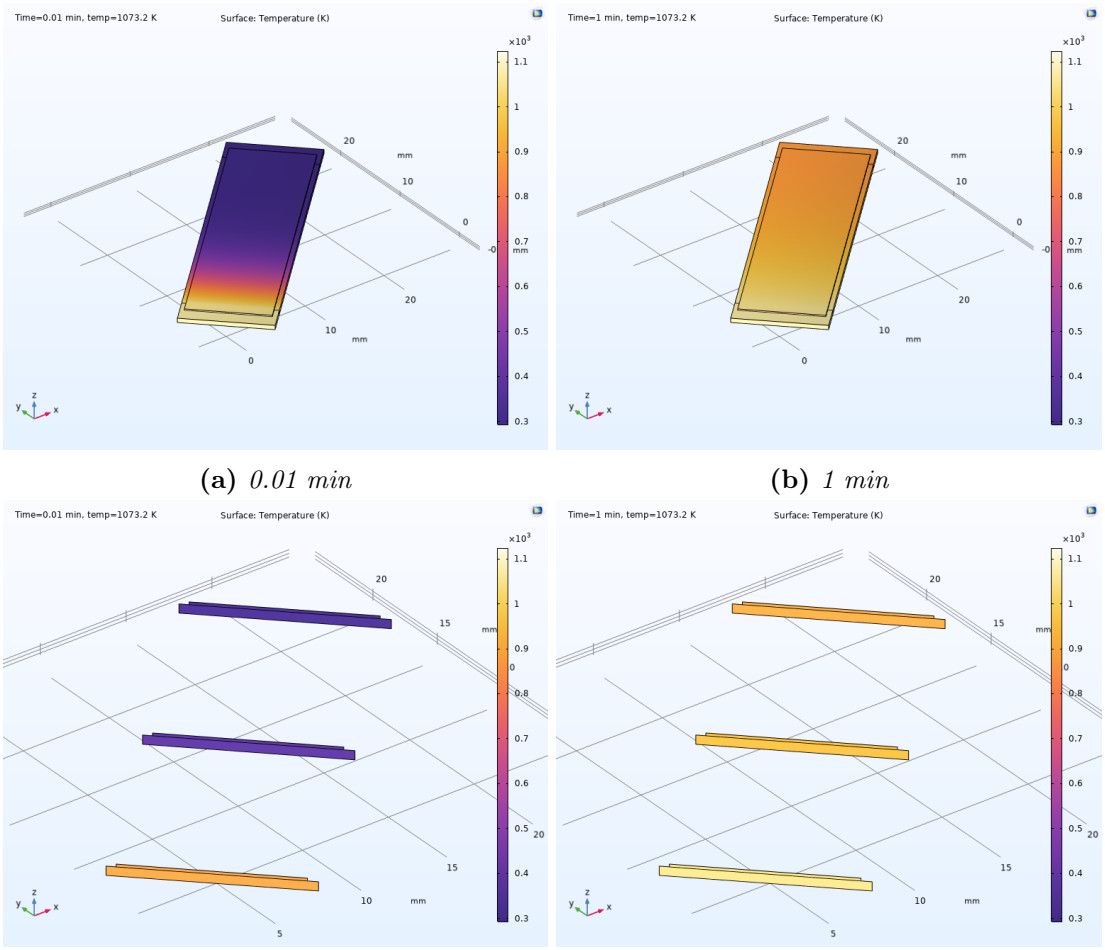

(a) *0.01 min* **(b)** *1 min*

(c) *0.01 min* **(d)** *1 min*

Figure 4.18. *Simulated sample 18 from 0.01 min to 1 min with a timestep of 0.01 min. The applied temperature is 800 °C. Both the whole sample and the cutout of the sample are shown.*

4.4 Assembly

For the assembly of GaN with Au, the GaN sample that was used were those with the best photoluminescence and roughness results. Three different methods were used for assembly, the first one was with MPTS. Thus, sample 20 of GaN was assembled with sample 1 of Au. Figure 4.19 shows the optical image, the AFM image of the flake, and the photoluminescence measurement. For this sample, only one AFM image was taken to check the surface of the flake.

For the Au surface a flake can be observed which came from the GaN sample. This can be observed in the images from 4.19a and 4.19b. The AFM image that is shown is from the flake on the Au sample. This shows a flat surface with 4 particles on top. The photoluminescence measurement shows a maximum in the black box at around 367 nm, giving a band gap energy of 3.38 eV.

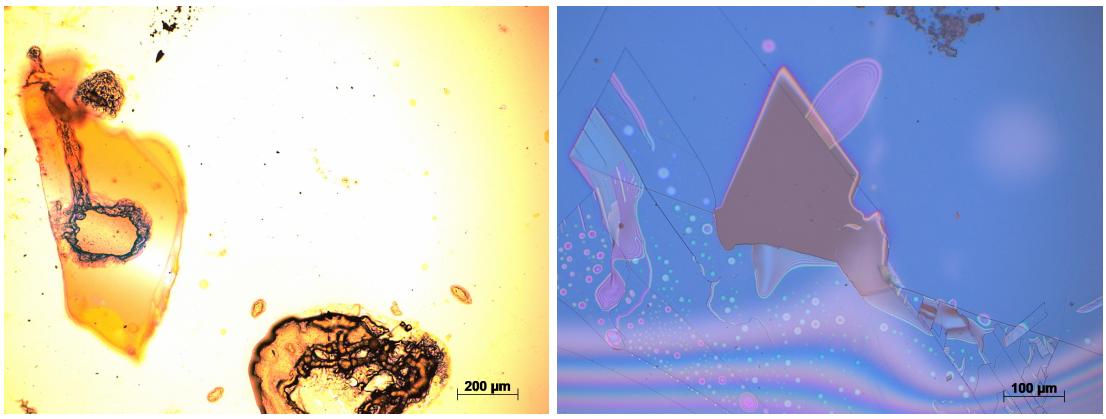

(a) (b)

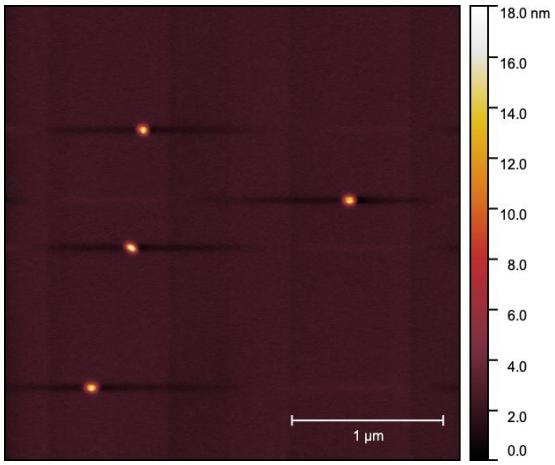

(c)

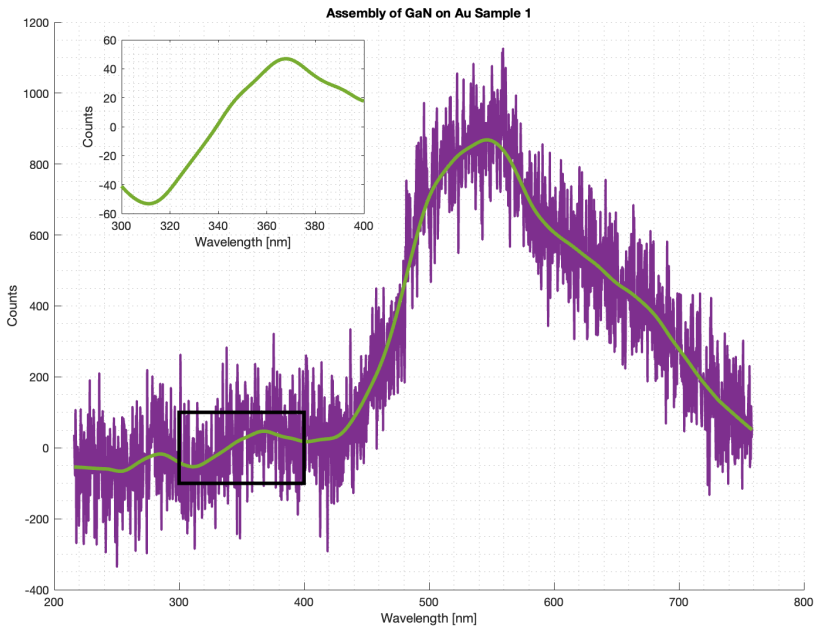

(d)

Figure 4.19. *Lift-off, of GaN to Au surface, where* ***(a)*** *is the optical image of the Au surface with a flake on top and a magnification of* $\times 10$ *and* ***(b)*** *is the optical image of the GaN surface with a magnification of* $\times 20$. ***(c)*** *is the AFM image.* ***(d)*** *is the photoluminescence measurement where purple is the raw data, green is the smoothed data, and the zoomed graph is from the black box on the original graph.*

The second assembled sample was GaN sample 21 and Au sample 2, which were assembled with silver epoxy. Figure 4.20, shows the optical images of the surface, where the GaN and the Au. The blue in the image is the GaN and the small particles are the silver particles in the epoxy. The AFM image shows a very flat surface with around 7 particles. From the photoluminescence graph, the expected maximum is not very distinct. A maximum can be observed at around 500 nm, which is very broad from around 300 nm to 750 nm.

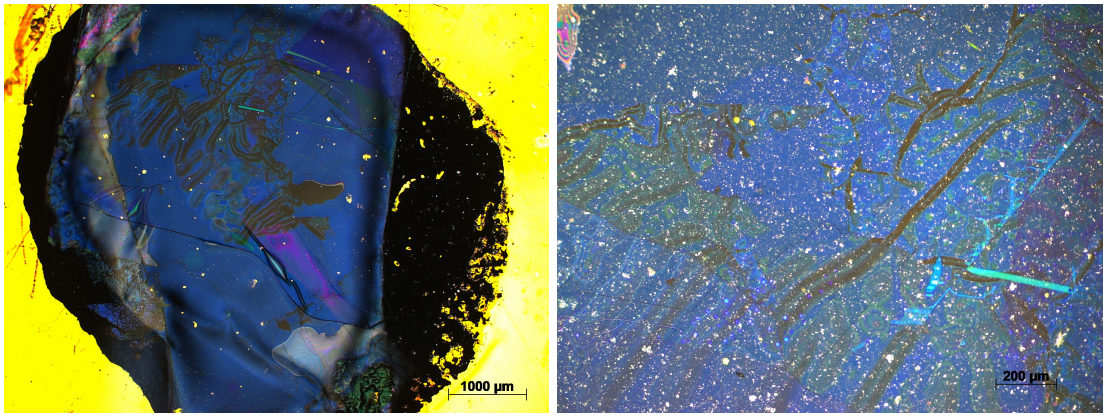

(a) **(b)**

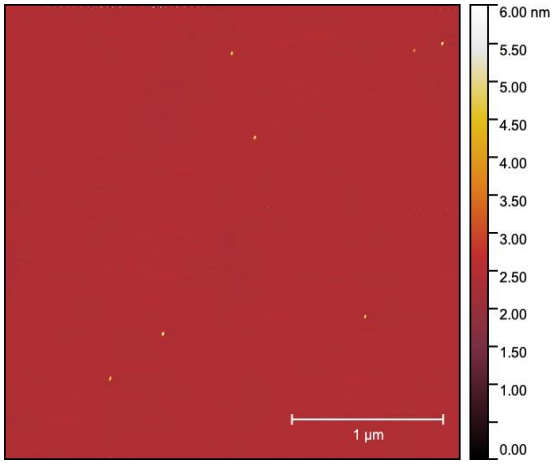

(c)

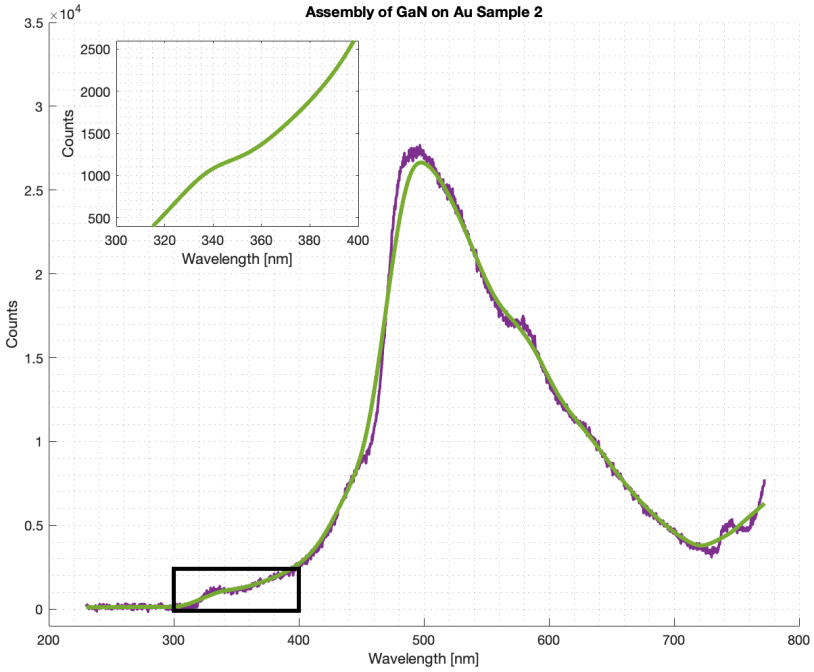

(d)

Figure 4.20. *Lift-off, of GaN to Au surface, where* ***(a)*** *is the optical image of the Au surface with GaN on top and a magnification of ×2.5 and* ***(b)*** *is the optical image of the GaN surface on the silver epoxy with a magnification of ×20.* ***(c)*** *is the AFM image.* ***(d)*** *is the photoluminescence measurement where purple is the raw data, green is the smoothed data, and the zoomed graph is from the black box on the original graph.*

For assembled sample 3 the GaN sample 22 and Au sample 3 were used. Here the GaN sample 22 was lift-off with adhesive tape until there was no visible mica left. Then isopropanol was used to lift the GaN off and fished out with the Au sample. The optical images of figure 4.21 show a GaN flake on top of the Au. Figure 4.21a shows the sample in reflective light and figure 4.21b shows the same with transmitted light. The AFM image of this sample shows one big particle compared to the rest of the surface. The surface is relatively flat. From the photoluminescence graph, no distinct maximum at the desired wavelength is visible, but there is still a maximum at around 344 nm which gives a band gap energy of 3.60 eV. There can again be observed a broad maximum from around 480 nm to 700 nm.

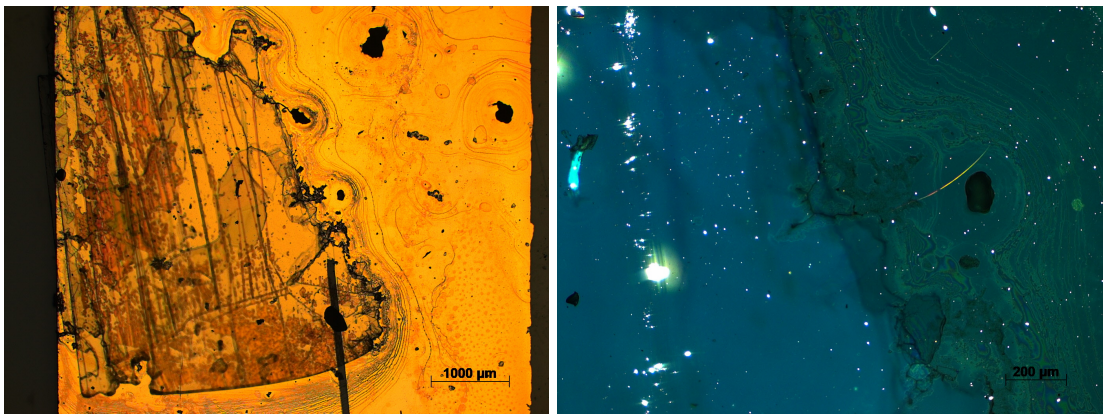

(a) (b)

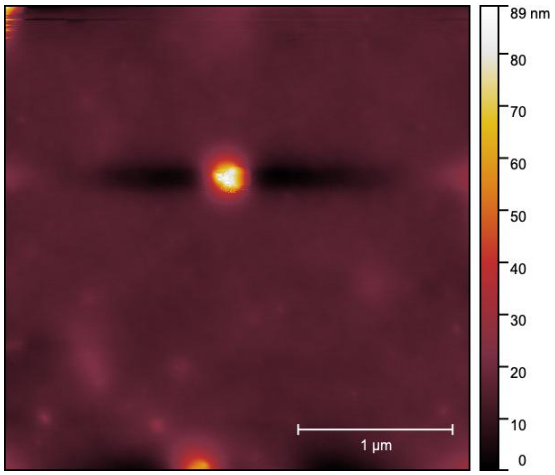

(c)

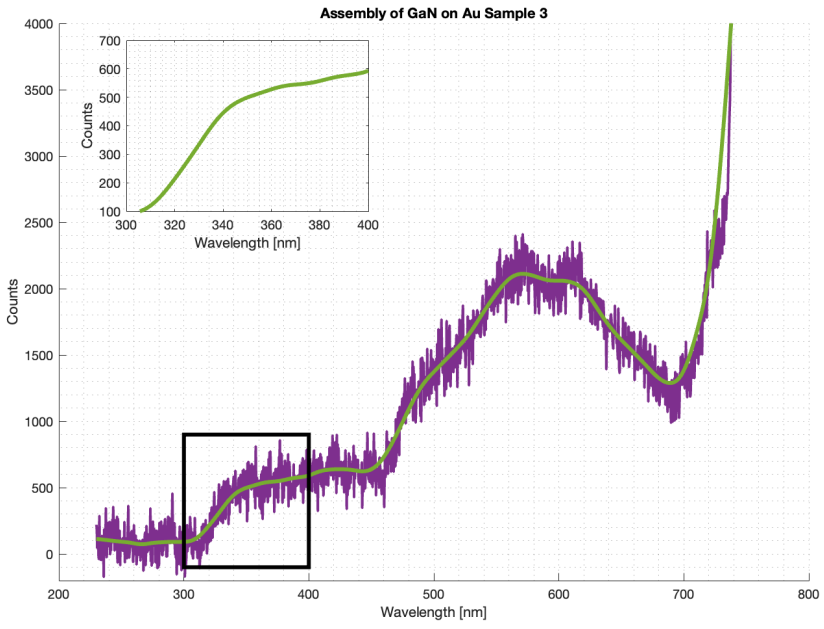

(d)

Figure 4.21. *Lift-off, of GaN to Au surface, where* ***(a)*** *is the optical image of the Au surface with GaN on top and a magnification of* $\times 2.5$ *and* ***(b)*** *is the optical image with transmitted light with a magnification of* $\times 10$. ***(c)*** *is the AFM image.* ***(d)*** *is the photoluminescence measurement where purple is the raw data, green is the smoothed data, and the zoomed graph is from the black box on the original graph.*

Discussion 5

The Au samples were all grown in the PVD system at the same temperature and same conditions. All 4 samples were grown on quartz glass with no intermediate between the Au and the substrate.

GaN was grown with MBE at different temperatures, substrate temperatures and substrates.

5.1 Au on Quartz Glass

The three Au films that were used show a similar optical image. Where the Au film has a homogenous surface with few imperfections, which can be better observed by the optical image with transmitted light, this is possible since the absorption and reflection of metal thin films are dependent on the frequency of the incident electromagnetic wave. Thereby they begin to be transparent and take on some new properties. This is investigated in the article of Axelevitch, A. et al. (2012)[39].

Not only did they investigate the transmittance of different metal films, but also investigated the surface of them by AFM. They concluded that the thicker the Au film is the higher the island growth is. This means that the surface also gets rougher. The AFM images of all the Au films in this project show relatively flat surfaces with island growth observed. The article of Axelevitch, A. et al. (2012)[39] states that this type of growth is typical for metal growth.

Usually to bind the Au thin films to the quartz glass substrate a thin film of chrome or metal oxide is used. This was done in the article of von Benken, W. and Kuwana, T. (1970)[40] where they investigated the different properties of the Au thin films. They concluded that when the thin films were deposited on an oxide layer they were perfect for different optoelectronic uses. The problem with this is that the thin films might react with the intermediate layer and create alloys.

Since the Au films in this project do not have an intermediate layer they must be able to hold on to the quartz glass by Van der Waals forces. The Van der Waals forces are attracting between any two atoms/molecules, which is separated by the distance larger than their dimension[41].

5.2 Ga and N Ratio

For the Si(100) substrate, the substrate temperature was first varied and then held constant for varying the Ga deposition temperature. As known Ga has a melting point of around 302.98 K, which is around 29.83 °C, and a boiling point of around 2676 K, which is around 2402.85 °C[7]. By heating the Ga up to 950 °C it would thereby be liquid in a way that it will free enough Ga atoms to deposit on the surface and react with the N in the system. By increasing the Ga temperature the ratio of Ga and N become different when the N_2 flow is held constant.

The article of koblmüller, G. et al.(2010)[42] investigated the surface properties, by changing the ratio of the Ga and N in the system. They figured that the smoothest surface was obtained with a Ga/N atomic ratio of ≈ 1 and that a too high Ga condition brings a rougher surface due to terraced surface growth. When the N is too high the surface becomes pitted due to

surface diffusion barriers. At the same time, they investigated the electrical properties of the GaN material and discovered that it was best at a slightly higher N rate. This increased the carrier concentration due to unintentional impurities.

5.3 GaN on Si(100)

After the Ga/N ratio was examined the sample temperature was varied. This was done to ensure the best crystallinity of the GaN thin films. For the article of Hughes, W. C. et al.(1995)[43] they also heated the substrate of SiC from between 600 - 800 °C, to achieve surface reconstruction.

From sample 1 where the GaN was grown at room temperature in ultra-high vacuum (UHV), and with a Ga temperature of 950 °C it showed a blue surface of the GaN but a roughness of around 2.2 nm which is relatively flat. This is also observed in the article of Bakri, A. S. et al. (2020)[44], even though it was deposited with magnetron sputtering and an AlN buffer layer underneath.

When looking at samples that had a higher sample temperature the optical images show that they go from a blueish to a yellowish look. For the first three samples the statement of, that colour could be related to thickness, interference. This thickness can also be related to roughness. For sample 4 where the Si(100) was flashed in the deposition chamber at around 1000 °C to remove the oxygen at the surface, the colour and roughness changed. From samples 4 to 6, the roughness goes down, and bigger grains are observed in the AFM images. These are observed in the Appendix 8. For sample 7 the roughness is increased again, but observing the optical images shows different surfaces on different places of the sample. This agrees with the study of Kum, D. and Byun, D.(1997)[45], where they investigated the roughness of GaN surface from MBE and the time the sample was nitridated. They also observed that the roughness increases and drops again, with nitridation time. This roughness increase is observed for the measured samples in this project after starting to flash the samples in the chamber.

Sample 1 gives a photoluminescence graph without a distinct maximum where GaN would be indicated to be. It is at around 367 nm and gives a band gap energy of 3.38 eV. The maxima at around 280 nm and 560 nm, were already explained to be the pump light leaking through the pass filter and the second-order diffraction, respectively. For sample 5 the photoluminescence has a distinct maximum at around 351 nm giving it a band gap of around 3.53 eV. It is observed that the band gap energy falls to 3.35 eV when the sample is heated too much, which is shown in sample 7.

The reason for this big energy gap can be because of the polarity of growth. This was discovered by Chichibu, S. F. et al.(2001)[46] where they grew GaN on sapphire with N$(000\bar{1})$ making it negative to the c plane of the sapphire and one with Ga(0001), making it positive to the c plane of the sapphire. With this polarisation, the difference of energy in the positive c plane is around 45 meV compared to the actual 3.4 eV for GaN. For the article, the samples were cooled down to around 8 K and investigated the difference between the differently cooled samples. Here they observed a stokes shift for the negative c plane of around 20 meV for 300 K.

The samples from this project were measured at room temperature and can have an influence on how sharp and precise the maximum signal can become. This is a possible reason why the maxima from all the different samples are not very strong.

For these samples, XRD was measured and analysed with the help of different articles as stated in the results. For sample 1 where it was grown at room temperature, the Si(100) has a very

distinct peak. This peak is shown for all the Si(100) samples. It can be observed that the higher the temperature, the more intensive the GaN(002) peak becomes, especially when the surface is flashed before deposition. Flashing the surface gives a clean Si(100) substrate, and thereby less strain for the thin film. Another explanation for the flashing could be that the Ga reacts with the Si and thereby creates a disordered surface. Samples 6 and 7 show that they were grown with too much temperature since they have smaller peaks. This peak indicates the wurtzite structure of GaN since it prefers to grow along the c axis which is perpendicular to the substrate surface. This is shown in the article of Fong, C. Y. et al.(2014)[47], where they have measured the same peak in XRD.

5.4 GaN on Muscovite Mica

For the GaN on muscovite mica the ratio of Ga and N were held constant which means the temperature of Ga was 970 °C and the flow of N_2 was constant.

Examining the muscovite mica samples that had the dimensions of 25 × 25 × 0.15 mm, shows some uniformly grown thin films. Sample 8 had a sample temperature of around 550 °C during deposition. This temperature seems not to be enough, since the surface on the AFM image is observed to have rather small grains, and the sample has no distinct maximum at the photoluminescence graphs black box. For all of these samples, the maxima at around 280 nm and 560 nm are observed as discussed above.

For sample 12 the sample temperature was 750 °C and the grains on the AFM image are bigger, which gives a rougher surface. For this type of sample 750 °C, seem to be a perfect temperature before the muscovite mica starts to dehydroxylate where the layers start to have a loss of the OH groups. This is very visible in sample 14, where the optical image shows the destruction of the muscovite mica. In the article of Zanazzi, P. F. and Pavese, A. (2002)[48] they investigated the properties of muscovite mica under pressure and high temperature. They concluded that temperatures around 800 °C and above do dehydroxylate. This sample also had no AFM image, since the surface was so uneven that it was impossible to make.

5.4.1 Smaller Muscovite Mica

For the muscovite mica samples that were cut to fit onto the Si(100) heating element, nearly the same trend is shown for heating the sample and for the AFM image structure. Here the samples grown with the temperature of 770 °C and 780 °C were the samples with the best signal in photoluminescence. For these samples maxima around 280 nm and 560 nm are visible in the photoluminescence graph.

For sample 18 the sample temperature was around 800 °C which is similar to the AFM image of sample 13 which is also grown at a sample temperature of around 800 °C. They both show that the substrate starts to dehydroxylate since the grains get smaller.

There can be observed a starting maximum at around 800 nm in the photoluminescence graphs for all of the muscovite mica samples. In figure 8.13 from Appendix 8 the photoluminescence was measured between 300 nm to 900 nm, to see what is above 800 nm. Here there is still shown a maximum at the 371 nm which is 3.34 eV. This is the maximum for GaN, but there is also a very big maximum at around 836 nm which is 1.48 eV. This fits with the simulation of the article of Mukherjee, J. et al (2022)[49], where they simulated the band gap of muscovite mica with an introduced defect of two K, one Al, two Si, four O and two H atoms in the structure.

The band gap thereby goes from 4.63 eV to 1.32 eV. The valence band is thereby composed of the s and p orbitals of Si and O, respectively. The s and p orbitals in the K atoms contribute more to the conduction band than the other atoms. This reduces the band gap energy.

5.5 Heat Distribution

There are simulations about the heat distribution for the two different sizes of muscovite mica. The reason for this is that mica is an insulator and needs to have a heating element (Si(100)) to be able to achieve the sample temperature as desired.[49]

All the different sample temperatures were simulated, with heating from one side of the sample since this was observed in the laboratory. As observed in all the mica samples, the heating element loses a little heat from one end to the other. This is due to heat transfer to the surroundings. In the article of Shanks, H. R. et al. (1963)[50] they looked at the thermal conductivity of Si and observed that up to 1000 K (726 °C), the thermal conductivity of pure Si is due to transmission of lattice vibrations. They also observed that for the thermal conductivity at temperatures from 1000 K to 1400 K (726 to 1126 °C) in pure Si the contribution by electron-hole pairs increases. Thereby at higher temperatures the heating element can be less efficient.

For the big mica samples the low temperature can be seen in figure 4.15. Here the temperature difference from one end to the other is around 180 °C. This is a big temperature difference to create a uniform thin film with the same conditions over the whole surface. For the sample that was heated to 850 °C, the difference was around 200 °C, which can be because of the thermal conductivity of the heating element as discussed above. This temperature difference in one sample is also observed in the produced samples. This extreme temperature difference is observable at the highest sample temperatures for both the Si(100) and mica samples since the surface differed from one end of the sample to the other end.

When the temperature was set for the samples in the laboratory, the temperature that is written for the samples is thereby the temperature measured at the heating end of the sample holder. This means that there was no perfect heat distribution condition. Therefore the samples produced in the laboratory, the whole sample differed in temperature, thereby giving different growth of GaN on the surface of the substrate.

The big mica samples also show that the higher the temperature gets the more the heat diffuses outwards from the heating element to the rest of the big sample.

There were also smaller mica samples to fit onto the heating element. This was to ensure that the heat did not need to be distributed to a larger area. Here the lowest temperature was 650 °C where the temperature difference throughout the sample is around 150 °C, which is less than the one for the big mica sample. The sample with the highest temperature also has a temperature difference of around 200 °C, which is around the same as for the big mica sample. Therefore the higher the temperature gets the more it goes to the surroundings.

5.6 Assembly

There were some different methods for the assembly of the two thin films that were produced. Before the assembly, all the thin films were cleaned with the procedure explained in the methods section.

5.6.1 MPTS

Looking at the chemistry of GaN, it is known that it is covalently bonded and thereby this semiconductor would not react with other chemicals. This is also calculated in the article of Dudesek, P. et al. (1998)[51] where they show that the covalent bonding is between the d and s orbitals overlapping. This means that the surface of GaN needs to be treated to be able to react with the silane. In this project, the surface treatment was by hydroxylating the surface by introducing OH groups to the surface by ozone treatment. The MPTS will then react with the surface at the alkoxysilane part of the chemical. The sulfur group will then make a covalent bond to the Au surface. This is also observed in figure 4.19, where a flake of the GaN was successfully placed on top of the Au surface. The article of Baur, B. et al. (2005)[52] shows that it is possible to silicate the GaN surface. They did it by hydrolyzing the surface with an acid and then treating the surface with APTES, which in general is the same, except that the sulfur group is switched with an amine group.

For this assembly, there were done 7 tries to make the sample. The different parameter changes for each try can be observed in table 3.5. After try number 2 the GaN and the Au were assembled. For this try, when the GaN sample was removed from the ozone machine it was possible to smell the ozone. For all the other tries this was not smelled. This thereby implies that the ozone treatment only worked once.

Here the band gap energy for the GaN flake on the Au surface is 3.38 eV, which is a bit lower than the measured GaN before the lift-off, which was 3.48 eV. This might be from the strain effect when growing the GaN on mica since there is a big lattice mismatch between the GaN and the mica substrate. The stress in the thin film can also cause a shift in the band gap, which is affected by the crystal field splitting and spin-orbital splitting, as described in the article of Orton, J. W. (1996)[53]. Not only is the stress in the film relevant but also the dislocations, which can influence the shift in the band gap energy.

From the photoluminescence graph, there is no big maximum at around 800 nm. This indicates that there is no mica but GaN that was lifted off. Then there is again shown the two maxima at around 280 nm and 560 nm, which already were discussed above.

The AFM image shows that the surface is flat on the other side of the grown GaN film. The RMS average of the sample before lift-off is around 4.4 nm. This change in surface can be caused by the substrate which is atomically flat.

5.6.2 Silver Epoxy

The second method of assembly of the two thin films was with silver epoxy. This was done since silver epoxy has one of the highest thermal conductivities, but the epoxy part is not conductive. The Ag nanoparticles (AgNP) in the epoxy make it conductive and create a conductive layer between Au and GaN.

From figure 4.20, there was one flake of GaN that stuck to the silver epoxy. There are AgNP, which can be seen through the GaN film as many small spheres. The AFM image also shows a very flat surface, like at the lift-off at the MPTS assembly. For this GaN sample the RMS value before lift-off was around 4.4 nm and had a lot of grains showing. This again indicates a very smooth surface as the sample from MPTS. Here the photoluminescence for the GaN sample was around 3.41 eV, but when it was assembled there was no distinct maximum anymore. The photoluminescence of AgNPs is around 332 nm to 340 nm, which was measured in the article of Zhao, Y. et al. (2006)[54] and from Smitha, S. L. et al. (2008)[55], respectively. This

could influence the photoluminescence and thereby give no distinct maximum at the desired wavelength.

The epoxy part of the silver epoxy has also a photoluminescence maximum of around 320 nm, which is not observed in the photoluminescence measurement of assembled sample 2[56]. It might be from the Au thin film together with some of the other materials since the photoluminescence of Au according to the article of Andersen, S. K. H. et al. (2015)[57] illuminates at around 532 nm, which would fit into the photoluminescence, But it might also just be noise from the instrument.

5.6.3 Adhesive Tape Lift-off

For the last assembly method, adhesive tape was used to do lift-off of the GaN from the muscovite mica. This method was done by fishing the visible flake out of an isopropanol solution. The GaN flake on top of the Au surface sticks by Van der Waals forces. The AFM image shows some small particles and one big particle, which might indicate that it is unknown if there is still some mica on the sample and which part of the original GaN sample is on the Au film and which part is upwards. From the photoluminescence graph of this sample the characteristic starting of the big maximum after 800 nm, which already was discussed before, came from the mica and thereby proves that there is still some mica. There is a step in the graph where the maximum for GaN should be, which gives the band gap energy of 3.60 eV. Before the lift-off, the band gap energy was 3.54 eV, which was an increase of around 0.06 eV.

It is known that isopropanol is an alcohol which has the functional group of OH. It is also known that the OH group can not react covalently with the mica, but there might still be some traces of it underneath the flake. The article from Balagurov, L. A. et al. (1996)[58] tested the influence of water and alcohols on the photoluminescence spectra. They concluded that the influence only affected the intensity of the maximum and that it would show around 700 nm. Another possibility would be that some of the epoxy of the adhesive tape was also sticking to the Au surface and thereby influencing the photoluminescence measurement.

Conclusion and Outlook 6

In this project, different methods were used to grow Au and GaN thin films, and different methods were used to assemble them. The Au thin films were successfully deposited on quartz glass without any intermediate layer and by physical vapour deposition. They were analysed to have island growth, which is typical for metal thin films.

For the deposition of the GaN with molecular beam epitaxy, the Ga/N ratio is important and was thereby tested on Si(100) substrate before trying to grow the thin films at different sample temperatures. This was achieved by having a Ga temperature of 970 °C and a constant flow of N. After achieving the best ratio for the deposition of the GaN, the sample temperatures were tested and the sample that gave the best results was identified to have a sample temperature of 710 °C. This sample reached the GaN(002) crystal structure which is identified as a wurtzite structure with the typical band gap energy of 3.4 eV. This substrate was the test substrate to have an idea of what parameters to use for the muscovite mica samples.

The muscovite mica samples had two different sizes $25 \times 25 \times 0.15$ mm and $9 \times 32 \times 0.15$ mm. The bigger samples were used to see what sample temperatures the mica would persist. Here the 550 °C was clearly too low of a sample temperature and 850 °C was too high of a sample temperature since the muscovite mica layers visibly started to separate because of hydroxylation. The big mica samples best sample temperature for deposition was at 750 °C. From the COMSOL[1] simulations of the big muscovite mica samples, the heat distribution gets less from one end to the other, but it does not distribute to the whole wafer, since muscovite mica is an insulator.

The small muscovite mica samples were made to ensure better temperature distribution from the heating element, which was a Si(100) wafer. The smaller samples had more of the same temperature over the whole wafer as seen in the COMSOL[1] simulations, of the heat distribution. Therefore they were used for assembly with the Au thin films. The best results for the small muscovite mica samples were those with a sample temperature of 770 °C and 780 °C.

For both muscovite mica sizes, a starting maximum can be observed in the photoluminescence graph at around 800 nm and above, giving a band gap energy of the muscovite mica of 1.4 eV.

The GaN samples with the best results were used for assembly with the Au thin films. There were tested three different methods, and of those the one with the silaneisation was the most promising. This was concluded since the silver epoxy can affect what properties the two thin films will have, but most importantly it is uncontrollable to achieve a thin film of silver epoxy between the two thin film materials. With the 3-mercaptopropyl(trimethoxysilane) the layer can be as thin as 1 nm.

Then there was the last method which in principle was good with assembly by Van der Waals forces, but it needs more research to know which side of the samples is on the interface and which is upwards.

This form of transfer of membranes is one step further to creating 3D stacking of thin films to create metamaterials with specific optical properties without alloy creation and less stress and dislocations in the thin films. The next step would be perfecting either the method of silane assembly or assembly by adhesive tape lift-off. Afterwards, try to produce a form of waveguide for specific optical properties.

Bibliography

[1] Multiphysics®, C. "COMSOL". In: *www.comsol.com* v 6.2 (). COMSOL AB, Stockholm Sweden.

[2] Kumar, S. and Krenner, N. "Review of the semiconductor industry and technology roadmap". In: *Journal of science education and technology* 11 (2002), pp. 229–236.

[3] Moore, G. E. "Cramming more components onto integrated circuits". In: *Proceedings of the IEEE* 86.1 (1998), pp. 82–85.

[4] Mollick, E. "Establishing Moore's law". In: *IEEE Annals of the History of Computing* 28.3 (2006), pp. 62–75.

[5] Oba, F. and Kumagai, Y. "Design and exploration of semiconductors from first principles: A review of recent advances". In: *Applied Physics Express* 11.6 (2018).

[6] Ponce, F. A. and Bour, D. P. "Nitride-based semiconductors for blue and green light-emitting devices". In: *nature* 386.6623 (1997), pp. 351–359.

[7] Moskalyk, R. R. "Gallium: the backbone of the electronics industry". In: *Minerals Engineering* 16.10 (2003), pp. 921–929.

[8] Yoshikawa, A. et al. "Crystal growth of GaN by ammonothermal method". In: *Journal of crystal growth* 260.1-2 (2004), pp. 67–72.

[9] Akselrod, M. S. and Bruni, F. J. "Modern trends in crystal growth and new applications of sapphire". In: *Journal of crystal growth* 360 (2012), pp. 134–145.

[10] Pal, S. and Jacob, C. "Silicon—a new substrate for GaN growth". In: *Bulletin of Materials Science* 27 (2004), pp. 501–504.

[11] Matsuki, N. et al. "Heteroepitaxial growth of gallium nitride on muscovite mica plates by pulsed laser deposition". In: *Solid state communications* 136.6 (2005), pp. 338–341.

[12] Daudin, B. et al. "Growth of zinc-blende GaN on muscovite mica by molecular beam epitaxy". In: *Nanotechnology* 32.2 (2020), p. 025601.

[13] Yamada, A. et al. "Layered compound substrates for GaN growth". In: *Journal of crystal growth* 201 (1999), pp. 332–335.

[14] Fali, A. et al. "Nanoscale spectroscopy of dielectric properties of mica". In: *ACS photonics* 8.1 (2020), pp. 175–181.

[15] Miskys, C. R. et al. "Freestanding GaN-substrates and devices". In: *physica status solidi (c)* 6 (2003), pp. 1627–1650.

[16] Wang, T. et al. “Experimental and numerical investigation on GaN/Al2O3 laser lift-off technique”. In: *Thin Solid Films* 515.7-8 (2007), pp. 3854–3857.

[17] Park, M. et al. “2D materials-assisted heterogeneous integration of semiconductor membranes toward functional devices”. In: *Journal of Applied Physics* 132.19 (2022).

[18] Kossoy, A. et al. “Optical and structural properties of ultra-thin gold films”. In: *Advanced Optical Materials* 3.1 (2015), pp. 71–77.

[19] Kittel, C. and McEuen, P. *Introduction to Solid State Physics*. 8th ed. John Wiley & Sons, 2005.

[20] Andiwijayakusuma, D., Saito, M. and Purqon, A. “Density functional theory study: Electronic structures of RE: GaN in wurtzite Gα15RE1N16”. In: 739.1 (2016), p. 012027.

[21] Schulz, H. and Thiemann, K. “Crystal structure refinement of AlN and GaN”. In: *Solid State Communications* 23.11 (1977), pp. 815–819.

[22] Godiksen, R. H. et al. “Two-photon photoluminescence and second-harmonic generation from unintentionally doped and semi-insulating GaN crystals”. In: *Applied Physics B* 123 (2017), pp. 1–7.

[23] Oura, K. et al. *Surface Science: An Introduction*. Advanced Texts in Physics. chapther 14. Springer Berlin Heidelberg, 2013.

[24] Reichelt, K. and Jiang, X. “The preparation of thin films by physical vapour deposition methods”. In: *Thin Solid Films* 191 (1990), pp. 91–126.

[25] Boden, A. C. et al. “Solution deposition conditions influence the surface properties of 3-mercaptopropyl(trimethoxysilane) (MPTS) films”. In: *Applied Surface Science* 602 (2022).

[26] Scott, A. and Gray-Munro, J. E. “The surface chemistry of 3-mercaptopropyltrimethoxysilane films deposited on magnesium alloy AZ91”. In: *Thin Solid Films* 517.24 (2009), pp. 6809–6816.

[27] Sun, Z. et al. “A review of the thermal conductivity of silver-epoxy nanocomposites as encapsulation material for packaging applications”. In: *Chemical Engineering Journal* 446 (2022), p. 137319.

[28] Jin, F.-L., Li, X. and Park, S.-J. “Synthesis and application of epoxy resins: A review”. In: *Journal of Industrial and Engineering Chemistry* 29 (2015), pp. 1–11.

[29] Adams, J. “Bonding Energy Models”. In: *Encyclopedia of Materials: Science and Technology*. Ed. by Buschow, K. J. et al. Elsevier, 2001, pp. 763–767.

[30] Hahn, D. W. and Özisik, M. N. *Heat conduction*. John Wiley & Sons, 2012.

[31] Tingting, Y. et al. “Impact of UV/ozone surface treatment on AlGaN/GaN HEMTs”. In: *Journal of Semiconductors* (2009).

[32] Chemtronics®. *CircuitWorks Conductive Epoxy*. Accessed: 2025-05-20. URL: https://www.chemtronics.com/circuitworks-conductive-epoxy-2.

[33] Nasr, F., Guermazi, H. and Guermazi, S. "Correlation between structural and optical properties of GaN epi-layers by the cathodoluminescence technique". In: *The European Physical Journal Plus* 131 (2016).

[34] Saron, K. M. A. et al. "Leakage current reduction in n-GaN/p-Si (100) heterojunction solar cells". In: *Applied Physics Letters* 118 (2021).

[35] Kumar, G. et al. "Facet-dependent electrical conductivity properties of 4H-SiC wafer". In: *Journal of Materials Chemistry C* 10 (2022).

[36] Masilamani, G. et al. "Structural and optical properties of GaN and InGaN nanoparticles by chemical co-precipitation method". In: *Materials Research Bulletin* 47 (2012).

[37] Kang, B. et al. "Formation of Highly Efficient Dye-Sensitized Solar Cells by Effective Electron Injection with GaN Nanoparticles". In: *Journal of The Electrochemical Society* 158 (2011).

[38] Martínez-Ara, L. et al. "Structural and Optical Properties of GaN Thin Films Grown on Si(111) by Pulsed Laser Deposition". In: *Materials Research* 22 (2019).

[39] Axelevitch, A., Gorenstein, B. and Golan, G. "Investigation of optical transmission in thin metal films". In: *Physics Procedia* 32 (2012), pp. 1–13.

[40] Benken, W. V. and Kuwana, T. "Preparation and properties of thin gold and platinum films on glass or quartz for transparent electrodes". In: *Analytical Chemistry* 42.9 (1970), pp. 1114–1116.

[41] Dzyaloshinskii, I. E. et al. "The general theory of van der Waals forces". In: *Perspectives in Theoretical Physics*. Elsevier, 1992, pp. 443–492.

[42] Koblmüller, G. et al. "Influence of Ga/N ratio on morphology, vacancies, and electrical transport in GaN grown by molecular beam epitaxy at high temperature". In: *Applied Physics Letters* 97.19 (2010).

[43] Hughes, W. C. et al. "Molecular beam epitaxy growth and properties of GaN films on GaN/SiC substrates". In: *Journal of Vacuum Science & Technology B: Microelectronics and Nanometer Structures Processing, Measurement, and Phenomena* 13.4 (1995), pp. 1571–1577.

[44] Bakri, A. S. et al. "Structural properties and surface roughness of heterostructure GaN/AlN on Si (100) substrate". In: *2020 IEEE Student Conference on Research and Development (SCOReD)*. IEEE. 2020, pp. 128–131.

[45] Kum, D. and Byun, D. "The effect of substrate surface roughness on GaN growth using MOCVD process". In: *Journal of Electronic Materials* 26 (1997), pp. 1098–1102.

[46] Chichibu, S. F. et al. “Impact of growth polar direction on the optical properties of GaN grown by metalorganic vapor phase epitaxy”. In: *Applied Physics Letters* 78.1 (2001), pp. 28–30.

[47] Fong, C. Y. et al. “Synthesis of wurtzite GaN thin film via spin coating method”. In: *Materials science in semiconductor processing* 17 (2014), pp. 63–66.

[48] Zanazzi, P. F. and Pavese, A. “Behavior of micas at high-pressure and high-temperature”. In: *Reviews in mineralogy and geochemistry* 46.1 (2002), pp. 99–116.

[49] Mukherjee, J. et al. “Band gap engineering of the top layer of mica by organized defect formation”. In: *Surfaces and Interfaces* 33 (2022), p. 102283.

[50] Shanks, H. R. et al. “Thermal conductivity of silicon from 300 to 1400 K”. In: *Physical Review* 130.5 (1963), p. 1743.

[51] Dudesek, P. et al. “d-to-s bonding in GaN”. In: *Journal of Physics: Condensed Matter* 10.32 (1998), p. 7155.

[52] Baur, B. et al. “Chemical functionalization of GaN and AlN surfaces”. In: *Applied Physics Letters* 87.26 (2005).

[53] Orton, J. W. “Effect of strain on GaN exciton spectra”. In: *Semiconductor science and technology* 11.7 (1996), p. 1026.

[54] Zhao, Y., Jiang, Y. and Fang, Y. “Spectroscopy property of Ag nanoparticles”. In: *Spectrochimica Acta Part A: Molecular and Biomolecular Spectroscopy* 65.5 (2006), pp. 1003–1006.

[55] Smitha, S. L. et al. “Studies on surface plasmon resonance and photoluminescence of silver nanoparticles”. In: *Spectrochimica Acta Part A: Molecular and Biomolecular Spectroscopy* 71.1 (2008), pp. 186–190.

[56] Mondragon, M. et al. “Photoluminescence of epoxy/clay nanocomposites”. In: *Polymer Engineering & Science* 51.9 (2011), pp. 1808–1814.

[57] Andersen, S. K. H., Pors, A. and Bozhevolnyi, S. I. “Gold photoluminescence wavelength and polarization engineering”. In: *Acs Photonics* 2.3 (2015), pp. 432–438.

[58] Balagurov, L. A. et al. “Influence of water and alcohols on photoluminescence of porous silicon”. In: *Journal of applied physics* 79.9 (1996), pp. 7143–7147.

Appendix A 7

7.1 Growth of Au

For Au sample 4 the Au layer also has a homogeneous surface with few imperfections. This is also observed in the optical image with the transmitted light. The AFM image shows many small grains on the surface with little space in between. The average roughness for this surface is 0.7 nm, shown in table 4.1c.

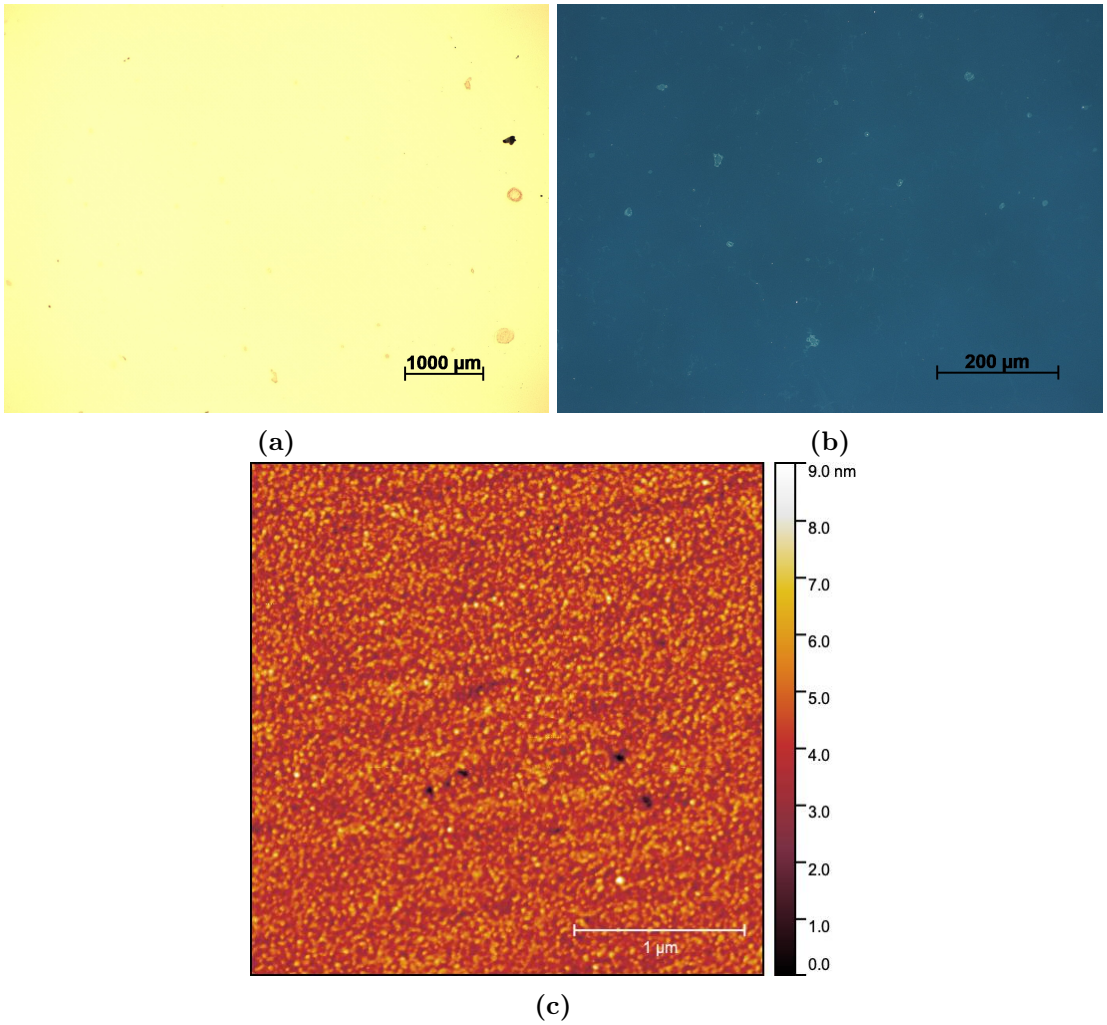

Figure 7.1. *Sample 4, Au surface on quartz glass without binding material between Au and quartz glass taken in an optical microscope and AFM. Here* ***(a)*** *is taken with a magnification of ×10 and* ***(b)*** *is with a ×20 magnification and with transmitted light.* ***(c)*** *is the AFM image of the surface.*

Appendix B 8

8.1 Growth of GaN on Si(100) Results

Sample number 2 is shown in figure 8.1, which is the surface in the middle of the sample. The optical image of figure 8.1a shows the image of the surface with a magnification of ×10. Here, it also shows a homogeneous growth of GaN with some imperfections, with a thickness of around 100 nm and the sample was heated to around 650 °C. The AFM images are shown in figure 8.1b where the image shows many grains with little space between them. The RMS for this surface is shown in table 4.2b which is 23.9 nm. The sample's photoluminescence is shown in figure 8.1c where 3 defined maxima can be observed at around 280 nm, 580 nm and 720 nm, respectively. The maximum in the black box is around 370 nm, which gives a band gap energy of 3.35 eV. This maximum is also very broad.

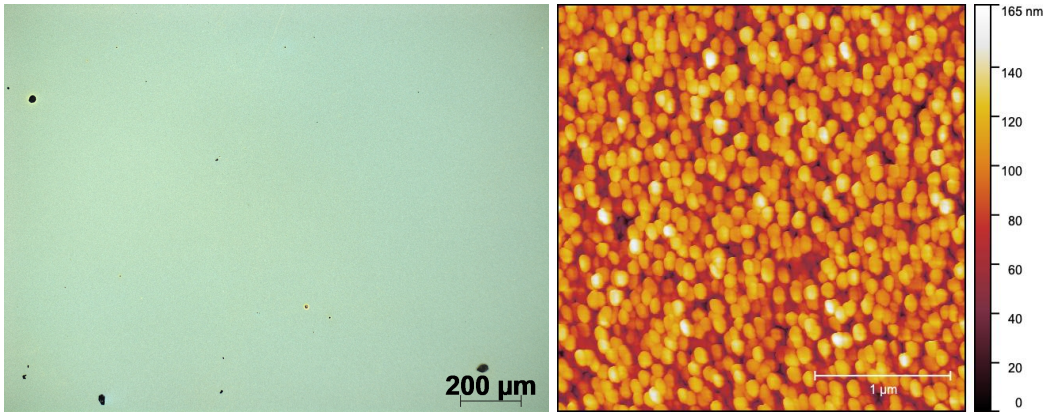

(a) **(b)**

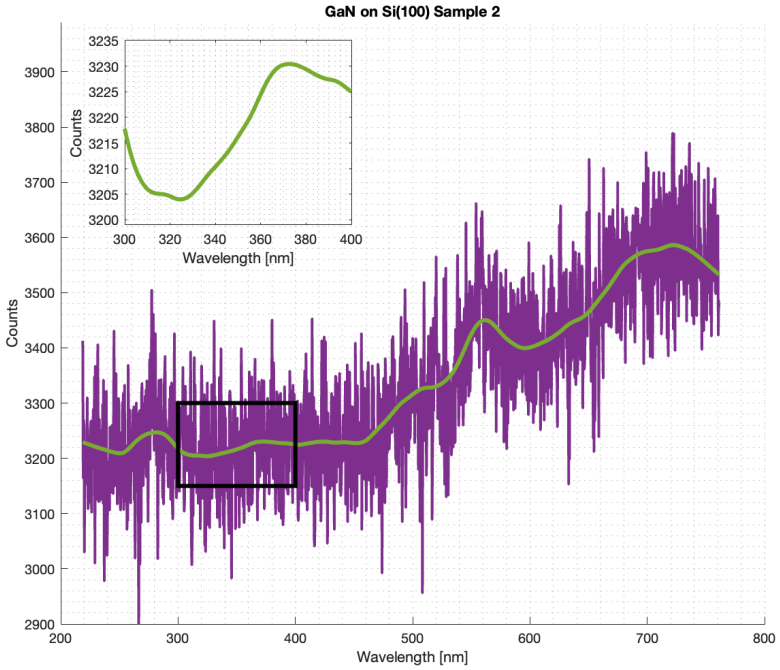

(c)

Figure 8.1. *Grown GaN on a Si(100) substrate where* ***(a)*** *is the optical image of the surface with a magnification of* $\times 10$ *and* ***(b)*** *is the AFM image.* ***(c)*** *is the photoluminescence measurement where purple is the raw data, green is the smoothed data and the zoomed graph is from the black box on the original graph.*

Sample number 3 in figure 8.2a is the optical image of the surface. The surface is homogenous without a lot of imperfections but with a few particles. From the AFM image, the surface has grains where some of the grains are higher than others. This makes the RMS of the surface 25.5 nm which is shown in table 4.2c. The photoluminescence of this sample shows 3 defined maxima at around 280 nm, 580 nm and 720 nm. This trend is observed in all samples for the Si(100). There are 2 maxima from the black box on the graph, where the first maximum is around 331 nm and the second is around 386 nm, which gives a band gap energy of 3.75 eV and 3.21 eV, respectively.

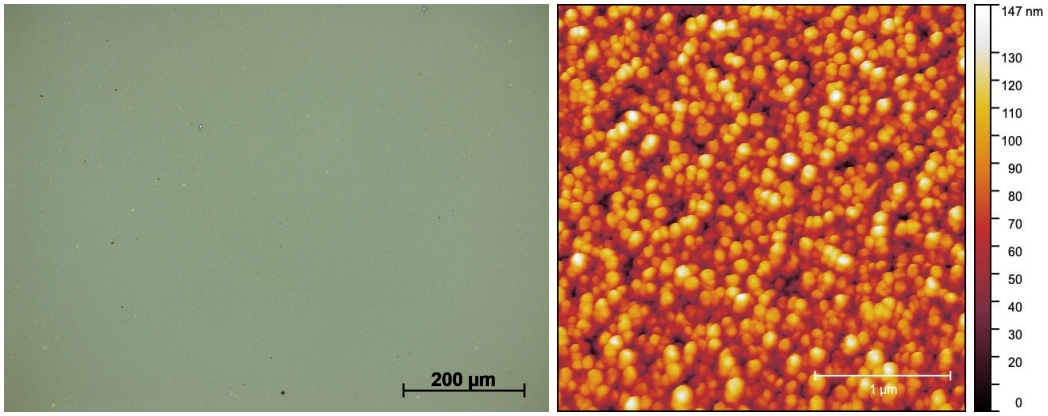

(a) **(b)**

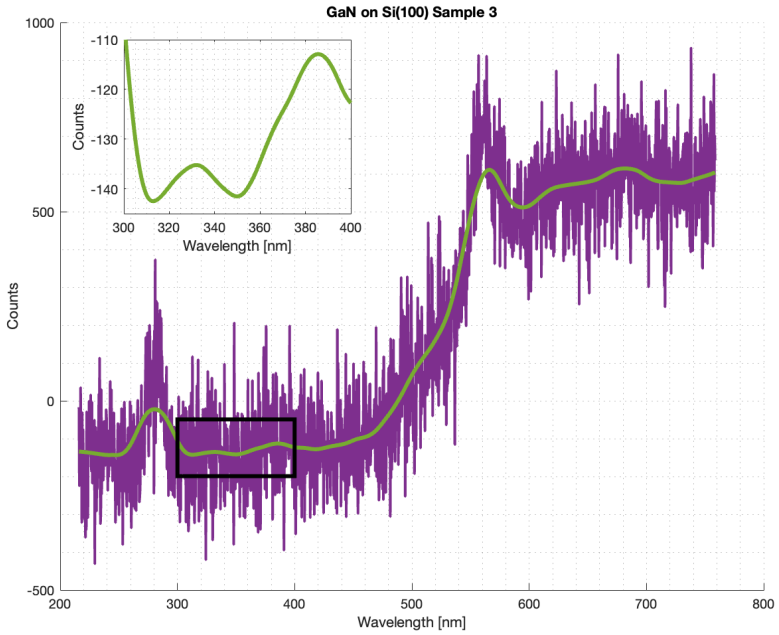

(c)

Figure 8.2. *Grown GaN on a Si(100) substrate where* ***(a)*** *is the optical image of the surface with a magnification of ×20 and* ***(b)*** *is the AFM image.* ***(c)*** *is the photoluminescence measurement where purple is the raw data, green is the smoothed data and the zoomed graph is from the black box on the original graph.*

For sample 4 the optical image shows a lot of grains on the surface. This is also shown in the AFM image where there is little space between the grains. Here the RMS value is 15.5 nm, which is shown in table 4.2d. The maximum photoluminescence for this sample is around 380 nm and very broad, which gives a band gap energy of 3.26 eV.

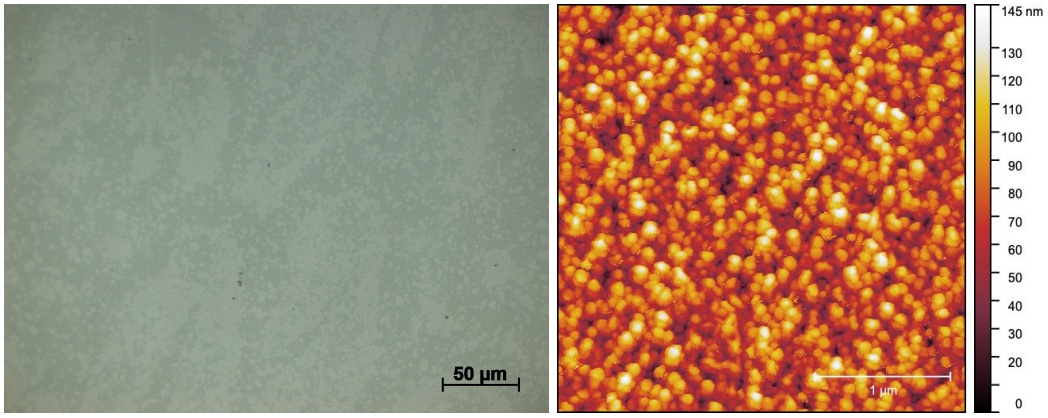

(a) **(b)**

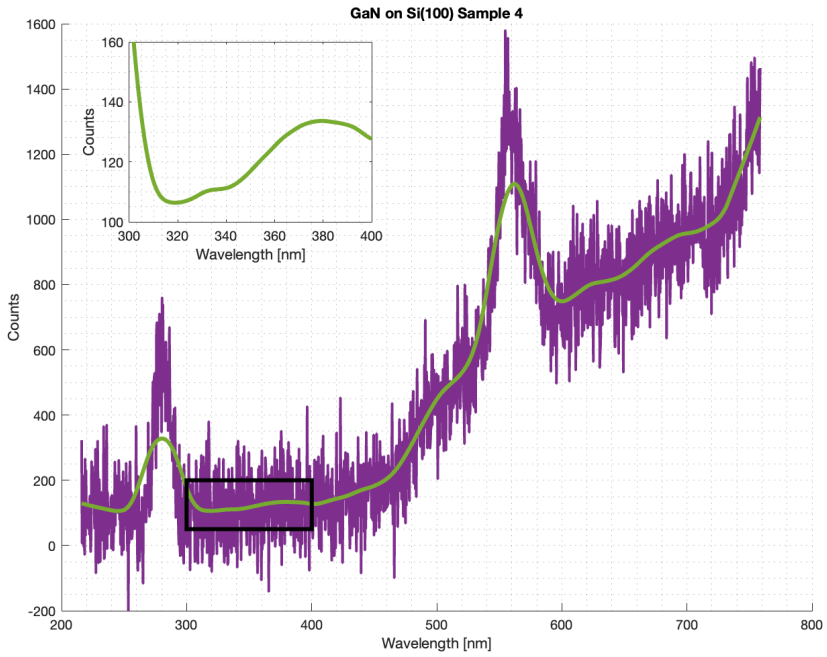

(c)

Figure 8.3. *Grown GaN on a Si(100) substrate where* ***(a)*** *is the optical image of the surface with a magnification of* $\times 50$ *and* ***(b)*** *is the AFM image.* ***(c)*** *is the photoluminescence measurement where purple is the raw data, green is the smoothed data and the zoomed graph is from the black box on the original graph.*

The optical image for sample 6 shows that the surface has a darker yellow colour and many grains. These grains can also be observed in the AFM image. Here there are big grains with no space in between. The RMS is 13.3 nm which is shown in table 4.2f. This sample's photoluminescence shows a distinct maximum at 354 nm and has a band gap energy of 3.50 eV.

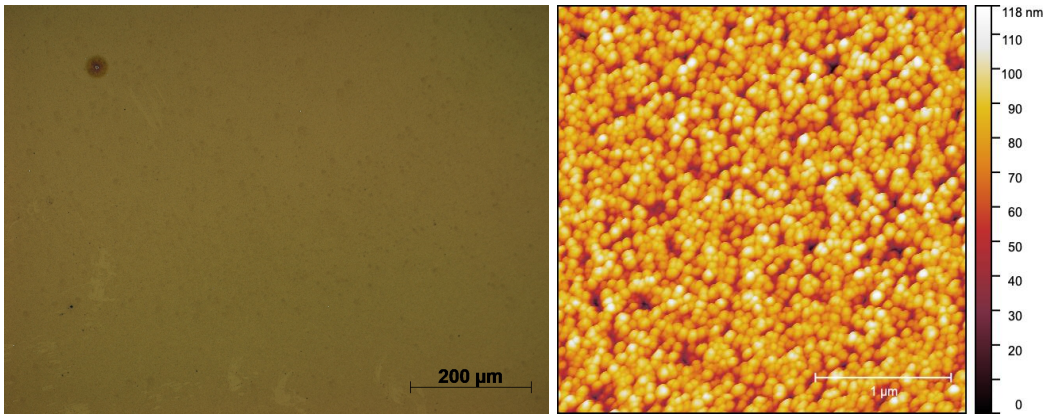

(a) **(b)**

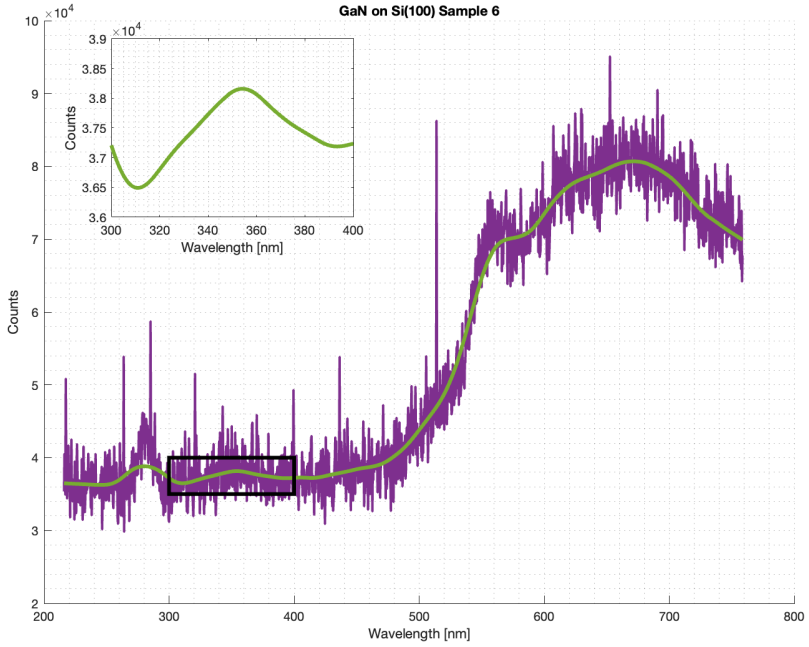

(c)

Figure 8.4. *Grown GaN on a Si(100) substrate where* ***(a)*** *is the optical image of the surface with a magnification of* $\times 20$ *and* ***(b)*** *is the AFM image.* ***(c)*** *is the photoluminescence measurement where purple is the raw data, green is the smoothed data and the zoomed graph is from the black box on the original graph.*

8.1.1 XRD of Si(100) Samples

Here are the XRD data from the GaN samples on Si(100) that are from the samples from the section above. They were analysed like the XRD data from the results section of XRD.

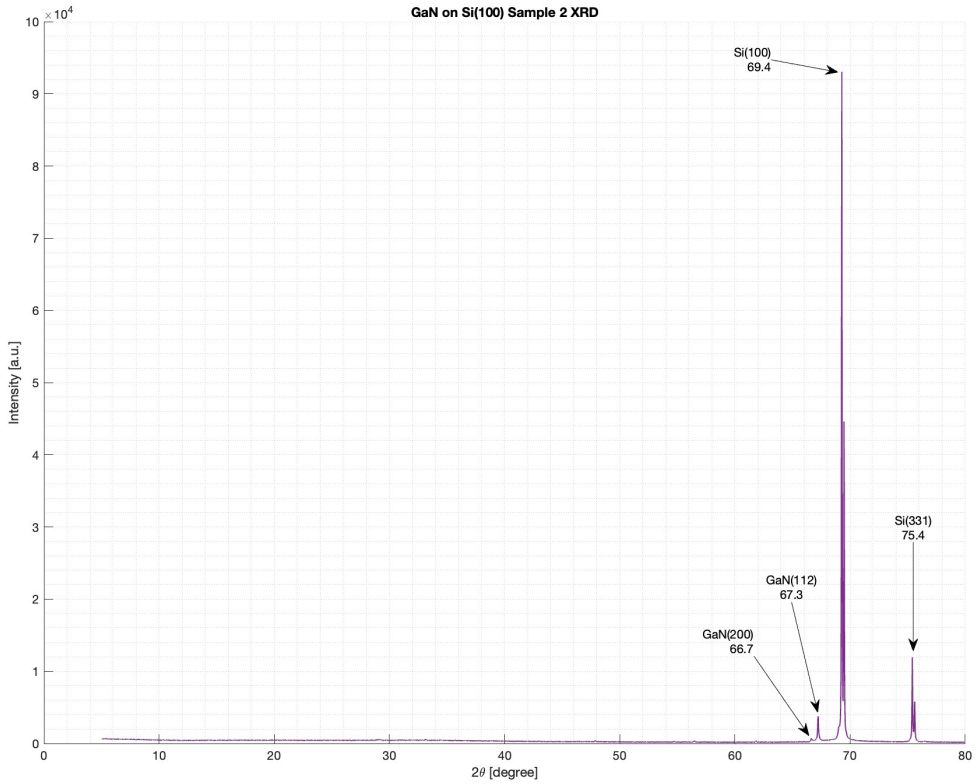
GaN on Si(100) Sample 2 XRD
×10^4
Intensity [a.u.]
2θ [degree]
Si(100)
69.4
Si(331)
75.4
GaN(112)
67.3
GaN(200)
66.7

(d)

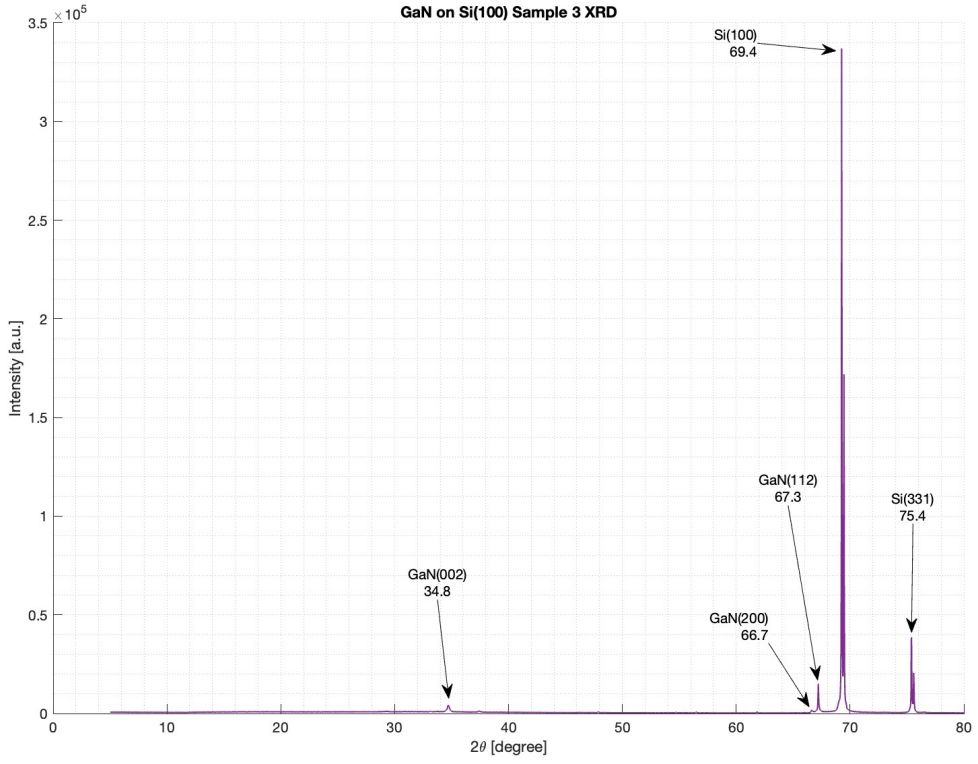
GaN on Si(100) Sample 3 XRD
×10^5
Intensity [a.u.]
2θ [degree]
Si(100)
69.4
GaN(112)
67.3
Si(331)
75.4
GaN(002)
34.8
GaN(200)
66.7

(e)

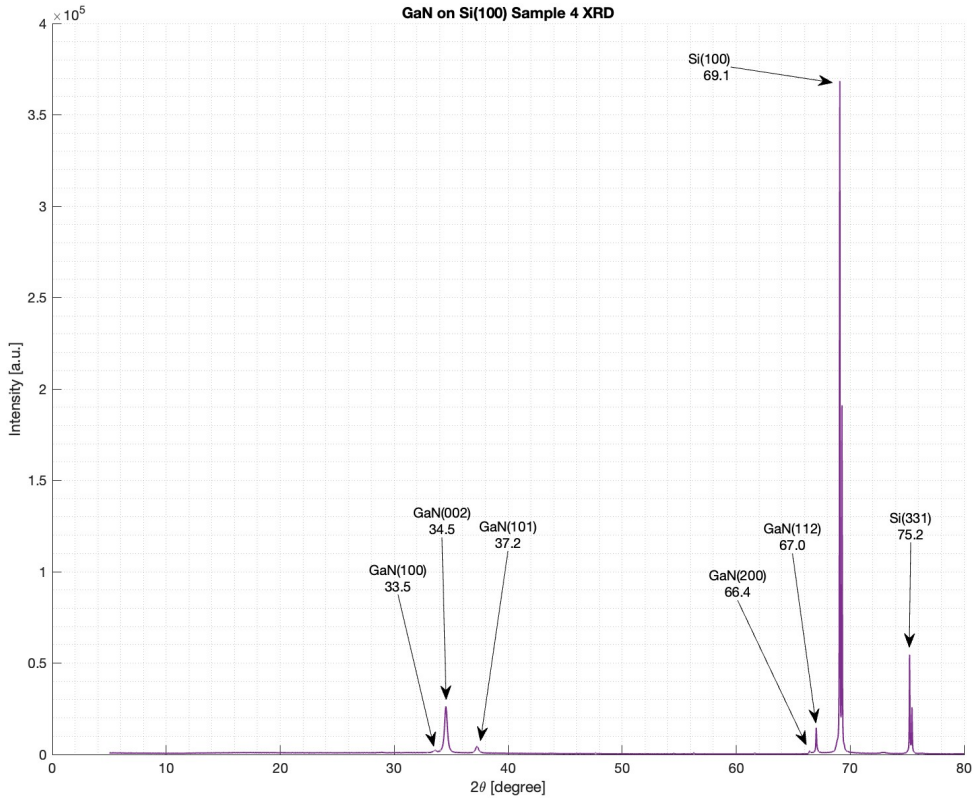

(f)

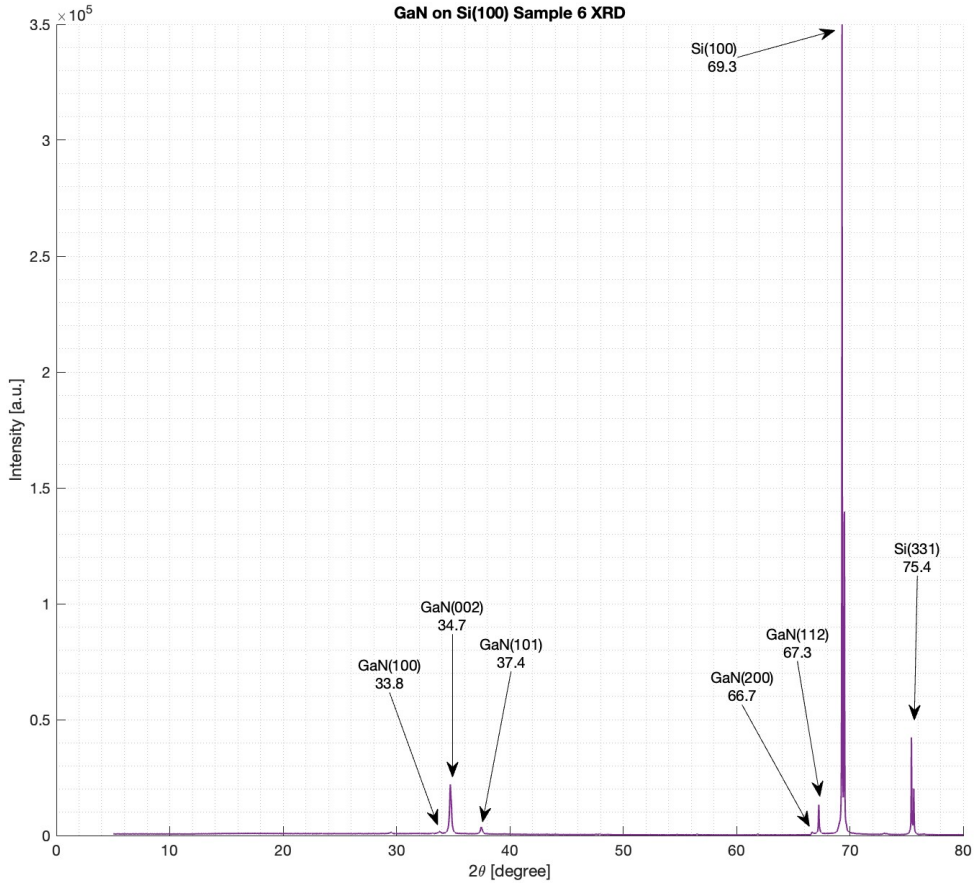

(g)

Figure 8.4. *The XRD data is shown with its defined peaks of the different crystal orientations for both the GaN and Si(100). Here* ***(a)*** *is from sample 2,* ***(b)*** *is sample 3,* ***(c)*** *is sample 4 and* ***(d)*** *is sample 6.*

8.2 Growth of GaN on Muscovite Mica Results

Sample 9 is shown in figure 8.5, where the surface is observed to be homogeneous with some imperfections from the substrate. The AFM image shows small grains, with some of the grains being higher than others, thereby giving an RMS of 3.2 nm, from table 4.3b. For photoluminescence, from the black box, no maximum was observed.

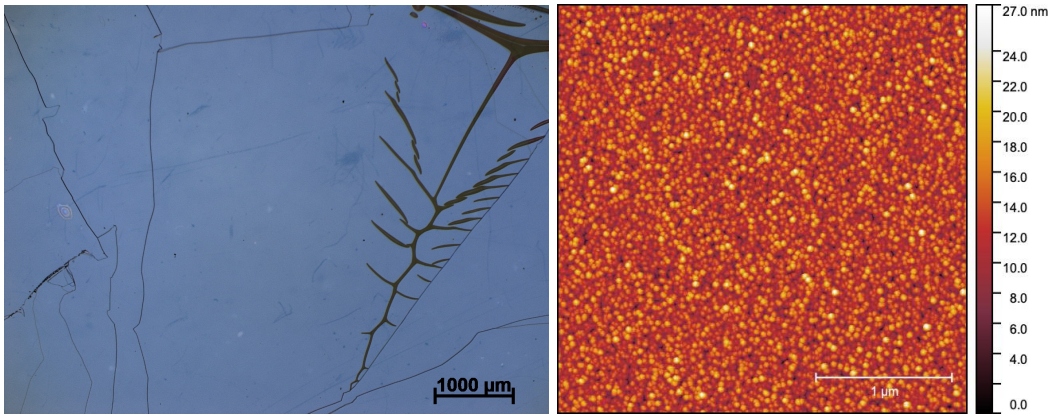

(a) **(b)**

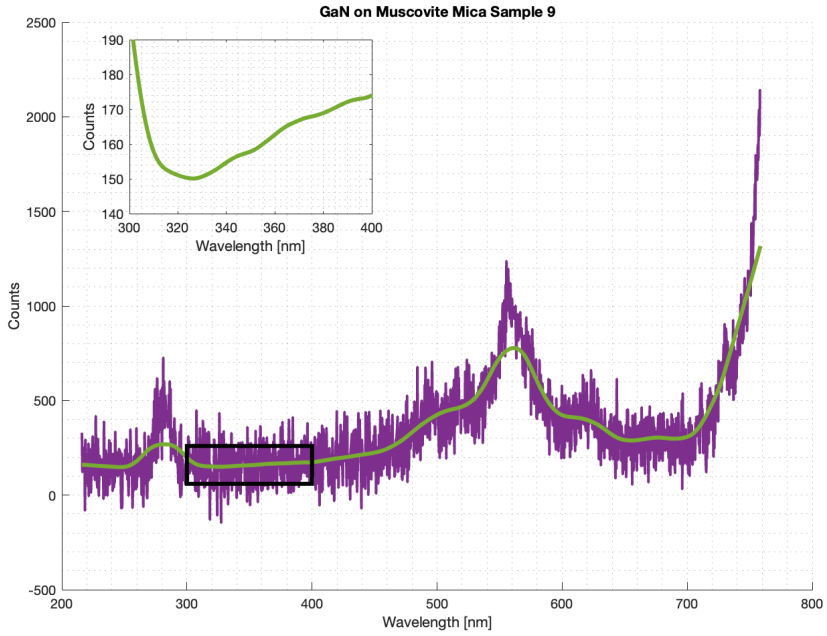

(c)

Figure 8.5. *Grown GaN on a muscovite mica substrate where* ***(a)*** *is the optical image of the surface with a magnification of* $\times 2.5$ *and* ***(b)*** *is the AFM image.* ***(c)*** *is the photoluminescence measurement where purple is the raw data, green is the smoothed data, and the zoomed graph is from the black box on the original graph.*

The results of sample 10 are shown in figure 8.6. Here, the optical image of the surface shows a homogeneous surface with few imperfections. There can be observed some small white dots on the surface. From the AFM image, the grains are relatively small and give an RMS value of 3.3 nm. For the photoluminescence, the maximum at the black box is 388 nm with little intensity, which gives a band gap energy of 3.20 eV.

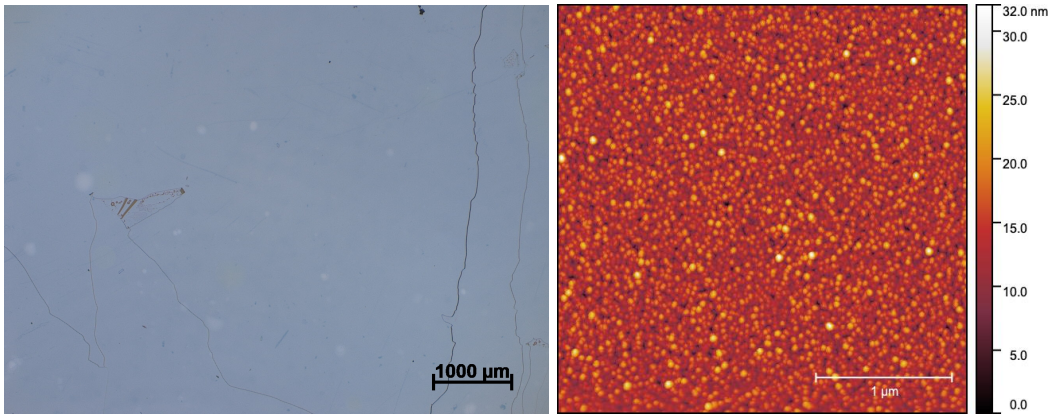

(a) **(b)**

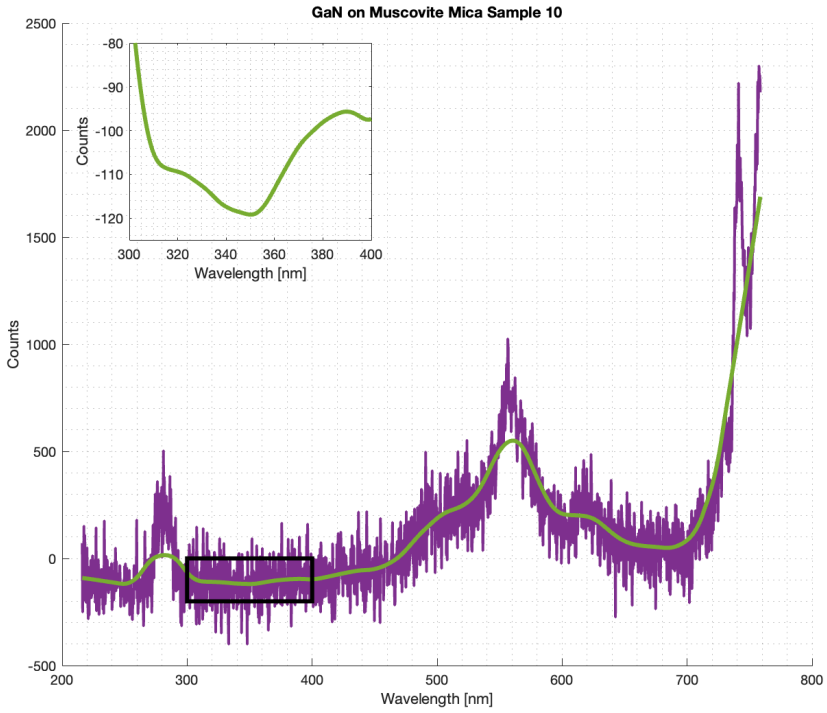

(c)

Figure 8.6. *Grown GaN on a muscovite mica substrate where* ***(a)*** *is the optical image of the surface with a magnification of* $\times 2.5$ *and* ***(b)*** *is the AFM image.* ***(c)*** *is the photoluminescence measurement where purple is the raw data, green is the smoothed data, and the zoomed graph is from the black box on the original graph.*

For sample 11, the optical image shows a uniform thin film with a few imperfections. In the image, a yellow circle and small circular imperfections with a purple colour are observed. For the AFM image, the surface has a lot of very small grains, one or two bigger grains in between. The RMS for this is around 2.4 nm. The maximum from the photoluminescence graphs black box is around 378 nm, giving a band gap energy of 3.28 eV.

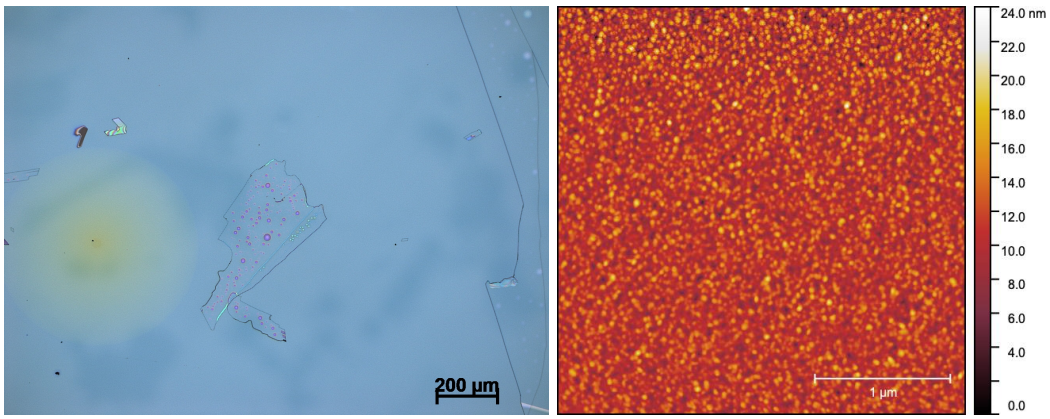

(a) **(b)**

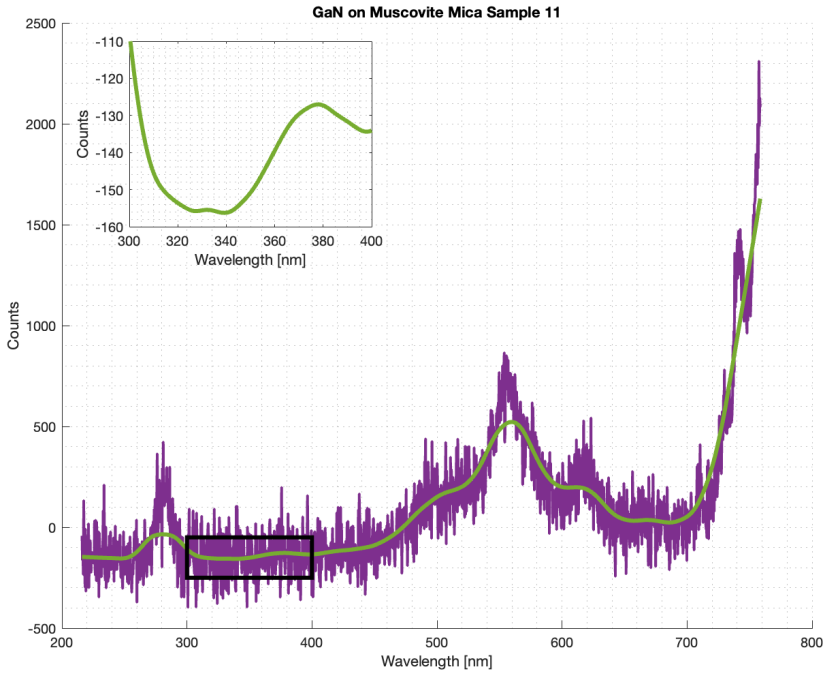

(c)

Figure 8.7. *Grown GaN on a muscovite mica substrate where* ***(a)*** *is the optical image of the surface with a magnification of* $\times 10$ *and* ***(b)*** *is the AFM image.* ***(c)*** *is the photoluminescence measurement where purple is the raw data, green is the smoothed data, and the zoomed graph is from the black box on the original graph.*

The optical image of sample 13 shows a couple of circles underneath the surface. The substrate also has some cracks, but the thin film shows a uniform surface, with some white circles on top. The AFM image shows many small grains. Therefore, the RMS for this sample is 1.9 nm. From the photoluminescence graph, this sample has two big maxima and one small maximum at the beginning. No maximum can be observed at the black box where the GaN should be indicated.

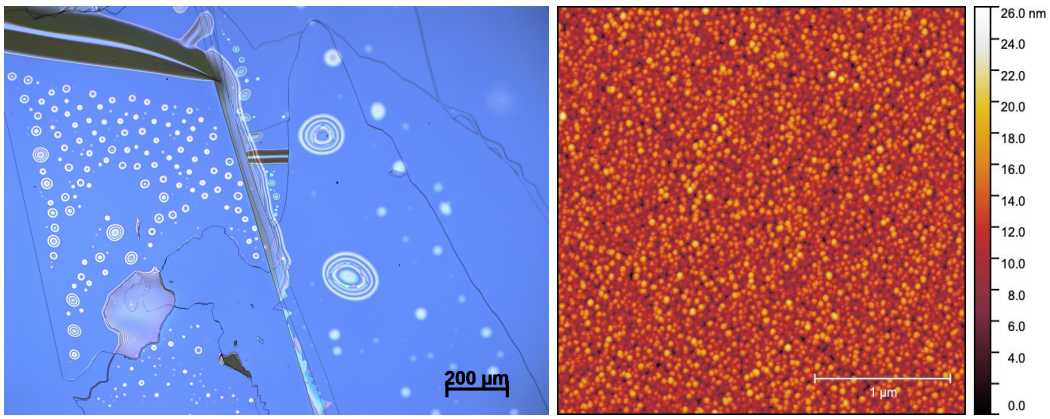

(a) (b)

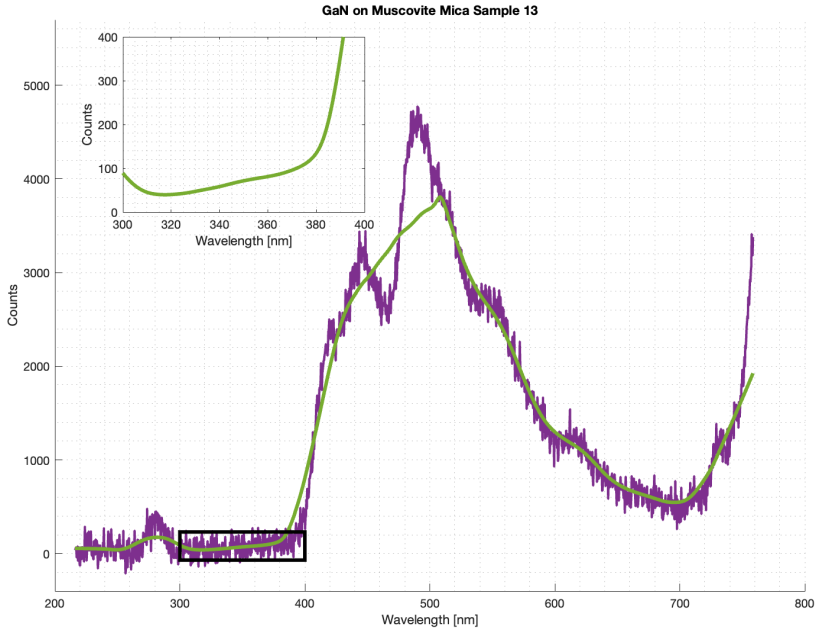

(c)

Figure 8.8. *Grown GaN on a muscovite mica substrate where* ***(a)*** *is the optical image of the surface with a magnification of* $\times 10$ *and* ***(b)*** *is the AFM image.* ***(c)*** *is the photoluminescence measurement where purple is the raw data, green is the smoothed data, and the zoomed graph is from the black box on the original graph.*

8.2.1 Small Muscovite Mica Samples Results

Sample 16 shows some destruction from the backside of the substrate, with a homogeneous film on top of the substrate. The AFM image shows a lot of grains with little space between them. The measured average RMS value is around 2.9 nm. From the photoluminescence measurement, the graph in the black box shows no maximum.

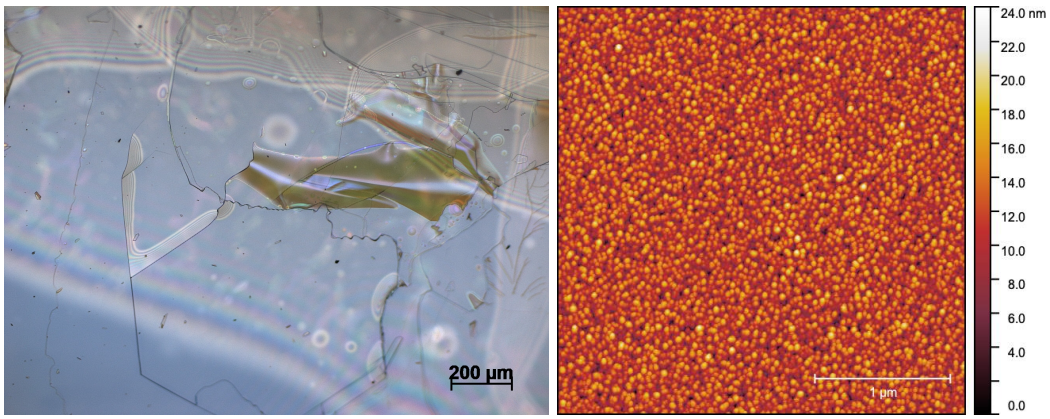

(a) **(b)**

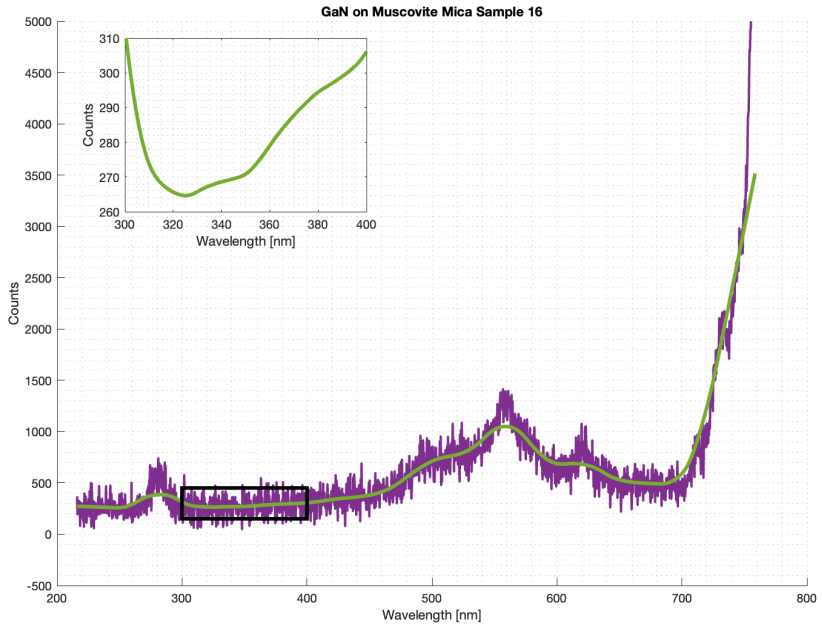

(c)

Figure 8.9. *Grown GaN on a muscovite mica substrate where* ***(a)*** *is the optical image of the surface with a magnification of* $\times 10$ *and* ***(b)*** *is the AFM image.* ***(c)*** *is the photoluminescence measurement where purple is the raw data, green is the smoothed data, and the zoomed graph is from the black box on the original graph.*

The optical image for sample 17 shows a homogeneous surface throughout the wafer. There are many grains in the AFM image with little space between them, giving it an RMS value of around 4.5 nm. The photoluminescence shows one maximum in the black box. This maximum is around 373 nm, giving the thin film a band gap energy of 3.32 eV.

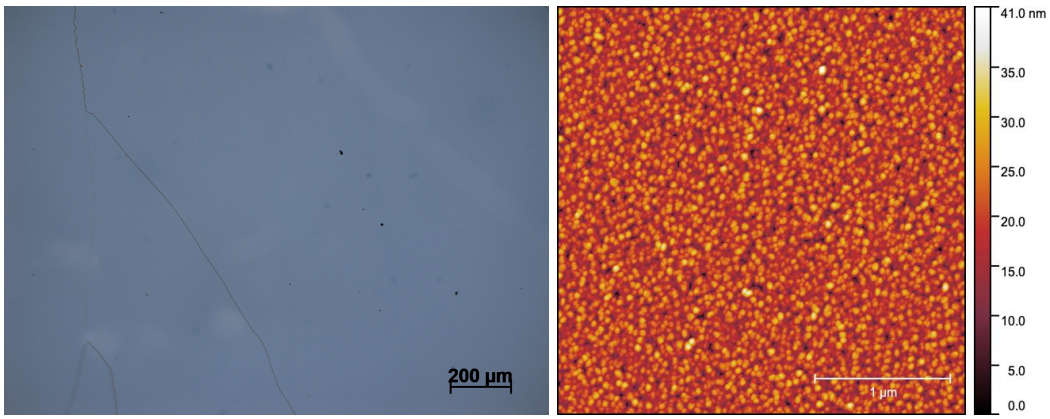

(a) **(b)**

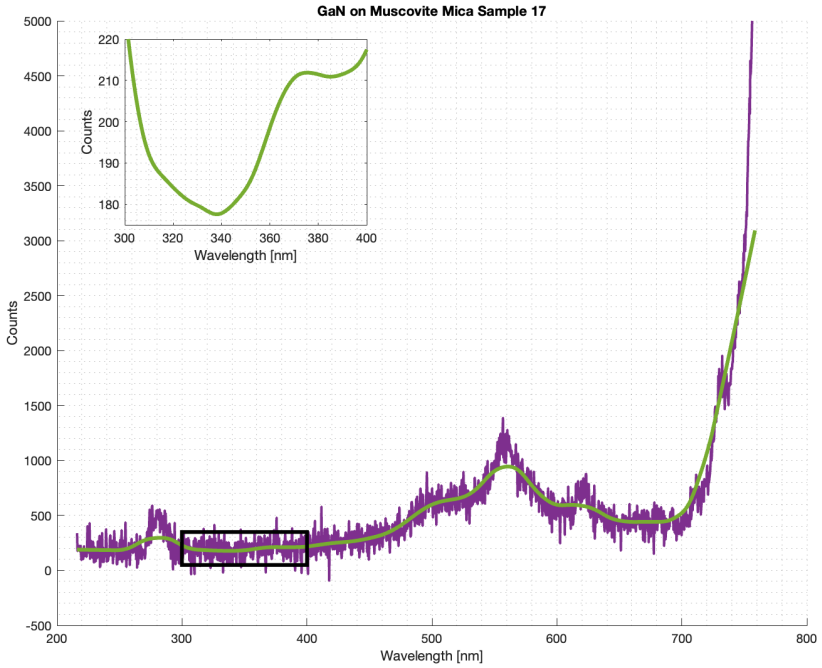

(c)

Figure 8.10. *Grown GaN on a muscovite mica substrate where* ***(a)*** *is the optical image of the surface with a magnification of* $\times 10$ *and* ***(b)*** *is the AFM image.* ***(c)*** *is the photoluminescence measurement where purple is the raw data, green is the smoothed data, and the zoomed graph is from the black box on the original graph.*

The surface of sample 18 shows a homogenous, thin film with few imperfections. There are some small white circles on the surface and underneath the surface. The AFM image shows many grains, with grains on top, which gives the surface an RMS value of 4.9 nm. Photoluminescence measurement shows a maximum at the black box at around 373 nm, thereby giving a band gap energy of 3.32 eV.

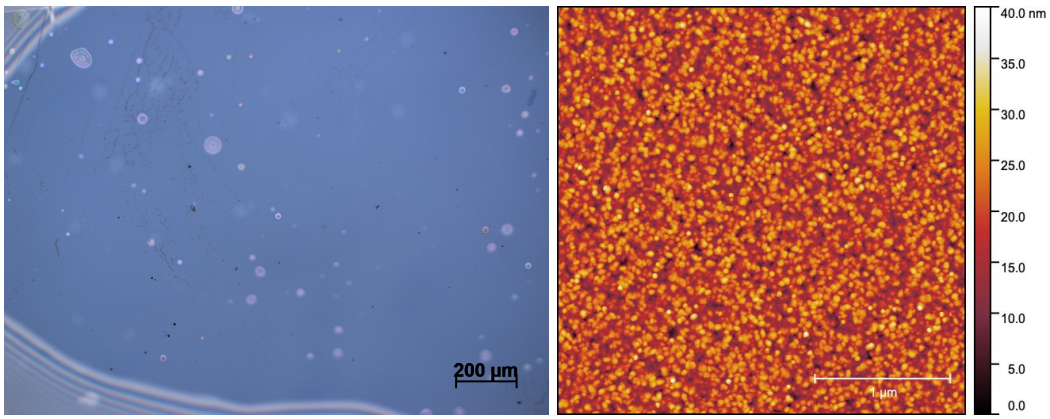

(a) **(b)**

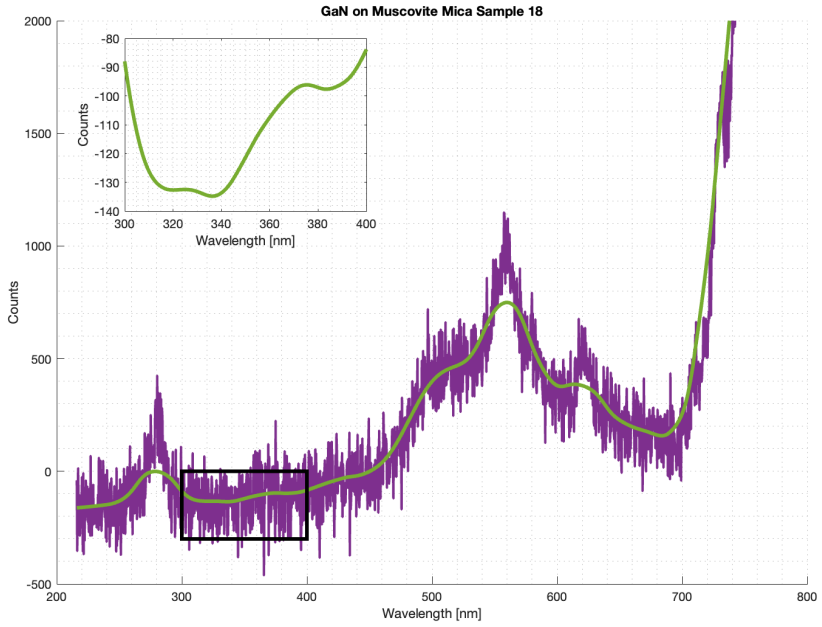

(c)

Figure 8.11. *Grown GaN on a muscovite mica substrate where* ***(a)*** *is the optical image of the surface with a magnification of* $\times 10$ *and* ***(b)*** *is the AFM image.* ***(c)*** *is the photoluminescence measurement where purple is the raw data, green is the smoothed data, and the zoomed graph is from the black box on the original graph.*

Sample 19 is shown in figure 8.12, where the optical image shows a homogeneous surface with few imperfections. The AFM image shows many big grains with some holes between some grains. This makes an average roughness of 7.3 nm, as seen in table 4.4e. For the photoluminescence the maximum that is of interest is shown in the black box of the graph, the maximum is around 366 nm which gives a band gap energy of around 3.38 eV.

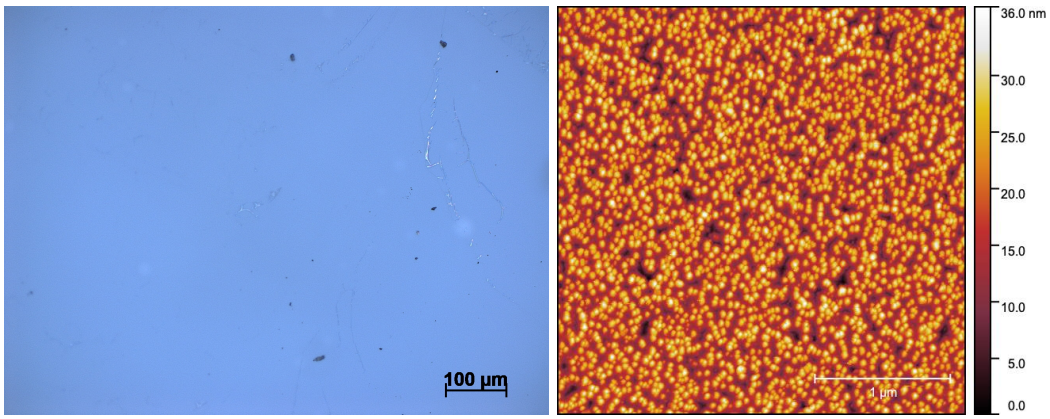

(a) **(b)**

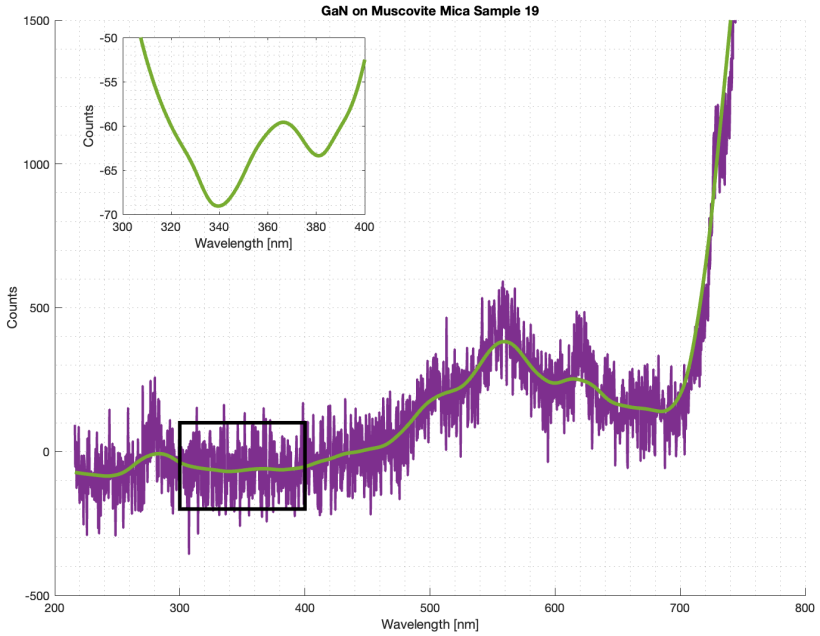

(c)

Figure 8.12. *Grown GaN on a muscovite mica substrate where* ***(a)*** *is the optical image of the surface with a magnification of* $\times 20$ *and* ***(b)*** *is the AFM image.* ***(c)*** *is the photoluminescence measurement where purple is the raw data, green is the smoothed data, and the zoomed graph is from the black box on the original graph.*

Figure 8.13 shows the photoluminescence graph from sample 19 where the measurements were done with more coverage. This was done to see how the graph looks at 800 nm and above. The measurement still shows the band gap energy of GaN at around 371 nm giving a band gap energy of 3.34 eV. For the maximum at around 836 nm, the band gap energy is 1.48 eV.

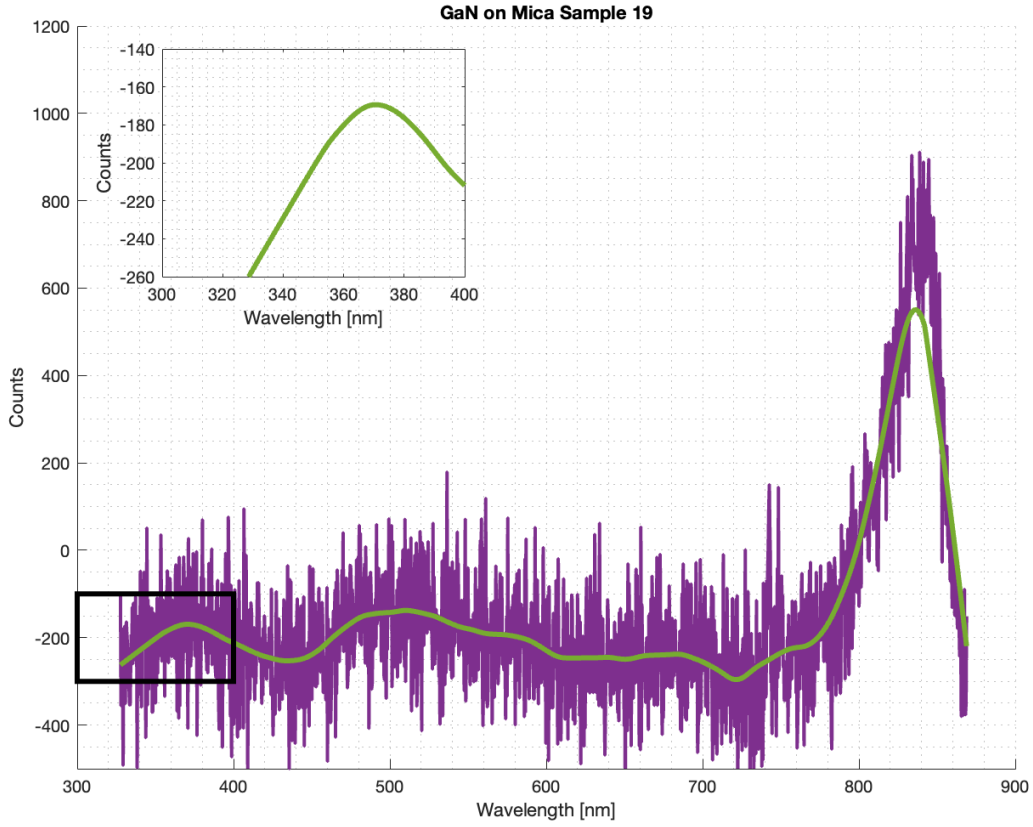

Figure 8.13. *This is the photoluminescence measurement of sample 19 from 300 nm to 900 nm, where purple is the raw data, green is the smoothed data, and the zoomed graph is from the black box on the original graph.*

Appendix C 9

9.1 Heat Distribution in Mica Results

For sample 9, which is shown in figure 9.1, the temperature is 600 °C and shows that after 1 min, the temperature has reached its limit over the whole sample. Only a small part of the sample edges get a higher temperature than the rest. There is again a temperature difference of around 180 °C from one end of the sample to the other end, that is heated.

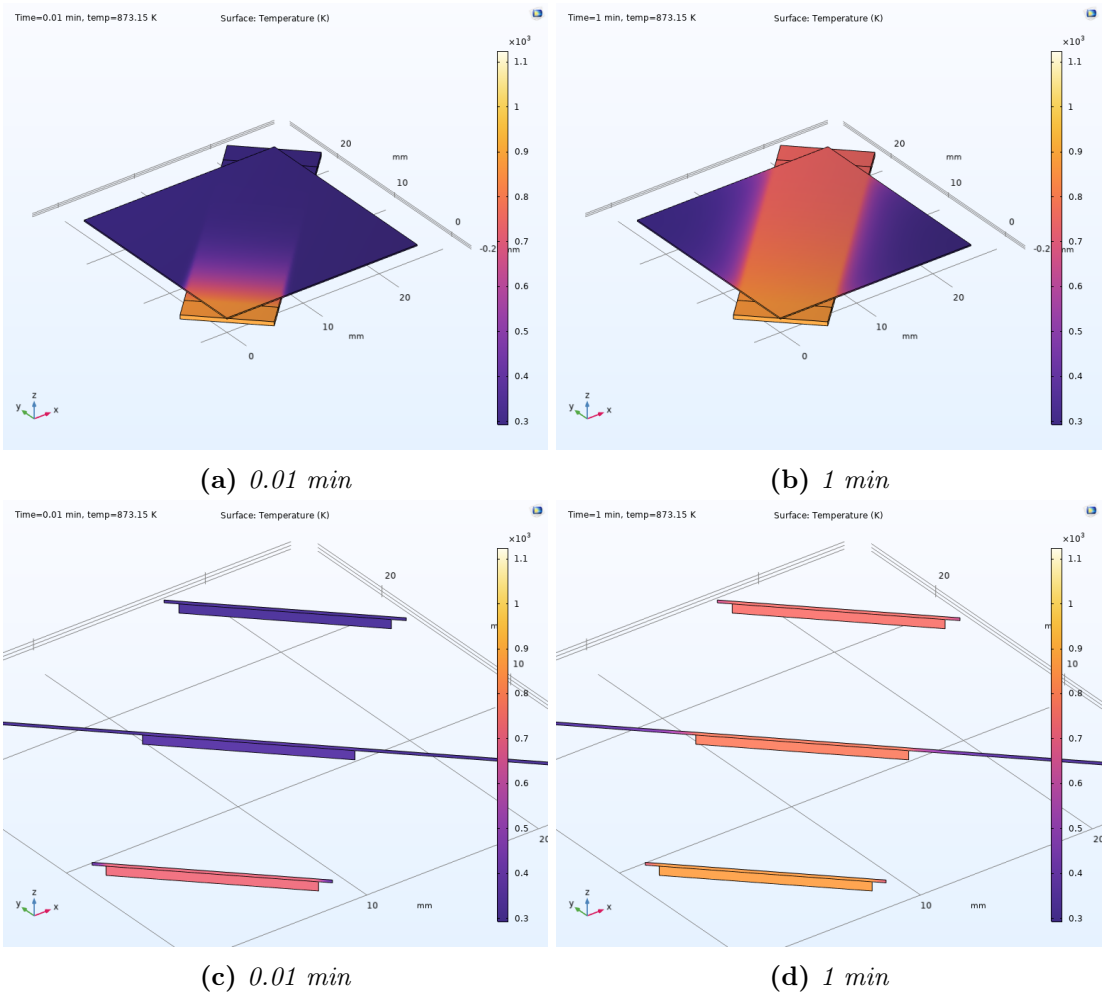

(a) *0.01 min* **(b)** *1 min*

(c) *0.01 min* **(d)** *1 min*

Figure 9.1. *Sample 9 simulated from 0.01 min to 1 min with a temperature of 600 °C and steps of 0.01 min. Both with the whole surface and cutouts from the sample.*

For sample 10, the heat can be observed to spread more over the entire sample. This is for a temperature of 650 °C, where after 1 min the heat is distributed. The temperature difference here can be observed to be around 200 °C.

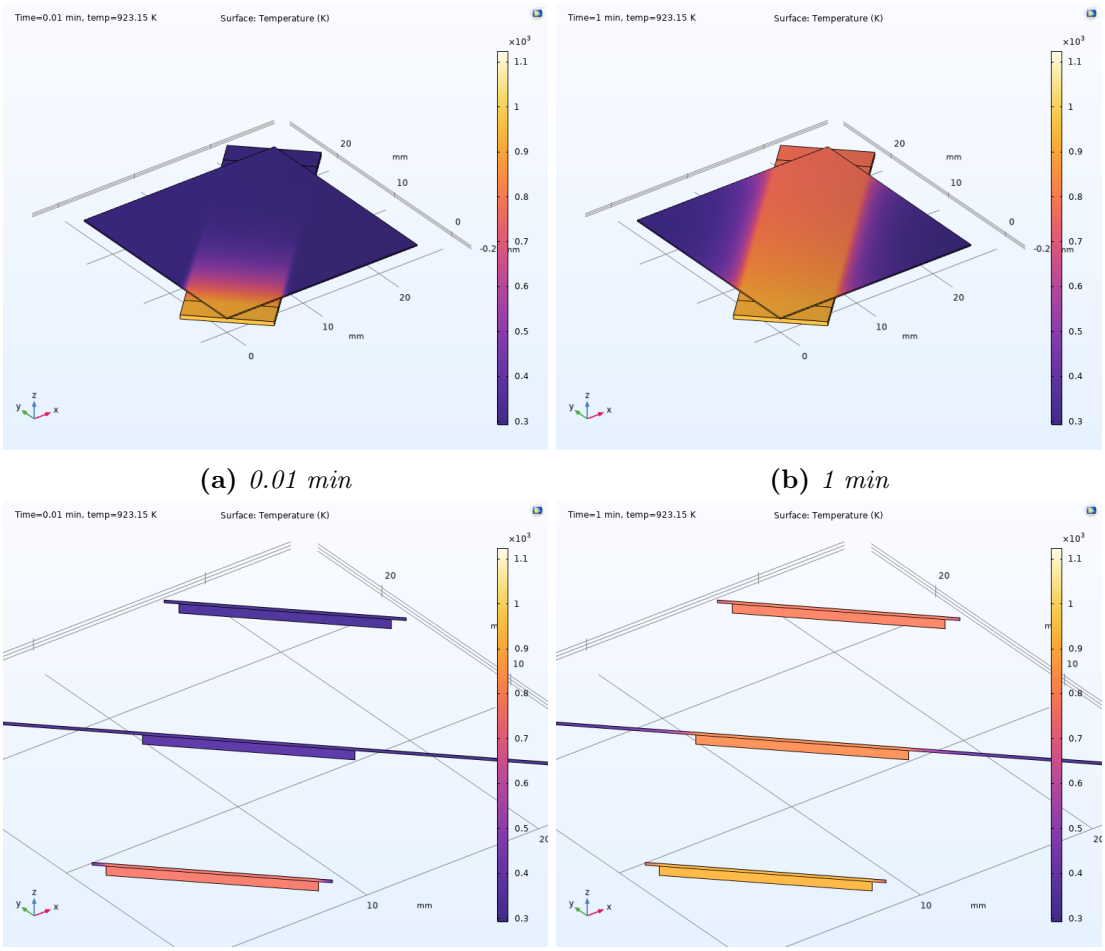

(a) *0.01 min* **(b)** *1 min*

(c) *0.01 min* **(d)** *1 min*

Figure 9.2. *Sample 10 simulated from 0.01 min to 1 min with a temperature of 650 °C and steps of 0.01 min. Both with the whole surface and cutouts from the sample.*

After 1 min, sample 11 reached 700 °C, with a temperature difference of around 200 °C. Here, the heat spreads more over the entire sample, which can better be observed in the cut of the sample.

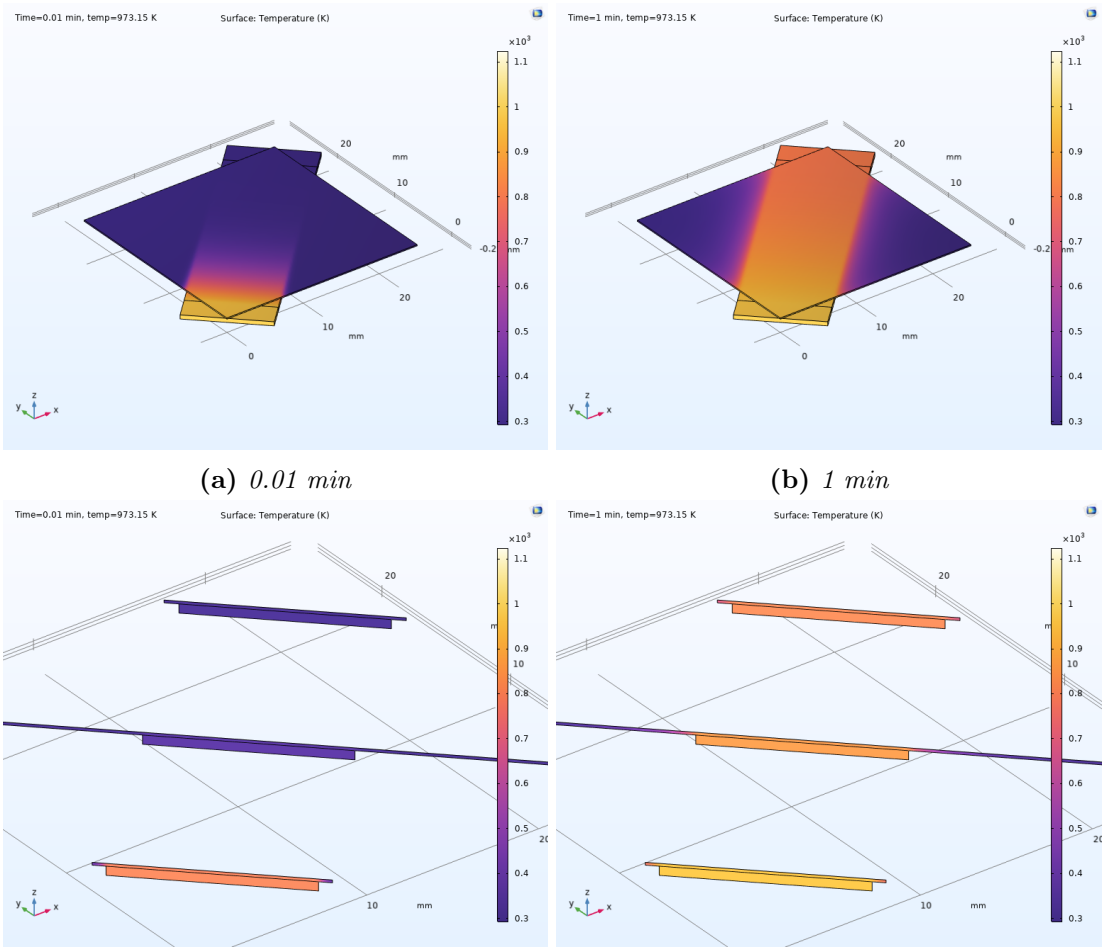

(a) *0.01 min* **(b)** *1 min*

(c) *0.01 min* **(d)** *1 min*

Figure 9.3. *Sample 11 simulated from 0.01 min to 1 min with a temperature of 700 °C and steps of 0.01 min. Both with the whole sample and cutouts from the sample.*

Sample 12 is shown in figure 9.4, where after 1 min, the sample has reached the 750 °C and has a temperature difference of around 250 °C. Both the whole sample and the cutout of the sample show that more heat is going through the mica.

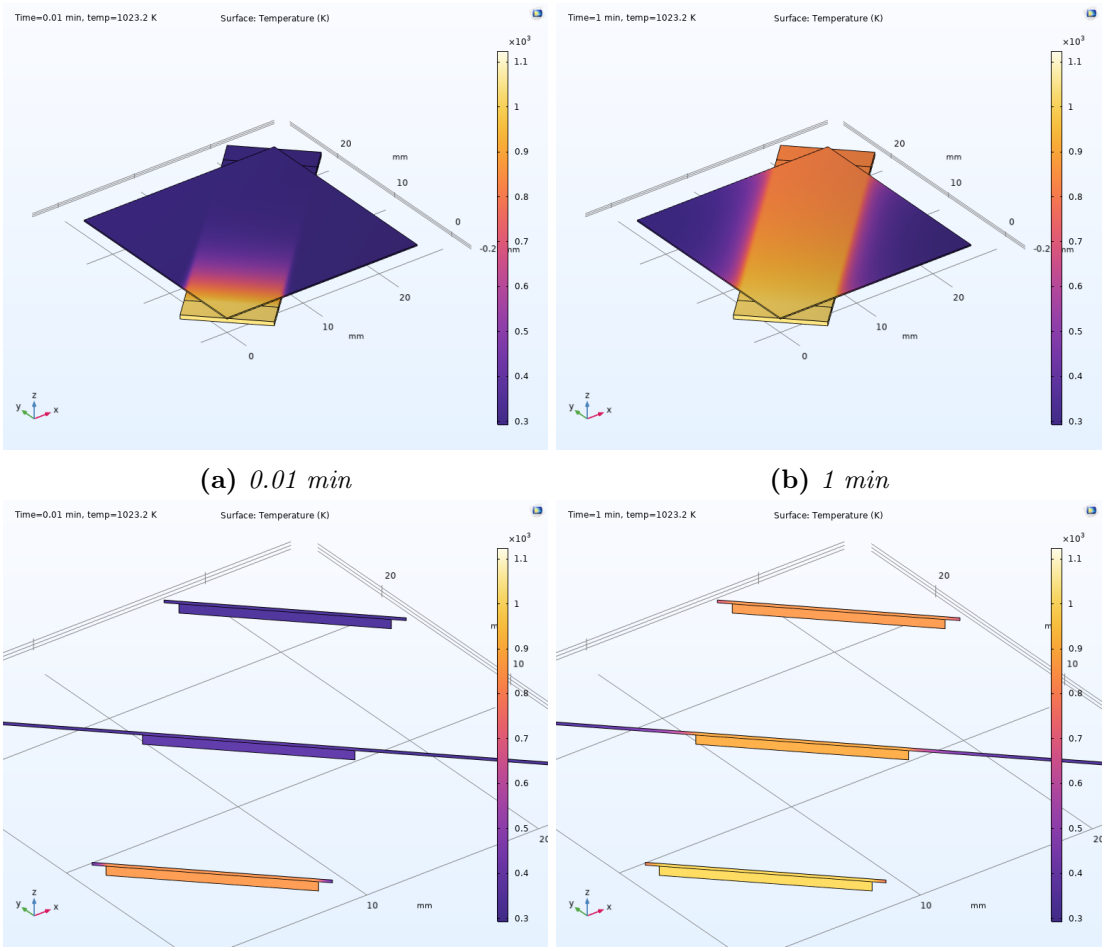

(a) *0.01 min* **(b)** *1 min*

(c) *0.01 min* **(d)** *1 min*

Figure 9.4. *Sample 12 simulated from 0.01 min to 1 min with a temperature of 750 °C and steps of 0.01 min. Both with the whole surface and cutouts from the sample.*

For sample 13, the muscovite mica surface after 1 min shows that the heated place reaches the 800 °C, but does not spread evenly over the entire surface. Thereby making a temperature difference of around 200 °C. From the cutout, the heat is shown to distribute a little through the mica outwards to the rest of the sample.

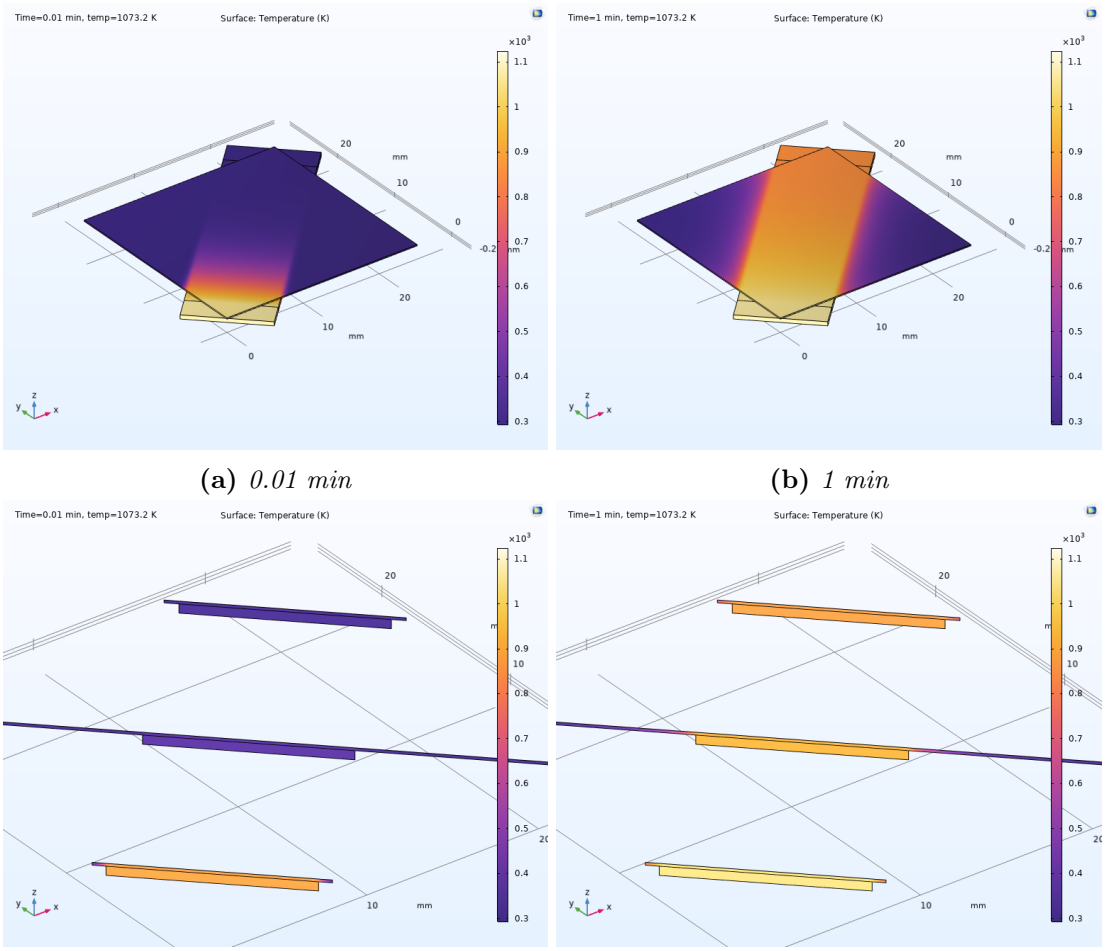

(a) *0.01 min* **(b)** *1 min*

(c) *0.01 min* **(d)** *1 min*

Figure 9.5. *Sample 13 simulated from 0.01 min to 1 min with a temperature of 800 °C and steps of 0.01 min. Both with the whole surface and the cutout from the sample.*

Sample 16 is shown in figure 9.6 where the applied temperature is 700 °C, which is already reached at the beginning of the simulation. After 1 min the heat has distributed throughout the sample with a temperature difference of around 150 °C. From the cutout images of the sample the heat distribution from the bottom of the sample to the top is uniformly heated.

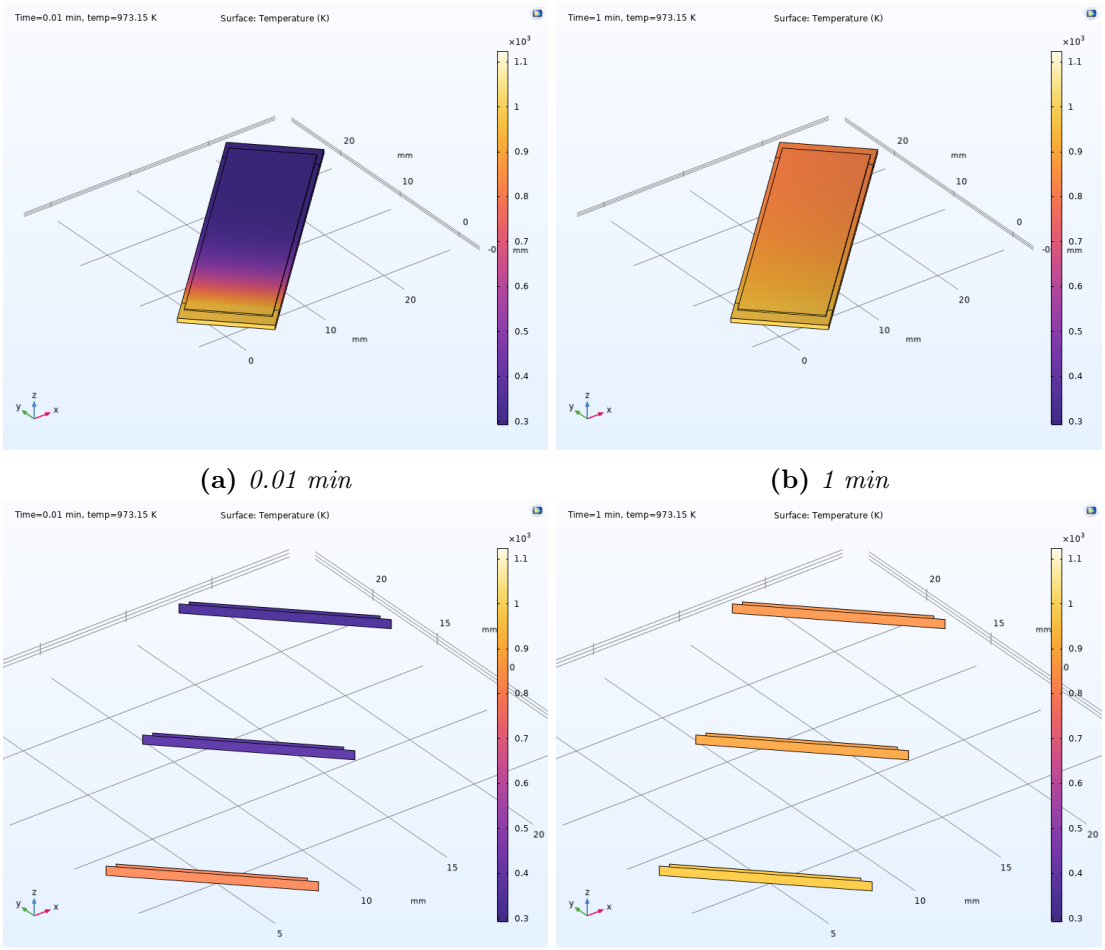

(a) *0.01 min* **(b)** *1 min*

(c) *0.01 min* **(d)** *1 min*

Figure 9.6. *Simulated sample 16 from 0.01 min to 1 min with a time step of 0.01 min. The applied temperature on the sample is 700 °C. Both the whole sample and the cutouts of the sample are shown.*

Sample 17 is shown in figure 9.7, where the applied temperature is 750 °C. After 1 min, the heat has distributed over the whole surface. Here, there is observed a temperature difference of around 200 °C.

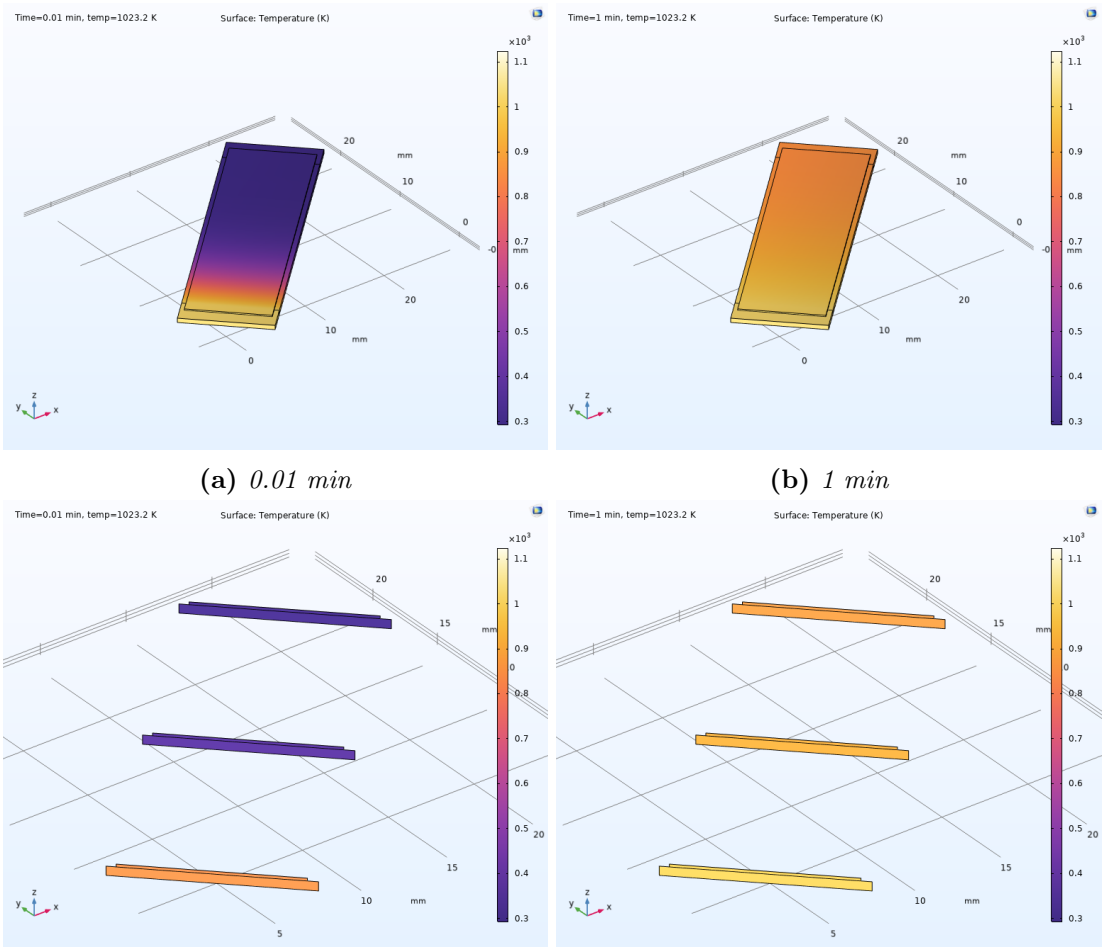

(a) *0.01 min* **(b)** *1 min*

(c) *0.01 min* **(d)** *1 min*

Figure 9.7. *Simulated sample 17 from 0.01 min to 1 min with a time step of 0.01 min. The applied temperature is 750 °C. Both the whole sample and the cutout of the sample are shown.*

Appendix D 10

10.1 First Try of Growth of GaN

The first attempt to grow GaN was made on a random Si(111) sample. The parameters for growing this sample are shown in table 10.1. This sample was grown by lab technician Peter Kjær Kristensen.

Table 10.1. *Deposition parameters of GaN.*

Sample	Substrate	T_S [°C]	Power [A]	T_{Ga} [°C]	t_{FS} [s]	thickness [nm]
GaN square	Si(111)	25	–	950	–	≈ 100

10.1.1 Optical Images

The optical images of GaN surface are shown in figure 10.1. Here, squares can be observed on the surface from the surface treatment before deposition of the GaN. In the squares, there are lines at a specific distance between them. This surface treatment was done by lab technician Peter Kjær Kristensen.

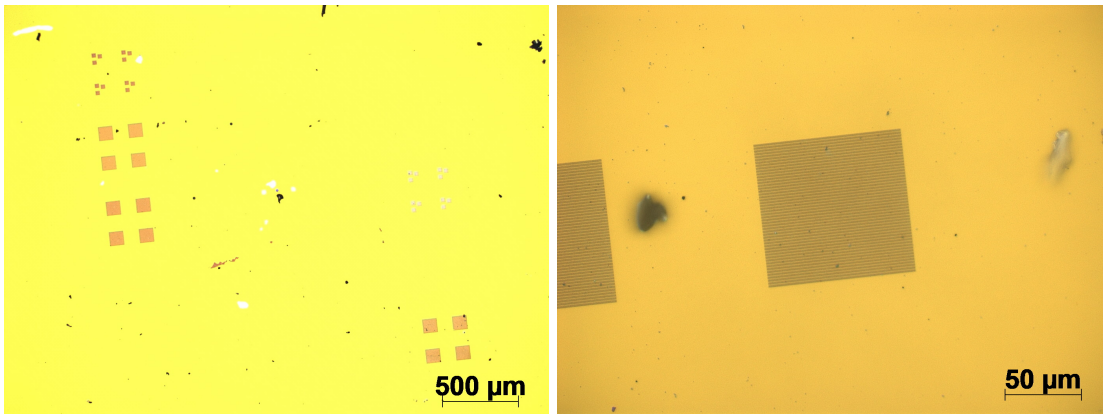

(a) **(b)**

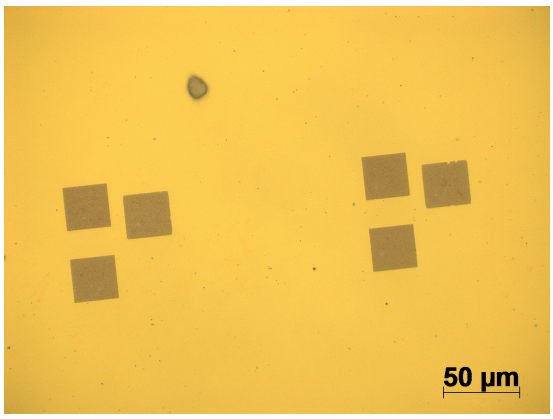

(c)

Figure 10.1. *The optical images of the first try of growing GaN on Si(111). Here* ***(a)*** *is the optical image with a magnification of ×5,* ***(b)*** *is ×50 and* ***(c)*** *is also with a magnification of ×50, only from a different place of the wafer.*

10.1.2 AFM

For this GaN sample the roughness was measured from the AFM images where some 3×3 images were analysed. Figure 10.2 shows the surface of the sample, where all of the different images had the same form of surface. Where there can be observed some grains at the surface and around 6 bigger particles on top of these grains.

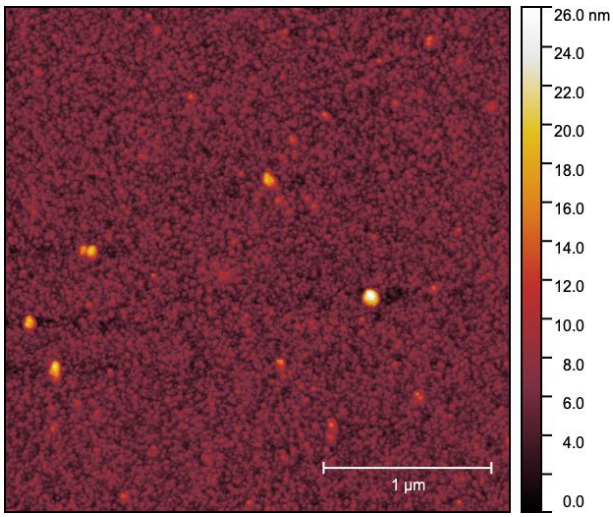

Figure 10.2. *AFM image of the GaN surface from figure 10.1.*

In table 10.2 the roughness of the surface is shown in nm and the average is then calculated from these measurements. This gives an average of around 3.3 nm, which is relatively smooth.

Table 10.2. *Roughness of the surface from figure 10.2.*

Image number	RMS [nm]
1	7.6
2	2.4
3	1.7
4	1.6
Average	3.3

Appendix E 11

11.1 Ionbonding

The Ion bonded Si to the glass substrate was measured in the AFM. This sample was made by Professor Kjeld Pedersen and lab technician Peter Kjær Kristensen. In Figure 11.1 the height images can be observed and the roughness of this surface can be seen in table 11.1.

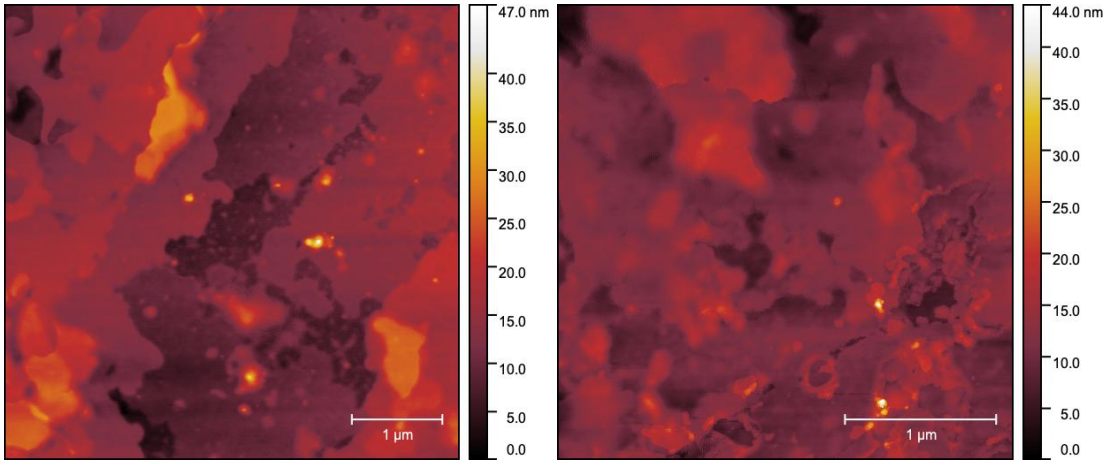

(a) **(b)**

Figure 11.1. *AFM images of Si transferred to a glass substrate, where* ***(a)*** *is the image of the surface with the size of 5×5.* ***(b)*** *is the image with the size of 3×3*

Table 11.1. *Roughness of the Si surface on different wafer places taken from the 3×3 images.*

Image number	RMS [nm]
1	1.6
2	2.7
3	2.8
Average	2.4